UNIVERSITY OF CALIFORNIA, SAN DIEGO

Primitive and differentiated achondrite meteorites and partial melting in the early Solar System

A Thesis submitted in partial satisfaction of the requirements
for the degree Master of Science

in

Earth Sciences

By

Christopher Andrew Corder

Committee in charge:

Professor James M. D. Day, Chair
Professor Geoffrey W. Cook
Professor David R. Stegman

2015

The Thesis of Christopher Corder is approved and it is acceptable in quality and form for publication on microfilm and electronically:

Chair

University of California, San Diego

2015

Dedication

This manuscript would be far from complete without thanking those who helped set the stage for the many hours of work it documents, and those thank-yous would be far from complete without recognizing my parents and their unwavering support throughout years of study. I know I was the one in the lab, but I never would have made it there, or to my defense, or through any of the long days and nights if it weren't for you both. Thank you, so much.

I'd love to thank my entire family, especially Stephen. You're a brother Stephen, and you encourage me more than you know. Whenever it seemed like research was going nowhere, you were there to remind me why science is always a worthwhile endeavor. Even more importantly you remind me, by example, that there are exceptional people in this world.

Many thanks are due to the lab group I worked with and other smart folks at SIO. First of all, thank you James for trusting this intriguing suite of meteorites to my care. I hope I did these beautiful samples justice. Caitlin and Jorge – you were the first M.S. students to graduate under James, and if it wasn't for you I'd have taken twice as long to graduate myself. You were tremendous helps during the first months when it was easy to feel lost. Jasmeet, I also would have never gotten here if I didn't have your support, and I hope I have or will someday return the favor. I can't think of anyone better to continue work on these samples. Tom – I am incredibly grateful I have such an intelligently practical friend to balance out my romantic ideas. Magali, your charm and positive attitude are rare, and I'm glad there are people that recognize those qualities in you. Brad, you have incredible brainpower and it's been a privilege to work along side you.

Thank you to all those, who throughout this scientific process have taught me what data, diagrams, publications, and theories cannot.

TABLE OF CONTENTS

LIST OF FIGURES

LIST OF TABLES

ABSTRACT OF THE THESIS

Primitive and differentiated achondrite meteorites and

partial melting in the early Solar System

by

Christopher Andrew Corder

Master of Science in Earth Sciences

University of California, San Diego, 2015

Professor James Day, Chair

This study aims to reveal details in the processes by which planetary bodies differentiate by using meteorites as snapshots of partial melting, metal segregation, and recrystallization in the early Solar System. A sample suite of twenty-two undifferentiated chondrite, slightly melted primitive achondrite, and differentiated achondrite meteorites was collected and subjected to petrographic, electron microprobe, whole-rock trace- and major-element, and oxygen isotope analyses. Graphite in a single meteorite, MIL 091004,

was subjected to Raman spectroscopy analysis. Because the sample set ranges between undifferentiated and fully differentiated, attempts to make links between different stages in petrologic processes can be attempted. Rare-earth and whole-rock siderophile element abundances can be used to establish basic behaviors in meteorites, especially in the primitive acapulcoites and lodranites. Acapulcoites have chondrite-like chemistries. In lodranites, chemical abundances help establish part of the group as metal cumulates, and others as having experienced metal loss. Recent finds MIL 090405 and MIL 090206 are likely brachinite-like achondrites, and MIL 090405 displays trace-element patterns complimentary to the felsic meteorites GRA 06128/9. The expanding compositional range of brachinite-like achondrites suggests that low degree partial melting was common on small planetesimals in the early Solar System. Petrologic diversity in LEW 88763 may reveal process-related links between meteorite groups. Its existence also points to diverse oxidation environments in the early Solar System. MIL 091004 is a ureilite that contains an intrusive region with an exceptional amount of graphite grains. The meteorite points to re-fertilization processes on the ureilite parent body.

1. Introduction

Our understanding of the composition and chronology of Solar System events is largely derived from meteorites – extra-terrestrial rocks ejected from parent bodies ranging from planets to asteroids. The present collection of meteorites – the majority of which come from the asteroid belt between Mars and Jupiter – offers a natural laboratory for studying planetary differentiation processes. To fully understand the details in the chemical composition and evolution of planetary bodies in our Solar System, it is important to briefly consider the beginning of the universe itself, and the evolution of its encompassing chemical composition. The widely supported Big Bang theory of the "birth" of the universe posits that at its beginning, all matter in the universe existed at a single point and subsequently began expanding outward from this point approximately 14 billion years ago (e.g., Olive et al., 2000). The crux of the Big Bang theory – the universe's rapid and continual expansion – has been observed (e.g., Hubble 1929, Hubble and Humason 1931, Penzias and Wilson 1965) and is supported by theoretical calculations (Lemaitre 1931).

The very first seconds or minutes of the expansion are thought to have produced most of the universe's light elements (nuclides of H, He, and Li; e.g., Burles et al. 2001). During this light-element nucleosynthesis, the universe was exceptionally hot and dense, but as expansion continued beyond the universe's infancy, temperatures dropped. As temperatures dropped potential gravitational attraction between tiny particles allowed larger and larger bodies to form, until stars were produced. The formation of stars, in turn, allowed the process of stellar nucleosynthesis, where fusion creates elements heavier than H, He, and Li, but lighter than Ni (Hoyle 1954). A number of different

physical processes, some of which take place during stellar explosions called supernovae, source the elements that are heavier than Ni (Seeger et al. 1965), although elemental abundance falls sharply as atomic mass increases.

Some 4.56 billion years ago, the process of accumulation of dust and gas particles led to the birth of the Solar System. A molecular cloud collapsed in on itself due to gravitational attraction and formed a solar nebula. As the Sun began to form from the nebula's aggregation of gas and dust, particles just outside of the feeding zone of the Sun began to aggregate themselves into planetesimals. These planetesimals eventually evolved into differentiated planets and small bodies (dwarf planets, asteroids, comets, moons, etc.), some of which persist today. The transition from early planetesimals to the bodies of today's Solar System was not a straightforward evolution. The early Solar System was likely a place of incredible petrologic diversity, with both "intra-body" (e.g., diverse differentiation and melting events) and "inter-body" (e.g., collisions between bodies) processes active throughout.

For the following study, focus is placed on the steps between undifferentiated accretionary materials (the oldest known rocks in our Solar System) and large differentiated bodies. Chondrite meteorites are thought to be the first solid materials to have condensed from the solar nebula, and the most striking piece of evidence supporting this is the presence of chondrules and calcium-aluminum-rich inclusions (CAIs), as well as the fact that carbonaceous chondrites have elemental abundances that approach the composition of the photosphere of the Sun (Lodders 2003). These small (Scott and Krot 2007; MacPherson 2007) structures are used to date the Solar System itself (4568.2 Ma from Bouvier and Wadhwa 2010; 4567 ± 0.6 Ma from Kita et al. 2005). CAIs in

particular have older absolute ages relative to initial Pb isotope values, and chondrules produce ages that are 1-3 million years younger (Kita et al. 2005).

In contrast, achondrite meteorites come from bodies of varying degrees of differentiation. Achondrites exist in two major varieties – primitive and differentiated. Primitive achondrites exhibit chemistries that are broadly chondritic, or only slightly fractionated from chondritic, along with metamorphosed, relatively equilibrated, non-chondritic textures. A very few primitive achondrites contain "relict chondrules" but for the most part, these remnants from the earliest Solar System have been completely recrystallized in primitive achondrites. The primitive achondrites are represented in this study by acapulcoite and lodranite meteorites. Acapulcoites and lodranites are early formed and genetically linked achondrites that preserve the initial stages of differentiation on an asteroidal body (Touboul et al. 2009, McCoy et al. 1996, McCoy et al. 1997a, Mittlefehldt et al. 1996, Palme et al. 1981, Rubin 2007), and thus can be considered a natural laboratory to study the beginning differentiation events involved in planet formation in the early Solar System. Acapulcoites have experienced temperatures high enough to partially melt FeNi metal and FeS (McCoy et al. 1996) while lodranites have experienced both Fe,Ni-FeS and silicate partial melting (McCoy et al. 1997a).

Differentiated achondrites, on the other hand, are characterized by chemistries that can fractionate significantly from those of chondrites, and contain textures that are clearly produced by igneous differentiation (partial or complete melting) and range from partially-melted to fully-differentiated meteorites. The extensive differentiation among achondrites is apparent in the presence of stony silicate-rich achondrites (Mittlefehldt 2007) and their metallic counterparts, the iron meteorites, as well as the intermediate

stony-iron meteorites (Haack and McCoy 2007). The achondrite meteorites are represented in this study by partially-melted brachinites, brachinite-like achondrites, and ureilites (some of which are anomalous or ungrouped samples). The brachinites comprise a relatively small ultramafic meteorite group and predominantly contain olivine and clinopyroxene, along with minor plagioclase, orthopyroxene, iron sulfide metal, chromite, phosphate, and iron nickel metal (Keil 2014, Day et al. 2012). Brachinite-like achondrites are similar to the brachinites but differ slightly in various geochemical properties (Day et al. 2012). In contrast to brachinites, the ureilite meteorite group is the largest of the partially melted achondrites. They are composed mainly of olivine and low- and high-Ca pyroxenes with minor sulfide, metal and elemental carbon (Goodrich 1992, Goodrich et al. 2004, Berkley et al. 1980, Mittlefehldt et al. 1998).

In the following study, the geochemical and petrographic characteristics of a set of achondrite meteorites are investigated and compared with results of the nebular chemical characteristics of chondrite meteorites in an effort to illuminate details in the petrological evolution from the primitive chondrites to differentiated achondrites. The overarching goal of this thesis is to place a diversity of partially melted achondrites into refined context for understanding the earliest phases of planetary melting and metal-silicate segregation.

2. Samples

A suite of twenty-two different chondrite and achondrite meteorites was collected and studied. Samples were obtained from the Meteorite Working Group (MWG), the Royal Ontario Museum (ROM), the University of California, San Diego (UCSD), and from Professor Lawrence A. Taylor (University of Tennessee, Knoxville). Meteorite samples are classified as either falls or finds – falls are collected immediately following the meteorite's impact on Earth's surface and finds are found after a meteorite spends an indeterminate length of time on Earth. The sample set included eight chondrites and fourteen achondrites and both major subgroups included falls and finds. For some meteorites we obtained more than one sample, so the entire suite included a total of twenty-seven bulk-rock samples for whole-rock chemical analyses, as well as nine polished thick-section samples and one polished chip sample (Acapulco) for petrographic and mineral chemical analyses. In this study, special emphasis is placed on investigation of the achondrites, and the chondrite meteorite samples were obtained for comparison to the achondrites, and for comparison with previously published datasets in order to verify external precision and accuracy. Non-analytical sample characteristics are listed in Table 2.1.

Table 2.1: The sample set used in this study.

Meteorite[1]	Sample ID	Fall/find[2]	Mass of original meteorite[2]	Meteorite type (original classification)[3]	New classification (per literature and this study)[4]	Type of sample(s)[5]	Mass of bulk rock sample (g)[6]	Sample source[7]
Allende	UCSD 142	fall	2 t	CV3	-	BR	2.370	UCSD
Murchison	chunk	fall	100 kg	CM2	-	BR	1.340	UCSD
Murchison	MTF 2005, v. large chunk	fall	100 kg	CM2	-	BR	36.053	UCSD
Chelyabinsk	JD + LAT (w/FC)	fall	100 kg	O - LL5	-	BR	2.730	UT
Chelyabinsk	JD + LAT (w/o FC)	fall	100 kg	O - LL5	-	BR	2.730	UT
Kunashak	LAT	fall	200 kg	O - L6	-	BR	1.620	UT
Kunashak	slice	fall	200 kg	O - L6	-	BR	21.520	UCSD
Larkman	3 fragments	find	15.75 g	-	O	BR	15.750	UCSD
NWA 869	chunk	find	2 t	O - L3-6	-	BR	23.360	ROM
Peace River	chunk	fall	45.76 kg	O - L6	-	BR	0.516	UCSD
Richardton	chunk	fall	90 kg	O - H5	-	BR	0.214	UCSD
Acapulco	-	fall	1.914 kg	Acapulcoite	-	PC and BR	2.066	UCSD
ALHA 81187	,7 and ,41	find	40 g	Acapulcoite	-	TS (,7) and BR (,41)	1.161	MWG
MET 01195	,30 and ,33	find	98.7 g	Acapulcoite	-	TS (,33) and BR (,30)	2.009	MWG
NWA 2871	larger mass	find	3.47 kg	Acapulcoite	-	BR	1.085	ROM
NWA 2871	smaller mass	find	3.47 kg	Acapulcoite	-	BR	0.189	ROM
EET 84302	,28 and ,47	find	59.6 g	Acapulcoite-lodranite	-	TS (,28) and BR (,47)	1.521	MWG
GRA 95209	,218 and ,258	find	0.949 kg	Lodranite	-	TS (,218) and BR (,258)	3.260	MWG
NWA 4833	-	find	0.608 kg	Lodranite	-	BR	1.857	ROM
NWA 4875	-	find	0.904 kg	Lodranite	-	BR	1.547	ROM
Norton County	5081	fall	1.1 t	Aubrite	-	BR	2.321	UCSD
Norton County	MTF536, N-184	fall	1.1 t	Aubrite	-	BR	0.844	UCSD
ALH 84025	,6 and ,31	find	4.6 g	Brachinite	-	TS (,6) and BR (,31)	0.161	MWG
LEW 88763	,14 and ,20	find	4.1 g	Brachinite	Brachinite-like/anomalous	TS (,14) and BR (,20)	0.202	MWG
MIL 090206	,8 and ,10	find	17 g	Achondrite - ungrouped	Brachinite-like achondrite	TS (,10) and BR (,8)	0.603	MWG
MIL 090405	,5 and ,7	find	58.8 g	Achondrite - ungrouped	Brachinite-like achondrite	TS (,7) and BR (,5)	1.151	MWG
MIL 091004	,4 and ,7	find	32.5 g	Lodranite	Ureilite	TS (,7) and BR (,4)	1.045	MWG

[1]Abbreviations: NWA=Northwest Africa; ALHA=Allan Hills; MET=Meteorite Hills; EET=Elephant Moraine; GRA=Graves Nunataks; ALH=Allan Hills; LEW=Lewis Cliff; MIL=Miller Range

[2]Information from Meteoritical Database except for Larkman sample (data from this study), abbreviations: t=tons; kg=kilograms; g=grams

[3]Information from Meteoritical Database except for Larkman sample (data from this study), single digit numbers indicate petrologic type, abbreviations: C=carbonaceous chondrite; V=Vigarano type; M=Mighei type; O=ordinary chondrite; LL=low-iron, low-metal; L=low-iron; H=high-iron

[4]Abbreviation: O=ordinary chondrite

[5]Abbreviations: BR=bulk-rock; PC=polished chip; TS=polished thick section

[6]Data from this study

[7]Abbreviations: UCSD=University of California, San Diego; UT = University of Tennessee; ROM=Royal Ontario Museum; MWG=Meteorite Working Group

3. Analytical Methods

3.1 Petrography

Petrographic analysis of the nine polished thick-sections and single polished chip (Table 2.1) was conducted using a Nikon POL transmitted/reflected light microscope. All samples were studied under plane-polarized light (PPL), cross-polarized light (XPL), and reflected light (RL) except for the polished chip, which was only studied under RL due to its thickness. After petrographic characteristics of each sample were noted, detailed composite sample maps were made by stitching together between fifteen and one-hundred (depending on sample size) 5× or 10× magnification photomicrographs, which were taken with a digital camera coupled to the microscope. Plane-polarized light, XPL, and RL maps were created for each sample (except for the polished chip where only a RL map was created).

Modal abundances for Miller Range (MIL) 091004, 7 were calculated using its PPL and RL maps in conjunction with Image J processing software (using methods similar to those in Day et al. 2006). The MIL 091004 maps (Figure 4.1.12a) were cropped to isolate the sample and eliminate "slide space" before processing. The cropped maps contained >5,000,000 pixels and were converted to grey-scale before being processed with Image J. Modes were obtained using a color contrast thresh-holding method where thresholds were selected based on knowledge of the mineral phases in the sample. Threshold selections were confirmed by cross-calibration with petrography and major mineral chemistry (see Results). Miller Range 091004, 7 contains two distinct lithological regions (main granoblastic region and carbon-rich region; see Results for detailed descriptions) and each were treated separately for modal analysis. Three

threshold bins were selected for the main granoblastic region: silicates (olivine, pigeonite, and augite), metals/sulfides (FeNi, FeS, and schreibersite) and alteration/fusion crust. Four threshold bins were selected for the carbon-rich region: metals/sulfides (as above), carbon, olivine and reduced olivine. A combined modal analysis of the entire section was calculated by including carbon along with the three threshold bins used for the main granoblastic region.

The same methods for calculating modal abundances were attempted for other samples (e.g., LEW 88763), but because of the graphic limitations of the method, modes for only certain mineral phases could be reliably calculated (most often FeNi and FeS metals). In some samples it was not possible to calculate modal percentages for any of the observable mineral phases because each of the mineral phases exhibited similar grey-scale values (or ranges of values). In these cases, mineral phases could not be distinguished from each other and the same procedures were attempted with color images to no avail.

3.2 Electron microprobe analysis

For each of the samples where a polished thick-section or polished chip was obtained, major- and minor-element mineral compositions were analyzed with a Cameca SX-100 electron microprobe (EMP) at the University of Tennessee. Mineralogies varied from sample to sample, but when present, each of the following mineral phases was analyzed using wavelength dispersive spectral mode – feldspar, iron-nickel (FeNi) metal, iron sulfides (FeS, or troilite), schreibersite, olivine, pyroxene (high- and low-Ca varieties), and spinel. Analyses were made in different regions within each sample and

multiple analyses were made in some mineral grains in order to determine if any mineral zoning was present. All analyses were made with an accelerating potential of 15 keV and a beam size of 1 μm. Beam currents were 30 nA for olivines, pyroxenes, and spinels, 20 nA for FeNi metals, Fe sulfides, and schreibersites, and 10 nA for feldspars. Both natural and synthetic standards were used to calibrate the EMP and standards were measured throughout analytical sessions to ensure data quality. Background and peak counting times used were 20-30 s and standard ZAF (PAP) correction procedures were used. Detection limits for silicates and spinels were <0.03 wt. % for SiO_2, TiO_2, Al_2O_3, MgO, CaO, and Na_2O, <0.04 wt. % for K_2O, V_2O_3, and Cr_2O_3, <0.05 wt. % for Cr_2O_3, MnO, FeO, and P_2O_5, <0.06 wt. % for NiO, and <0.1 wt. % for BaO. For FeNi, FeS, and schreibersite analyses, detection limits were <0.03 wt. % for Si, P, Mg, Al, and Ti, <0.04 wt. % for S, Fe, Cr, Mn, and Mg, and <0.05 wt. % for Co and Ni. Throughout the EMP analytical sessions, back-scattered electron images were also taken of important regions of each sample section.

3.3 Whole-rock sample preparation

Twenty-seven bulk-rock samples were acquired for analysis of whole-rock chemistry (trace- and major-element compositions, and oxygen isotopes). Upon acquisition of bulk-rock samples, the allocated stones were weighed with a high precision scale (see Table 2.1 for weights of samples) prior to powdering aliquots of the samples. Precise weights were needed in order to ensure there would be adequate amounts of material for future research. For each sample, less than or approximately half of the original allocation was powdered, even if a single bulk-rock sample was very small (e.g.,

ALH 84025 and LEW 88763; Table 2.1). If a sample contained fusion crust, effort was made to avoid powdering fusion crust, as the chemical composition of fusion crust is likely not representative of the bulk rock (Clayton et al. 1986). Powders were made in an agate mortar and pestle that was cleaned between each sample by fine-powdering copious amounts of quartz sand and rinsing with ultra-pure water. Sample loss was kept to a minimum for each sample (typically <10 mg). The amounts of powder created for each bulk-rock sample are included in Table 3.1.

Table 3.1: Bulk-rock powder masses and oxygen isotope analysis masses. Only portions of the powders were used in this study, but all material set aside for oxygen isotope analysis was used.

Meteorite	Weight of powder (mg)	Weight of material for oxygen isotopes (mg)
Allende, UCSD 142	411	30
Murchison, chunk	34	48
Murchison, MTF 2005, v. large chunk	230	69
Chelyabinsk, JD + LAT (w/FC)	151	36
Chelyabinsk, JD + LAT (w/o FC)	103	15
Kunashak, LAT	192	19
Kunashak, slice	274	27
Larkman, 3 fragments	701	40
NWA 869, chunk	120	16
Peace River, chunk	142	54
Richardton, chunk	77	15
Acapulco	201	21
ALHA 81187, 41	215	49
MET 01195, 30	256	61
NWA 2871, larger mass	228	54
NWA 2871, smaller mass	68	40
EET 84302, 47	223	78
GRA 95209, 258	253	25
NWA 4833	274	59
NWA 4875	284	61
Norton County, 5081	245	23
Norton County, MTF536, N-184	185	16
ALH 84025, 31	54	36
LEW 88763, 20	75	30
MIL 090206, 8	183	57
MIL 090405, 5	251	59
MIL 091004, 4	182	68

3.4 Parr bomb digestions, trace-element analysis, and major-element analysis

For each bulk-rock sample, small amounts (typically ~40 mg; exact masses in Table 3.2) of the powder masses were digested in Teflon Parr bomb vessels for trace- and major-element analysis at the Scripps Isotope Geochemistry Laboratory (SIGL). The powders were digested at 170°C in Optima grade concentrated HF (4 mL) and HNO_3 (1 mL) for >72 hrs in a standard processing oven. After digestion in the HF/HNO_3 mixture, the solutions were dried down and sequentially taken up in Optima grade HNO_3 two times in order to remove fluorides. After the final dry-down, stock solutions were prepared with Optima grade HNO_3 and were doped with an In (1 ppm) internal standard to monitor instrument drift and sensitivity. Final stock solutions contained sample powder, 1 mL Optima HNO_3, 1 mL 1ppm In solution, and 8 mL ultra-pure water (Σ = 10 mL). A maximum of 12 Parr bomb digestion vessels were available for processing, so stock solutions were created in four cycles (Table 3.2). One total procedural blank and multiple standards were included in each cycle. For trace-element abundance analyses, 250 µL of stock solution was further diluted in 5 mL of 2% HNO_3 for each sample. For major-elements, 100 µL of the trace-element solution was further diluted in 9.9 mL of 2% HNO_3. One trace- and one major-element solution was created for most samples, but two of each type were made for the recently collected Antarctic finds (samples with the MIL prefix).

With these solutions, major- and trace-element abundance analyses were performed using a ThermoScientific iCAP Qc quadrupole inductively coupled plasma mass spectrometer in normal, low resolution mode. Analyses were standardized versus reference material BHVO-2 that was measured throughout the analytical run. In addition,

three reference materials were analyzed as "unknowns" (BIR-1, BHVO-2, and BCR-2) in order to monitor instrumental drift and to assess external reproducibility and accuracy. For trace-elements, reproducibility of the reference materials was generally better than 5-8% (RSD), with the exception of V (9%), Cr (9%), and Ge (10%). Likewise for major-elements, reproducibility of the reference materials was generally better than 6-8% (RSD), with the exception of P (11%) and Ni (22%).

3.5 Oxygen isotope analysis

Un-powdered portions (exact weights in Table 3.1) of the bulk-rock samples were processed and analyzed for oxygen isotopes at the Institut de Physique du Globe-Paris. Complete analytical methods are similar to those documented in Rumble and Hoering (1994). Prior to analysis, silicate grains were separated from each other under alcohol in a tungsten-carbide mortar and pestle, ultrasonicated in dilute HCl at room temperature for 240 s to remove weathering products, and separated into magnetic and non-magnetic fractions.

Before analyzing any meteorite sample, small masses of the well-known San Carlos olivine were analyzed to ensure external precision and accuracy. The non-magnetic fractions of the meteorite samples were then analyzed via laser fluorination. The garnet standard UWG-2 from the Gore Mountain mine, Adirondack Mountains, New York (Valley et al. 1995) was analyzed after every two to four meteorites analyzed. Towards the end of oxygen isotope analysis, a glass connection in the apparatus that transferred sample material to the mass spectrometer was broken. A fix was improvised with an ultra-torr vacuum fitting and 10 runs (on 6 different meteorite samples; ALH

Table 3.2: Stock solution list for whole-rock chemical analysis. Stock solutions were prepared in four different cycles (column 1).

Cycle	Analysis ID #[1]	Sample[2]	Loaded mass (mg)
First	1	TPB	-
	2	BHVO-2	39.10
	3	BHVO-2	41.88
	4	BCR-2	40.35
	5	BIR-1	41.04
	6	Chelyabinsk w/FC	38.63
	7	Allende, UCSD 142	53.41
	8	Kunashak, Lg. slice	40.30
	9	Kunashak, LAT	41.47
	10	Murchison, MTF 2005	41.19
	11	Chelyabinsk w/o FC	39.47
	12	MIL 091004, 4	40.82
Second	13	TPB	-
	14	BHVO-2	40.85
	15	BHVO-2	43.70
	16	BCR-2	41.91
	17	MIL 090206, 8	38.90
	18	MIL 090405, 5	38.32
	19	Acapulco	39.46
	20	GRA 95209, 258	38.69
	21	MET 01195, 30	38.29
	22	ALHA 81187, 41	39.75
	23	NWA 2871, larger	39.59
Third	24	TPB	-
	25	BHVO-2	39.85
	26	BCR-2	27.81
	27	LEW 88763, 20	15.77
	28	ALH 84025, 31	14.36
	29	EET 84302, 47	38.64
	30	NWA 869, chunk	15.73
	31	NWA 4833	39.66
	32	NWA 4875	39.22
	33	NWA 2871, smaller	14.81
	34	Larkman	43.82
Fourth	35	TPB	-
	36	BHVO-2	41.06
	37	BIR-1	40.82
	38	Richardton, chunk	18.75
	39	Peace River, chunk	44.11
	40	Murchison, chunk	13.38
	41	Norton County, 5081	41.21
	42	Norton County, MTF536, N-184	41.95
	43	MIL 091004, 4	21.03
	44	MIL 090206, 8	20.75
	45	MIL 090405, 5	40.47

[1]Analysis identification # used in order to keep track of samples throughout stock solution preparation as well as trace- and major-element analyses

[2]Abbreviations: TPB=total procedural blank; BHVO=basalt, Hawaiian Volcanic Observatory; BCR=basalt, Columbia River; BIR=basalt, Icelandic Reykjavic; all other abbreviations as in Table 2.1

84025, Allende, Chelyabinsk w/o fusion crust, Murchison MTF 2005, Norton County MTF 536, and NWA 2871 smaller mass) were completed with the setup. Because it was unknown whether or not these analyses are reproducible, they have been discarded from the final data set. The Murchison sample with identification suffix "MTF 2005" does not have any publishable oxygen isotope data as a result of the improvised fix. All other samples were analyzed at least once.

Oxygen isotope data is reported in delta notation ($\delta^{18}O$, $\delta^{17}O$), which is the per mil (‰) deviation of $^{X}O/^{16}O$ (where X = 18 or 17) from the international standard (std) V-SMOW given by the following equation: $\delta^{X}O_{unk} = 1000 \times ((^{X}O/^{16}O)/(^{X}O/^{16}O_{std})-1)$, where *unk* is the unknown. From the delta notation values, $\Delta^{17}O$ (representing deviation from the terrestrial fractionation line and given by the following equation: $\Delta^{17}O = \delta^{17}O - 0.526 \times \delta^{18}O$) is then calculated.

3.6 Raman spectroscopy of MIL 091004

The MIL 091004, 7 polished thick-section was sent to the Carnegie Institution in Washington, D.C. to confirm the presence of graphite grains in the sample's carbon-rich region. Confirmation of graphite was carried out by confocal Raman spectroscopy (methods similar to those in Steele et al. 2012). A Witec α-scanning Near-Field Optical Microscope was used to collect Raman spectra. The excitation source that drives the analysis is a frequency-doubled solid-state YAG laser (532 nm) operating between 0.3 and 1 mW of output power. Two objective lenses were used (×100 and ×20) and spectra were collected on an Andor EMCCD chip after passing through a 300 mm f/4 imaging spectrometer (600 lines/mm grating).

Two operating modes were typically used in this study. The first mode, imaging mode, allows acquisition of images of the sample region in question. The second, single spectra mode, allows the collection of a spectrum from a single small spot on the sample. Weak spectral features are verified by collecting spectra with 10 accumulations at 30 seconds per accumulation. The field of interest observed through imaging mode guides the instrument's collection of spectra – a Raman spectrum is taken at each pixel using an integration time of between 1 and 6 s/pixel. To arrive at an average spectrum a number of corrections were used to mitigate the effects of stray radiation, isolated bright pixels, fluorescence, and interfering peaks. As an example, a typical scan with the ×100 lens of a 30 mm^2 area produced 10,000 separate and spatially aligned Raman spectra, from which average spectra were calculated.

4. Results

4.1 Petrography

Acapulcoites and lodranites – The primitive acapulcoites and lodranites studied – Acapulco, MET 01195, ALHA 81187, EET 84302, GRA 95209 – can be broadly described as granoblastic with moderate to high amounts of FeNi and FeS metal (usually FeS metal appears in lesser amounts). Silicate grain sizes are typically ≤ 1 mm in EET 84302 and MET 01195, ≤ 0.7 mm in GRA 95209, and ≤ 0.5 mm in Acapulco and ALHA 81187. The five samples display a range of textural equilibration, with EET 84302 as the most equilibrated meteorite, ALHA 81187 and Acapulco as the least equilibrated, and GRA 95209 and MET 01195 as moderately equilibrated. The meteorites contain low-Ca pyroxene, high-Ca pyroxene, plagioclase, olivine, FeNi metal, FeS metal, and chromite as major mineral phases, except for EET 84302, which lacks chromite. Acapulco, MET 01195, and ALHA 81187 also contain schreibersite as a minor mineral phase.

The new petrographic results agree well with previously published petrography for acapulcoite-lodranites (e.g., Palme et al. 1981, Zipfel et al. 1995, McCoy et al. 1996, McCoy et al. 1997a, McCoy et al. 2006, Mittlefehldt et al. 1996). In the following paragraphs, members of the acapulcoite-lodranite group are described in approximately increasing order of partial melting. The acapulcoites (Acapulco, ALHA 81187, and MET 01195) have experienced melting in the Fe-Ni-S system (Mittlefehldt et al. 1996) and are described first. The next description is for EET 84302, a meteorite considered to be transitional between acapulcoites and lodranites (McCoy et al. 1997a). The one lodranite for which a polished section was obtained – GRA 95209 – is described last and has experienced Fe-Ni-S melting as well as silicate partial melting (McCoy et al. 1997a).

Because a polished chip of the well-studied meteorite Acapulco (the archetype of the acapulcoite meteorite group) was generated from a whole-rock sample in the SIGL, only reflected light petrographic analysis was possible, but the petrographic results herein (Figures 4.1.1, Figure 4.1.5a, and 4.1.5b) agree with major mineral petrography included in previous publications (Palme et al. 1981; Zipfel et al. 1995). Studies of Acapulco minor and trace minerals have also been conducted (e.g., phosphate in Zipfel et al. 1995, carbon in El Goresy et al. 2005).

The Acapulco meteorite displays a range of grain sizes (≤ 0.5 mm) and shapes (most often subhedral to euhedral) with silicate grains often creating 120° triple junctions (Figure 4.1.1). Many of the silicates in the meteorite poikilitically enclose smaller grains of the major mineral phases. This is especially evident in feldspars that enclose smaller (~20-40 μm) rounded grains of other silicate minerals (Figures 4.1.1, 4.1.5a, and 4.1.5b). Although it is difficult to identify because pyroxenes and olivines have similar appearances in reflected light, the same poikilitic behavior is also seen in these minerals. Iron-nickel and FeS metals display unusual morphologies in Acapulco (Figure 4.1.1). In addition to the coarse (≤ 0.5 mm) irregularly shaped FeNi and FeS grains visible in the sample, the metals also appear within silicates as swarms of tiny (≤ 15 μm) blebs. Although, under the microscope, the size of any single swarm is only visible in two dimensions, there is remarkable similarity in the sizes of these swarms. Many of the swarms measure to be ~150 × 75 μm, although some are smaller or larger, but never longer than 300 μm on any side. The swarms also seem to have remarkably well defined boundaries within their silicate hosts. The sample of Acapulco contains a small length

(~1 mm) of fusion crust. Terrestrial weathering was difficult to identify in reflected light, but is likely minimal since Acapulco is a fall.

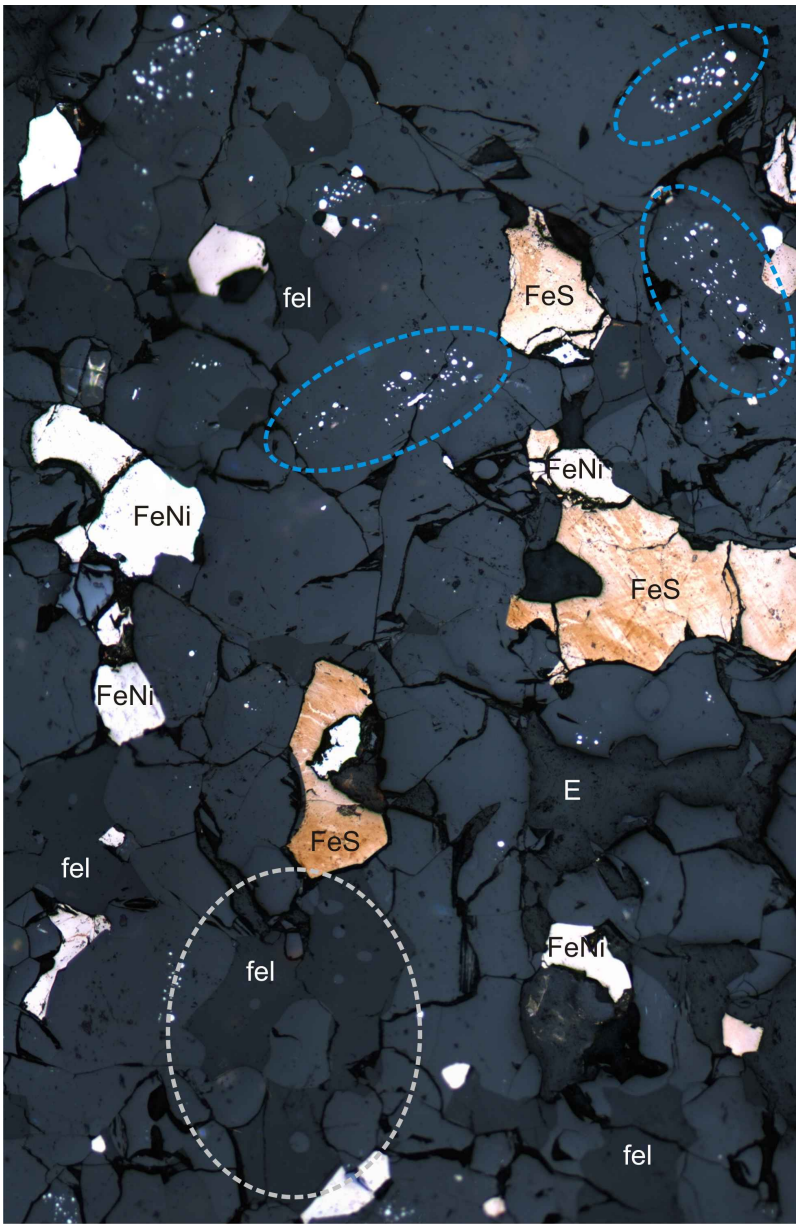

Figure 4.1.1: Portion of the reflected light photomicrograph map for the Acapulco meteorite. Field of view is 1.93 mm high × 1.27 mm wide. Blue dashed ovals surround well-defined swarms of tiny FeNi blebs and the gray dashed oval highlights feldspars poikilitically enclosing olivines and/or pyroxenes. Abbreviations: FeNi – iron-nickel metal, FeS = iron-sulfide metal, fel = feldspar, E = epoxy (no sample).

The fusion crust free polished section of acapulcoite ALHA 81187 obtained for this study (ALHA 81187, 7) contains a finer grained granoblastic texture than that in Acapulco (Figures 4.1.4c, 4.1.4d, 4.1.5f and g). This relatively unequilibrated sample contains often-rounded subhedral silicate grains up to 0.5 mm in diameter (with most only up to 0.25 mm in diameter) and an abundance of anhedral metallic grains (FeNi and lesser amounts of FeS) up to 0.5 mm in the long dimension. Very mild undulatory extinction is visible in a few silicate grains. Large grains of FeS are often adjacent to large FeNi grains, but large FeNi grains do not always have adjoining FeS grains. Notable features found in ALHA 81187 are remnants of small (~0.25 mm radius) layered globular structures (Figure 4.1.5g) of FeNi metal and an unidentified mineral (these are iridescent in reflected light, possibly phosphates). These features were not studied in detail, but could prove important in future studies. Chromite displays smaller grain sizes than the other major mineral phases, with the largest grain measuring about 0.3 mm in the long dimension. Throughout the sample, grain sizes for FeNi, FeS, and chromite are highly variable, with the smallest grains occurring on the μm scale. In plane-polarized and cross-polarized light ALHA 81187, 7 looks dark because of the ubiquity of a black material that exists interstitially, and even seems to “overwhelm” silicate grains (Figures 4.1.4c and 4.1.4d). When “overwhelmed” by the dark material, silicate grains become less bright and grain boundaries are weakly defined. This darkening is caused by a combination of processes. One of the contributors is weathering of metallic material. Larger anhedral metallic grains in the meteorite have embayments around their entire edge and rarely have straight boundaries. Although most of the anhedral morphology is likely a primary feature of the meteorite, at least some of it can likely be attributed to

terrestrial weathering, since the meteorite displays small amounts of rusty colored weathering products in plane-polarized light. Backscattered electron images of ALHA 81187 reveal reduction as another contributor to the darkened appearance (Figure 4.1.5f). Silicates proximal to metallic phases often appear darker in BSE images, and silicates also often contain fractures that are darkened compared to the rest of the grain. Reduction in ALHA 81187 has been previously reported by Yugami et al. (1995).

The moderately equilibrated acapulcoite MET 01195 contains the same major minerals as Acapulco and ALHA 81187 and also displays much of the same granoblastic texture (Figures 4.1.4b, 4.1.5h-j). Silicate grain sizes in the fusion crust free MET 01195, 33 approach 0.8 mm in a few cases, but for the most part remain between 0.1 and 0.4 mm, with abundant 120° triple junctions. As with ALHA 81187, undulatory extinction is rare, showing up mildly in only a few silicate grains. Terrestrial weathering is present throughout the sample as rust colored alteration along grain boundaries and fractures in silicates. Iron-nickel, FeS, and chromite grains in MET 01195 have many of the same petrographic characteristics as Acapulco and ALHA 81187, with a few major morphological differences. Iron-nickel displays a larger maximum grain size, with the largest measuring ~1.5 × 0.5 mm. This large metal grain adjoins a large chromite grain that measures ~1.2 × 0.5 mm. The majority of FeNi grains are anhedral to subhedral with longest dimensions spanning 0.1-0.5 mm. Besides the one large grain associated with FeNi, chromite generally remains ≤ ~0.1 mm in the long dimension. Iron-sulfide metals normally exist as grains 50-250 μm in size, but also are present as tiny μm-scale blebs within silicates or in interstitial spaces. In many instances FeS grains adjoin FeNi grains. In reflected light, a few narrow (≤ 50 μm wide, discontinuous vein “systems” can extend

up to 3 mm in length) veins of grey weathered material (likely iron oxide) are observed. In some FeNi grains, short "splashes" of dark material seem to infiltrate their metallic host, and this material may be carbon (Figure 4.1.5i). It was possible to calculate modes accurately for three mineral phases in MET 01195, 33 – 7.4 modal % for FeNi, 3.7 modal % for FeS, and 2.0 modal % for chromite.

The "transitional" acapulcoite-lodranite EET 84302 is the most equilibrated of the acapulcoite-lodranites in this study and displays the coarsest granoblastic texture (Figures 4.1.2, 4.1.4e and f, 4.1.5c-e). The polished section obtained (,28) was previously studied by Yugami et al. (1998) and Takeda et al. (1994), and is fusion crust free (Figure 4.1.2). As in previous members of the group, silicate grain sizes are variable (≤ 1 mm, with most in the range of ~0.2-0.5 mm) and abundant 120° triple junctions are visible. Silicates are euhedral to subhedral, often have one or more fractures and rarely display undulatory extinction. The polished section displays terrestrial weathering throughout as rusty colored alteration along grain boundaries and intergranular fractures, but EET 84302, 28 is also noticeably less weathered than ALHA 81187, 7 and MET 01195, 33. Takeda et al. (1994) reported dusty cores in EET 84302 orthopyroxene grains, and we confirm this observation along with the new observation that the cores' dusty appearance is associated with well-defined (often ~0.1-0.3 mm in the long dimension) swarms of tiny (μm-scale) metallic blebs, much like the ones in Acapulco. Because of this association, the cloudy appearance that Takeda et al. (1994) refers to seems to be caused by shallow subsurface metallic blebs, or possibly by tiny holes from which metallic blebs may have been plucked during creation of the section. The metallic blebs are usually FeNi, but also

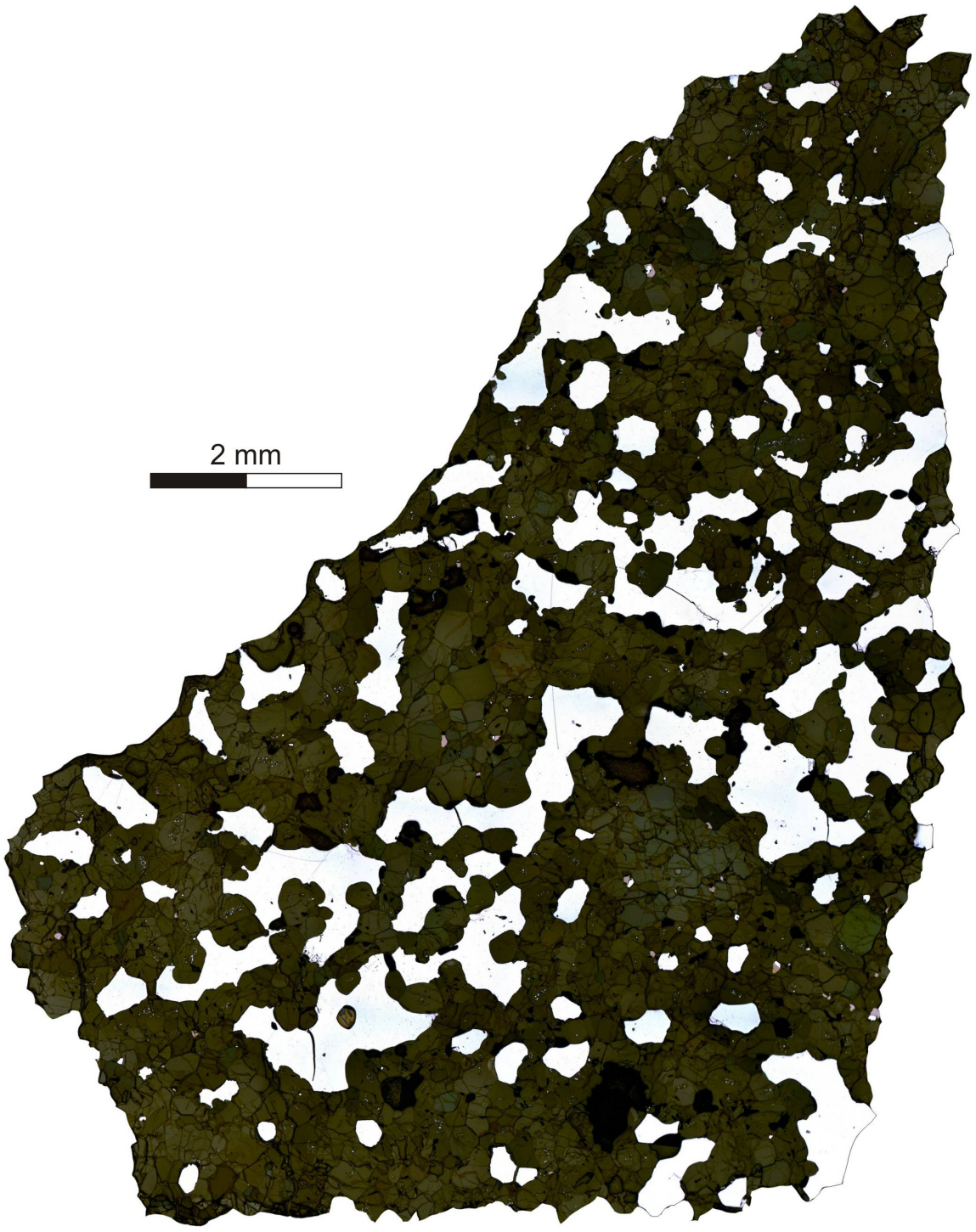

Figure 4.1.2: Reflected light photomicrograph map of the transitional acapulcoite-lodranite EET 84302, 28. This meteorite serves as a particularly useful demonstration of the migration of metal in primitive meteorites – the FeNi metal in this sample (large reflective minerals that appear white in this map) appears to have "pooled" into large anhedral grains.

occasionally appear as FeS. In contrast to the blebs' tiny size, the remainder of the meteorite's FeNi appears as large (elongate grains up to ~2 mm in length in some cases) "pooling" grains that often are connected by narrow metallic "arms" and appears as if the grains were migrating towards each other. Iron-sulfide is also present in the sample, but is more rare and has much smaller (≤ 0.1 mm) grain sizes than the FeNi metal.

Graves Nunataks 95209, the single lodranite for which we obtained a polished section (,218; free from fusion crust; Figures 4.1.3, 4.1.4a, 4.1.5k and l) is a moderately coarse granoblastic metal-rich stone that displays many of the same petrologic characteristics as the acapulcoites (and acapulcoite-lodranite EET 84302) described above. McCoy et al. (2006) studied the meteorite in detail and described three different lithologies present – "prominent metal veins, the metal-poor regions, and the matrix that serves as the host for the other two lithologies and is the dominant lithology." Polished section ,218 is consistent with the matrix lithology they described, although a discrepancy is noted in observed maximum silicate grain size. McCoy et al. (2006) report a maximum silicate size of 2 mm while in this study the maximum silicate grain size observed is 0.8 mm in the long dimension (in a single grain). Most silicate grains in section ,218 are ≤0.5 mm. Although this is considered a large discrepancy when analyzing grains on the mm scale, the difference is not troublesome because of the textural heterogeneity that GRA 95209 displays (Mittlefehldt and Lindstrom 1998, McCoy et al. 2006). Silicate grains display mainly subhedral to euhedral shapes, are moderately to highly fractured, and create numerous 120° triple junctions. Mild undulatory extinction is observed in only a few grains and rust colored terrestrial weathering is present along some fractures in silicates and grain boundaries. In reflected light, narrow (≤40 μm wide, often mm-scale in

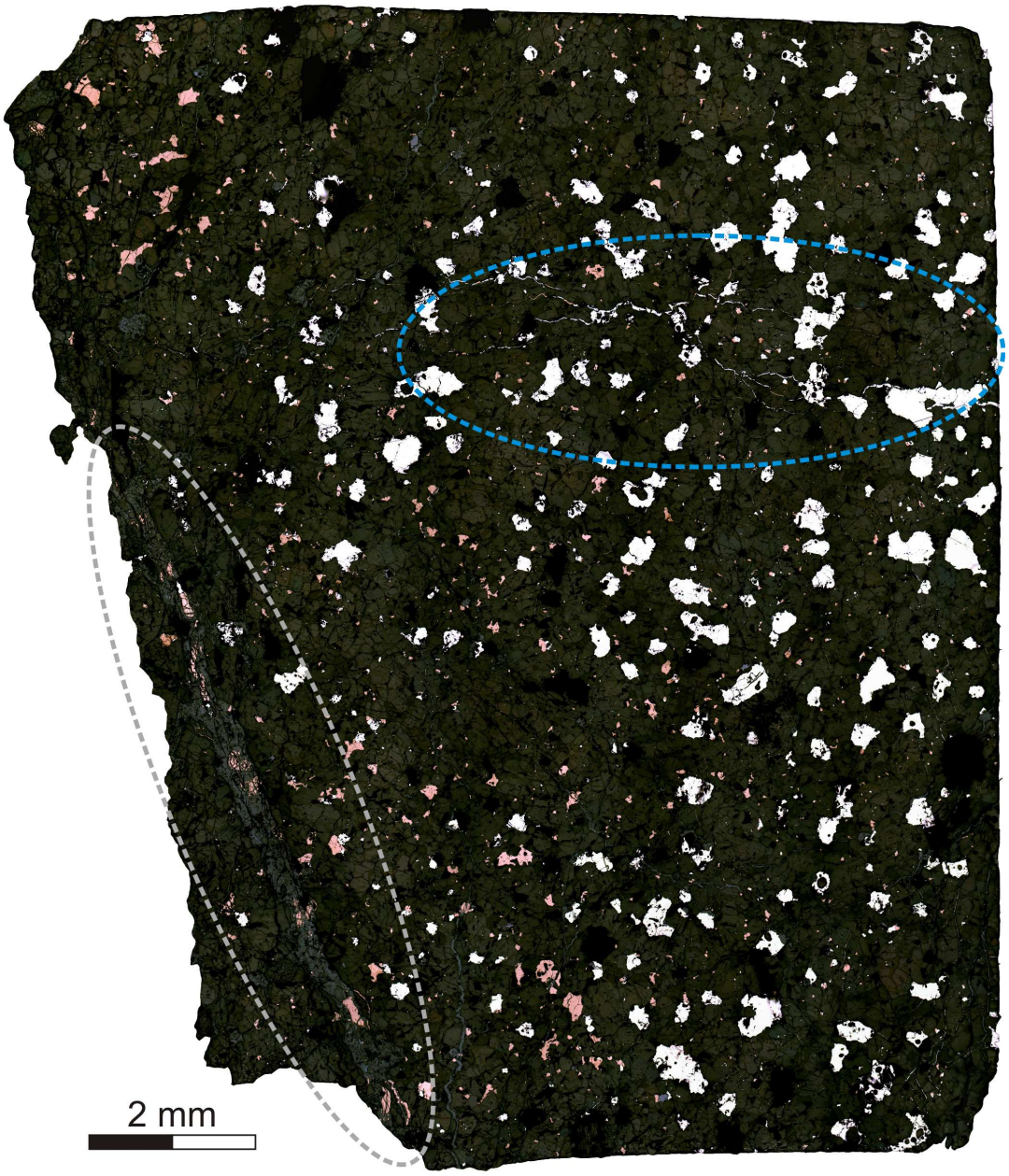

Figure 4.1.3: Reflected light photomicrograph map of lodranite GRA 95209, 218 again demonstrating behavior of metal migration in primitive meteorites. The gray dashed oval highlights the ~10 × 3 mm weathered vein with non-weathered sections of FeS demonstrating mass movement of metallic material on the meteorite's parent body. The weathered portions likely existed as primary metallic material before weathering. The blue dashed oval highlights a region with smaller unweathered veins of FeNi metal. Both type of vein suggest melt migration processes were active on the meteorite's parent body. Moreover, the decrease of still-primary FeNi grains near the large weathered vein (gray dashed oval) suggests that the FeNi in this region was migrating away via the large vein.

length with one vein measuring 6 mm long) grey weathered veins (likely of iron oxide) are visible and similarly sized counterpart veins of FeNi ± FeS are also visible. A single long (~ 10 × 3 mm) vein of the same grey weathered material (likely iron oxide) stands out in one corner of the polished section. The vein contains FeS grains (≤ ~0.5 mm in longest dimension) that at first glance look like inclusions, but these grains are more likely unweathered portions of the vein. The large vein intersects two sides of the section, so it is possible that the vein was much longer than what is seen in section ,218. This could potentially have important implications for metal melt migration in the meteorite's parent body (McCoy et al. 1997b, McCoy et al. 2006). Large FeNi grains are abundant and can be up to 1.3 mm in the long dimension, and smaller, often μm-scale grains and blebs are present in equal numbers. Included within FeNi metals are graphite rosettes also reported in McCoy et al. (2006). Iron-sulfides are also abundant, but are present in lesser numbers and in smaller sizes (≤ ~0.5 mm in longest dimension). An interesting observation is that there is a decrease in the number of FeNi grains in the region of the large weathered vein, suggesting that the vein may have been serving as a conduit for metallic material to migrate out of the lithology (Figure 4.1.3). Iron-sulfide seems to increase in number near this same weathered vein – this observation may serve as evidence against the previous observation.

All five members of acapulcoite lodranite group studied here have very similar petrologic properties, properties that are distinct from meteorites described below that are representative of other meteorite groups.

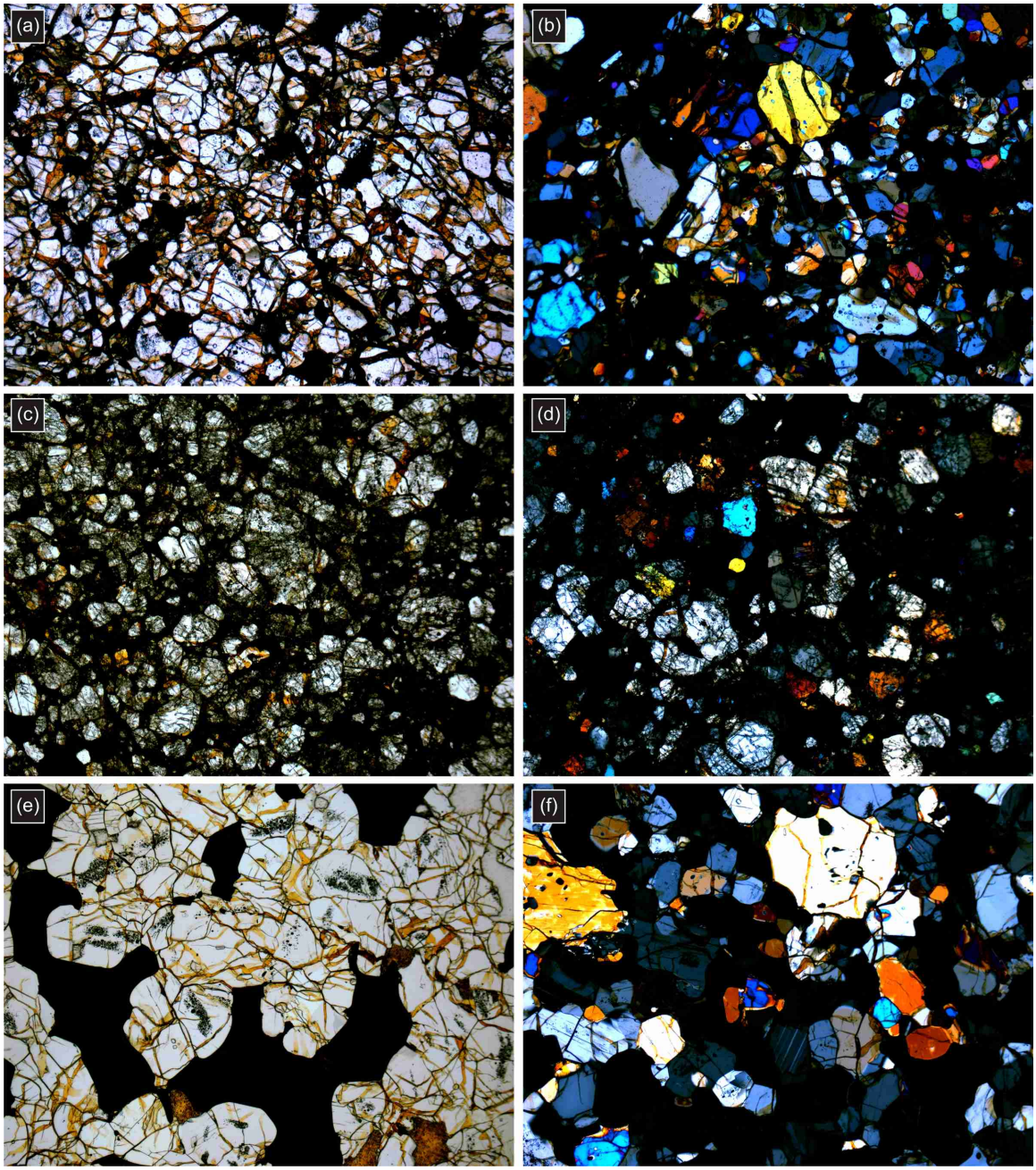

Figure 4.1.4: Plane-polarized (a, c, and e) and cross-polarized (b, d, and f) light photomicrographs of a) GRA 95209, b) MET 01195, c) and d) ALHA 81187, and e) and f) EET 84302. Each photomicrograph was taken at 5× magnification and has a field of view 1.95 mm tall × 2.60 mm wide.

Figure 4.1.5: Back-scattered electron images of portions of (a), (b) Acapulco; (c)-(e) EET 84302, 28; (f) ALHA 81187. In (a) and (b), Acapulco's granoblastic, poikilitic texture is visible with abundant 120° triple junctions. Also visible are well-defined swarms of metallic blebs, as well as coarse metal grains. Panels (c)-(e) show a granoblastic texture with abundant 120° triple junctions in EET 84302, 28, as well as slightly larger grain size in some grains. Similar to Acapulco, EET 84302, 28 also contains swarms of metallic blebs. In (f), the granoblastic texture and more weathered nature of ALHA 81187, 7 is apparent. The mottled appearance of intergranular material as well as the silicates in (f) is due in large part to weathering. Note also (f) is a BSE image taken at lower resolution, causing a grainy appearance; this is not due to petrology. Abbreviations: FeNi = iron-nickel metal, FeS = iron-sulfide metal, fel = feldspar, cr = chromite, opx = orthopyroxene, cpx = clinopyroxene, ol = olivine.

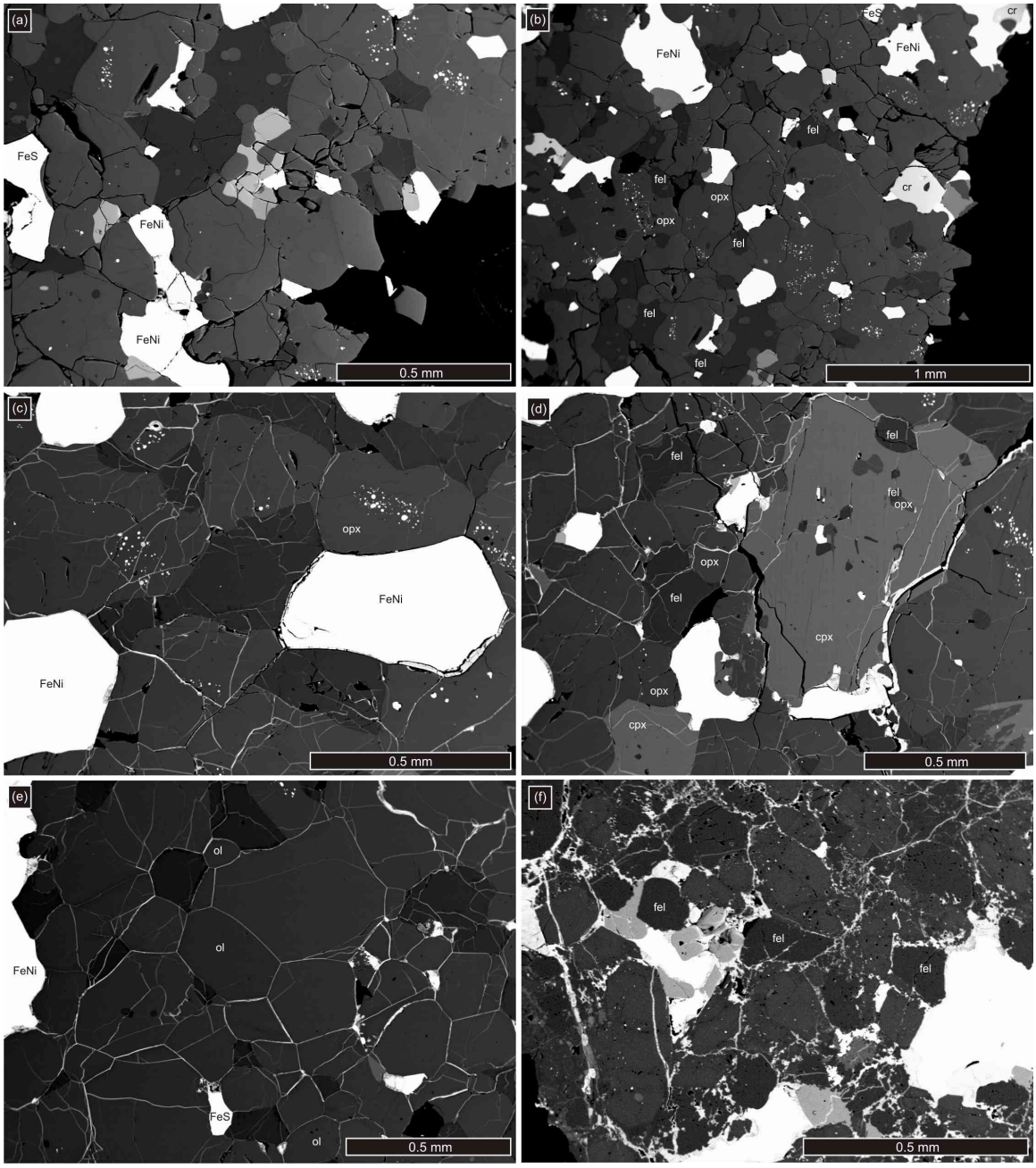
(a)
FeS
FeNi
FeNi
FeNi
0.5 mm
(b)
FeS
cr
FeNi
FeNi
fel
fel
opx
cr
opx
fel
fel
fel
1 mm
(c)
opx
FeNi
FeNi
0.5 mm
(d)
fel
fel
fel
opx
opx
fel
cpx
opx
cpx
0.5 mm
(e)
ol
ol
FeNi
FeS
ol
0.5 mm
(f)
fel
fel
fel
0.5 mm

Figure 4.1.5, continued: Back-scattered electron images of portions of (g) ALHA 81187, 7; (h)-(j) MET 01195, 33; (k), (l) GRA 95209, 218. Frame (g) displays a remnant of one of the layered globular structures in ALHA 81187. The structure is largely composed of FeNi metal, as well as tiny structures that appear iridescent in reflected light and may be phosphates. The granoblastic, sometimes poikilitic, metal-rich texture of MET 01195, 33 is presented in (h) and (j). Frame (h) also displays veins of weathered material that completely surround silicate grains (note that non-weathered metal grains may exist in the same frame, but are difficult to distinguish from weathered material in the BSE image). In (i), a MET 01195, 33 FeNi grain is shown with what is thought to be carbon (small elongate black areas within the large white FeNi grain), which creates a "splashed" pattern in the metal grain. The final two frames, (k) and (l), display textures in GRA 95209, 218. Note again that lower image resolution in (l) gives the figure a grainy appearance not caused by petrology. Abbreviations: FeNi = iron-nickel metal, FeS = iron-sulfide metal, fel = feldspar, opx = orthopyroxene, cpx = clinopyroxene, ol = olivine.

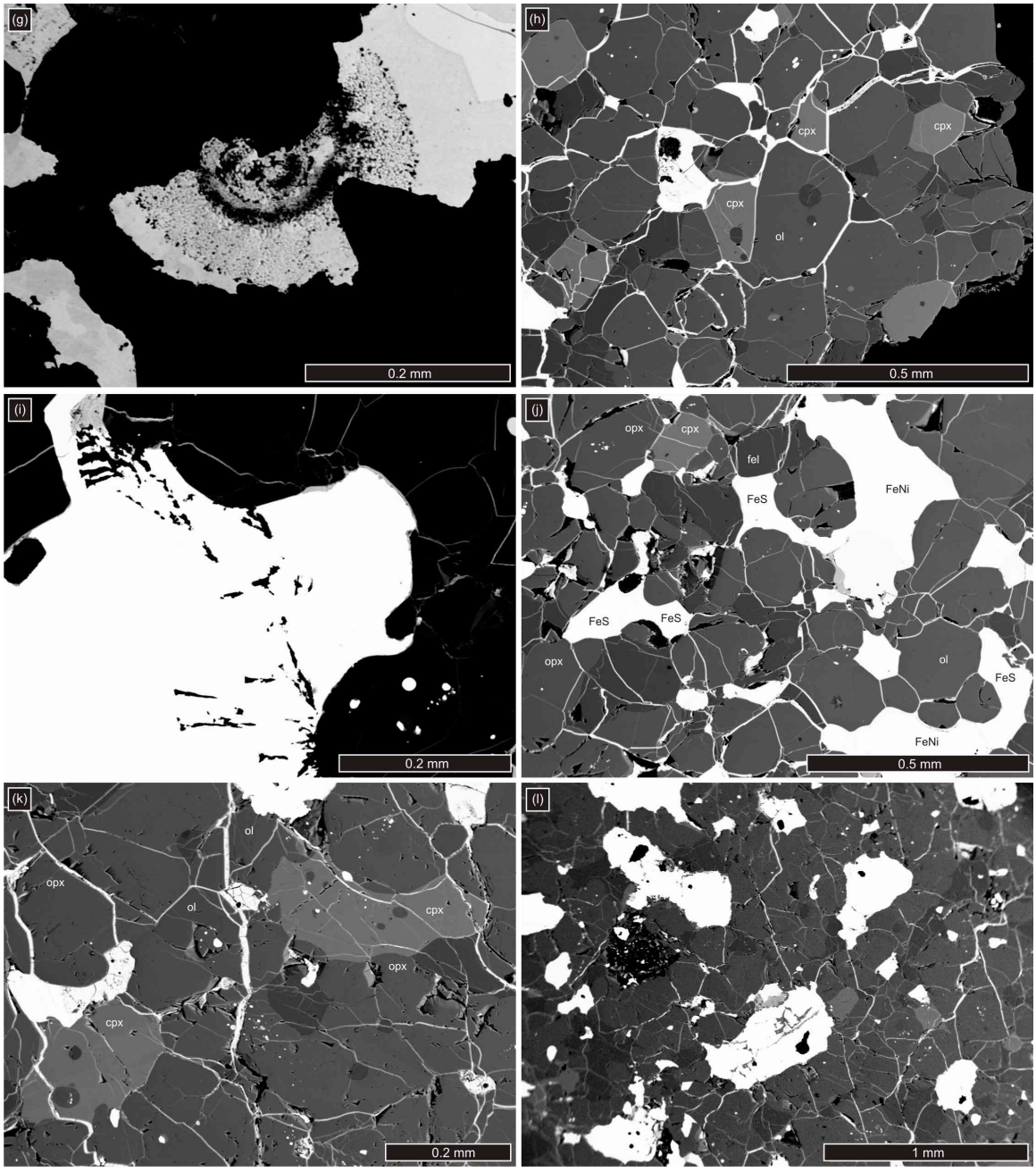
(g)
0.2 mm
(h)
cpx
cpx
cpx
ol
0.5 mm
(i)
0.2 mm
(j)
opx
cpx
fel
FeS
FeNi
FeS
FeS
opx
ol
FeS
FeNi
0.5 mm
(k)
ol
opx
ol
cpx
opx
cpx
0.2 mm
(l)
1 mm

ALH 84025, MIL 090206, and MIL 090405 – The brachinite Allan Hills 84025 is a relatively well-studied meteorite (Warren and Kallemeyn 1989, Mittlefehldt et al. 2003, MacPherson 1985, Prinz et al. 1986). The study by Warren and Kallemeyn (1989) described the meteorite's petrography in detail and compared their results to previous studies of ALH 84025. Warren and Kallemeyn's description of ALH 84025 texture can be summarized as "polygonal-granular" recrystallized, with some portions of certain samples exhibiting only mild recrystallization. These authors also found average silicate grain size to be roughly 0.7 mm across, with clinopyroxene and olivine maximum sizes up to 2.7 and 1.8 mm across, respectively. Troilite, chromite, and Ni-rich FeNi grains were generally anhedral and up to 1.6, 0.7, and 0.4 mm across, respectively. Although large in size, the previous studies reported these opaque phases to be interstitial to the silicates.

The polished section of ALH 84025 obtained for this study (,6), which was also studied by Mittlefehldt et al. (2003), displays petrologic features that are consistent with previous descriptions. The meteorite is composed mainly of olivine but also contains high-Ca pyroxene, troilite, chromite, and Ni-rich FeNi as major mineral phases (Figure 4.1.6). One grain of chlorapatite was identified and is considered a trace phase. The meteorite's texture is coarse with an average grain size between ~0.5-0.8 mm in maximum dimension. Grains generally appear euhedral to subhedral and many 120° triple junctions between silicates are visible. Silicate grains are largest (up to 1 mm in size) and most numerous in the section, and many exhibit minor to moderate fracturing. Identification of high-Ca pyroxenes was aided by the presence of parallel fractures and fractures at roughly 87/93°. Minor undulatory extinction of silicates can be observed in

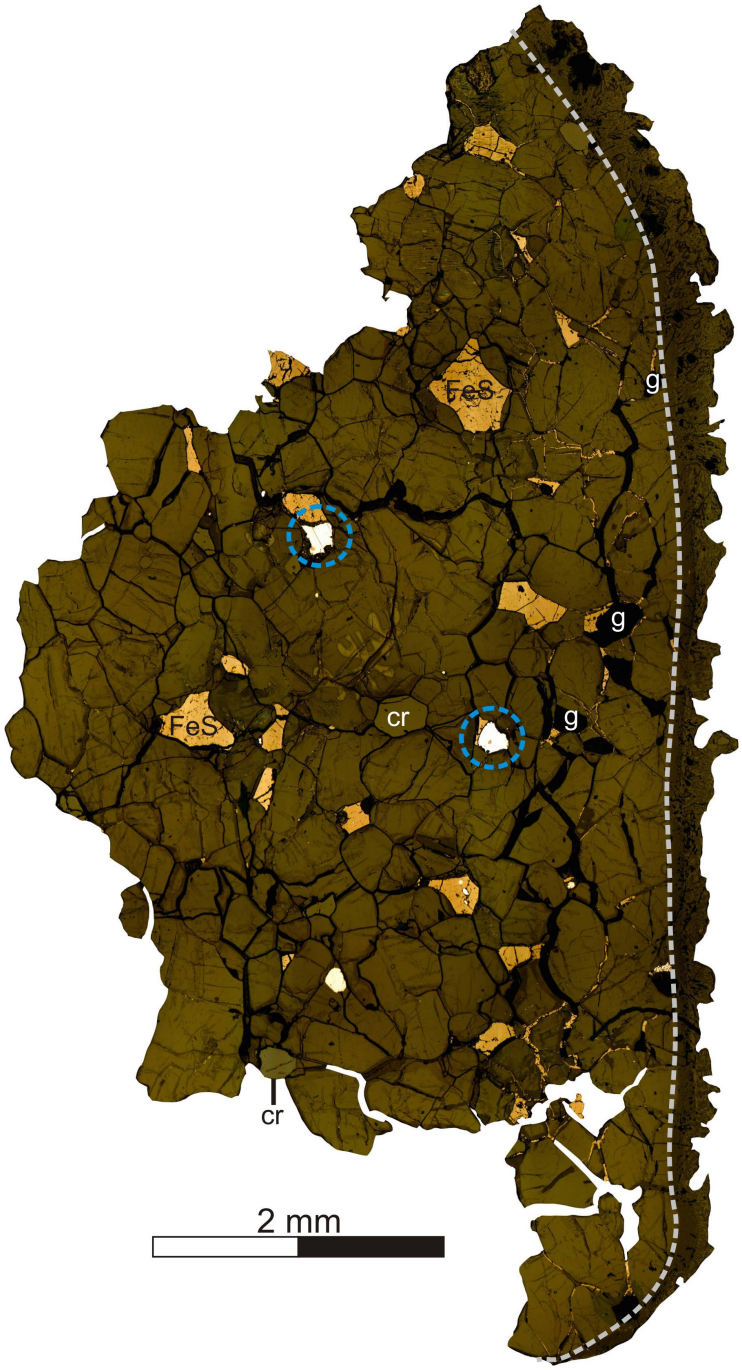

Figure 4.1.6: Reflected light photomicrograph map of ALH 84025, 6. Coarse recrystallized texture, large sulfide grains, and recrystallized fusion crust all visible. Close to the fusion crust, short narrow veins of FeS exist and may be caused by the meteorite's passage through Earth's atmosphere. The dashed blue circles highlight large FeNi grains. The gray dashed line follows the boundary between fusion crust (right) and the meteorite's primary mineralogy. Abbreviations: FeS = iron-sulfide metal, cr = chromite, g = epoxy/gaps in sample.

cross-polarized light. Most grains of major opaque phases (FeNi, troilite, chromite) are smaller than the average grain size. Metallic Ni-rich FeNi grains are comparable in size (200-400 μm) and frequency (~0.5-1.0 modal %) of chromite grains. Troilite (~1.9 modal %) displays the largest grain size out of the major opaques, with the largest at ~0.7 mm across and average grain size at ~0.2-0.3 mm. Troilite also displays veining that emanates from some troilite grains and veining that is detached from larger grains. Veins can extend up to ~0.8 mm in length and are narrow (<50 μm). A noteworthy feature of the troilite veins is their location within the sample – all veins are located close (≤ ~1.5 mm distance) to the sample's fusion crust, suggesting the veins may be associated with heating caused by the stone's passage through Earth's atmosphere. The sample's fusion crust is itself notable for multiple reasons. Most striking is that the recrystallized fusion crust is in optical continuity with the silicate grains that border it, even though portions of those silicate grains have melted and have recrystallized to exhibit a much finer grained acicular texture. Adjacent to the acicular fusion crust, the silicate grains have a very continuous, consistently ~100 μm darkened band. Terrestrial weathering in ALH 84025 is minimal compared to other samples in the set, and is most often found along grain boundaries.

Two of the Miller Range meteorites in the sample set, MIL 090206 and MIL 090405, are similar petrologically (Figure 4.1.7). Because they are relatively recent finds from the 2009 Antarctic collection season (Satterwhite and Righter 2011b; Satterwhite and Righter 2012), they have not been extensively studied, but preliminary studies have found them to be similar to each other (Corder et al. 2014a) and to other 2009 MIL samples (090340, 090356, 090805, and 090963; Satterwhite and Righter 2012). Goodrich

et al. (2012) reported that MIL 090340 and MIL 090206 have petrographic characteristics similar to brachinites, and lack characteristics that would distinguish them as ureilites, although they were originally classified as such (Satterwhite and Righter 2011a; Satterwhite and Righter 2011b).

The Miller Range 090206, 10 polished section (Figure 4.1.7a and b) is ~12 × 10 mm, is free of fusion crust, and contains olivine, high- and low-Ca pyroxene, chromite, plagioclase, FeS, and FeNi metal as major mineral phases. The sample displays a crystalline texture, with silicate grains displaying a range of sizes and shapes. Both coarse elongate silicates (≤ ~1.5 mm on long axis and ≤ ~0.5 mm on short axis) and finer subhedral silicates (often between ~ 0.1 and ~0.5 mm on long axis) are numerous. The coarse elongate silicates display relatively strong alignment along their long axis, which combined with the existence of the finer grains creates a moderately lineated texture. Silicate grains display only mild undulatory extinction, but also many fractures. Many fractures in the elongate silicates are oriented roughly perpendicular to the long axis of the same grains. Another notable feature of MIL 090206 petrography is the existence of a single ~10 × 2.5 mm orthopyroxene grain positioned along one edge of the sample. Because the grain's long edge creates the border of the polished section, it is possible that the grain was even larger than ~2.5 mm in the short dimension. The grain poikilitically encloses silicate grains, FeS, and FeNi, all of which have similar mineral shapes and sizes as the grains in the meteorite's main region. Elongate silicate grains within the large orthopyroxene grain even occasionally display the same alignment as elongate silicates in the main region. Rounded grains of chromite are also poikilitically enclosed (~0.1-0.3 mm diameter) in the large orthopyroxene whereas the remainder of the sample contains

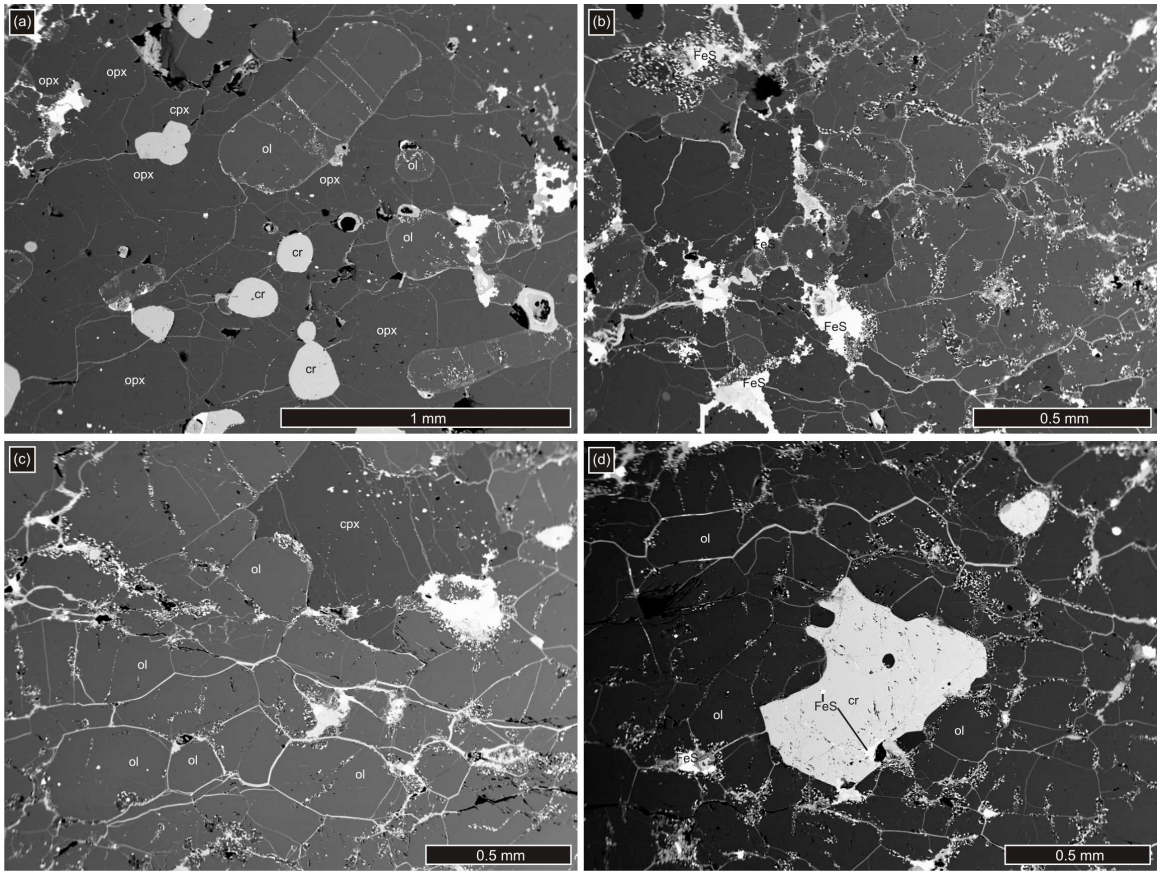

Figure 4.1.7: Back-scattered electron images of regions of (a), (b) MIL 090206, 10 and (c), (d) MIL 090405, 7. Image (a) displays a portion of MIL 090206's large orthopyroxene grain poikilitically enclosing different minerals – most notably elongate olivine grains and rounded chromite grains. Elongate silicate grains showing relatively strong alignment along their long dimension are present throughout the sample and create a moderately lineated texture in MIL 090206, 10. Image (b) depicts the prevalence of tiny FeS grains in the main lithology of MIL 090206, 10 (areas of the sample excluding the large orthopyroxene grain). This same behavior of FeS is evident in MIL 090405, 7 in images (c) and (d). Miller Range 090405, 7 exhibits the same lineated texture as in MIL 090206, 10 but it is difficult to identify in (c) and (d).

more angular, sometimes larger grains of chromite. The large orthopyroxene grain does not have a sharp contact with the remainder of the sample. The study by Goodrich et al. (2012) reported petrography of MIL 090206, 5 that contained a ~10 mm-long orthopyroxene, and it is assumed that this is the same grain as in section ,10. Iron-sulfide

and FeNi metals do not display very large grain sizes (FeS ≤ ~0.1 mm on long axis and FeNi ≤ ~0.05 mm on long axis) and exist along silicate grain boundaries as intergrowths of each other and Fe-oxide weathering products. The diffuse boundary between the large orthopyroxene grain and the remainder of the sample displays an increase in these FeS, FeNi, Fe-oxide intergrowths. Iron-sulfide also pervades the meteorite as tiny "micro-droplets" scattered along silicate grain boundaries as well as fractures in silicates. In plane-polarized light, MIL 090206, 10 is stained with rust colored alteration along some grain boundaries and some fractures.

Miller Range 090405 ,7 (Figure 4.1.7c and d) is ~11 × 9 mm and the moderately coarse, moderately lineated crystalline texture that is evident in MIL 090206 is evident in MIL 090405, 7 as well. A cursory petrographic analysis would suggest the possibility that the two meteorites should be paired, but upon closer inspection a few differences appear. These differences do not necessarily exclude the possibility of pairing. Both meteorites contain the same major mineralogy except MIL 090405 lacks low-Ca pyroxene. The mineral alignment (or lineated fabric) in MIL 090405 is more pronounced than in MIL 090206 and MIL 090405 has a slightly smaller maximum silicate grain size (≤ 1.0 mm on long axis). Miller Range 090405 also lacks the large ~10 × 2.5 mm orthopyroxene grain that two different sections of MIL 090206 contain (or any grain comparable in size). Finally, comparing plane-polarized light maps of each of the meteorites reveals slightly less rust colored alteration in MIL 090405, but the difference is not pronounced enough to suggest that the two meteorites had been weathering on the surface of the Earth for different lengths of time.

The petrography of MIL 090206 and MIL 090405 is similar to published petrography of brachinites and brachinite-like achondrites (see Day et al. 2012, Mittlefehldt et al. 2003).

Lewis Cliff 88763 – The tiny 4.1 g Antarctic find LEW 88763 was originally announced as a Brachina-like achondrite with a dark crystalline interior and fusion crust covering 95% of the sample (Lindstrom 1991). In the same announcement, LEW 88763 was described as containing mostly anhedral olivine with minor amounts of plagioclase, pyroxene, and opaque material. A comprehensive study of LEW 88763 by Swindle et al. (1998) found the meteorite to be mainly composed of olivine with accessory augite, pigeonite, plagioclase, chromite, whitlockite, ilmenite, troilite, and taenite.

The polished section (,14; total surface area = 0.27 cm^2; Figures 4.1.8-4.1.10) of LEW 88763 obtained for this study (as well as for a preliminary study published in Corder et al. 2013) agrees well with previous studies of the meteorite's petrology. The small section is roughly triangular in shape and two of its sides are covered with a thin fusion crust. One side's fusion crust is ~200 μm thick, and the second side's fusion crust is ~50 μm thick. Terrestrial alteration is pervasive (see rustiness, Figure 4.1.8) but a region of decreased alteration is associated with the ~200 μm thick section of fusion crust (also see Figure 4.1.8). The major mineral phases observed were olivine, clinopyroxene, orthopyroxene, plagioclase, chromite, FeNi, and FeS. Olivines make up most of the silicate grains, are euhedral to subhedral, and generally do not exceed 0.4 mm in diameter. All other mineral phases are generally less than 0.25 mm in diameter. Iron sulfides make up 1.3 modal % of the section, and FeNi grains and chromite grains each make up 0.5 modal % of the section. The remainder of the section (97.7 modal %) is

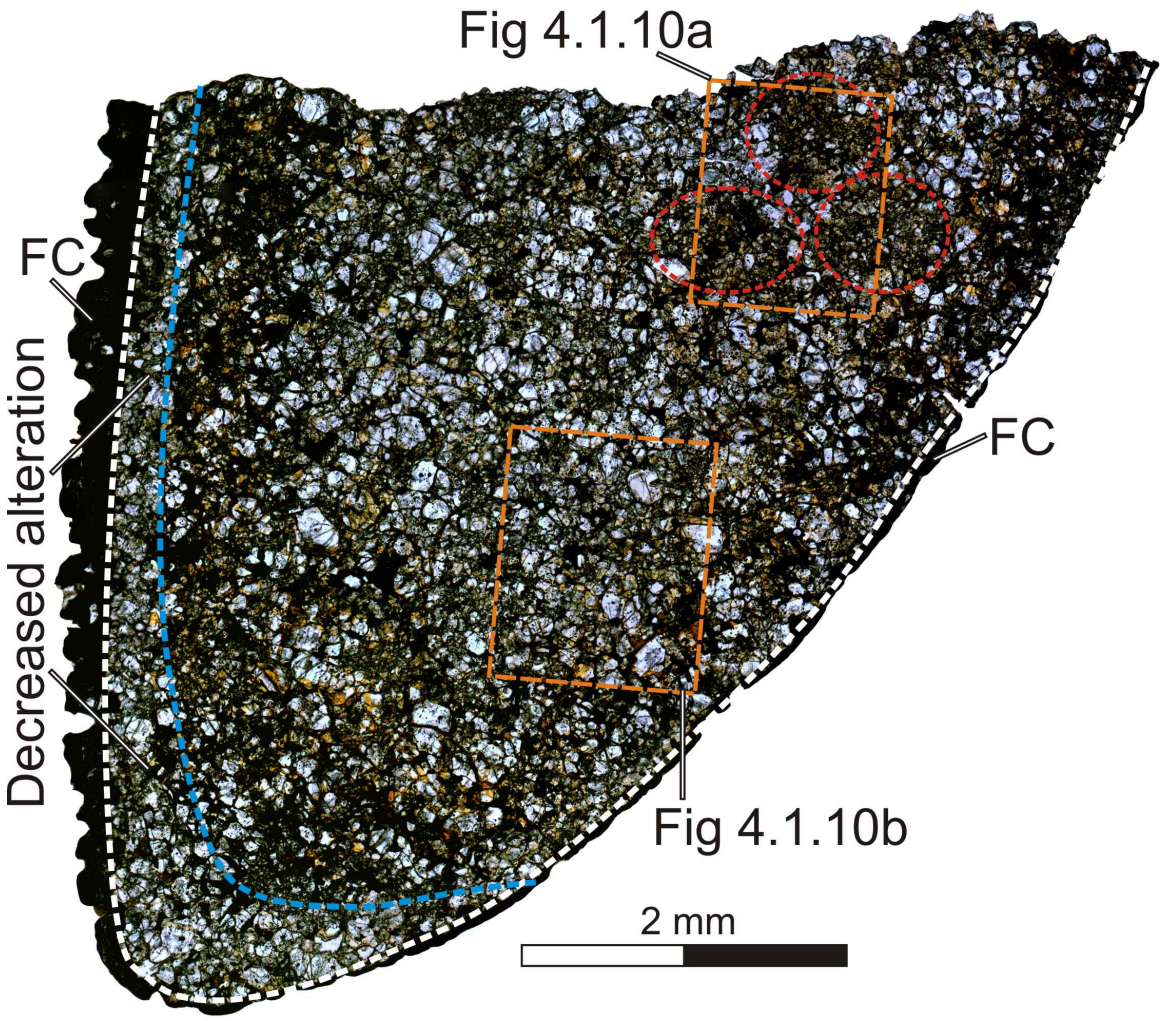

Figure 4.1.8: Plane-polarized transmitted light map of LEW 88763, 14. The meteorite's granoblastic texture and small grain size is visible. Areas (roughly circular) of smaller grain size are circled by red dashed ovals. Fusion crust lies outside of the white dashed line and is noted by the abbreviation "FC." The region between the white dashed line and the blues dashed line towards the left and bottom left of the sample has experienced less alteration than the rest of the sample. Orange dashed rectangles refer to the areas depicted in Figures 4.1.10a and 4.1.10b.

composed of silicate grains, fusion crust, and alteration. Because modes were determined with simple imaging processing techniques and silicates in LEW 88763 had similar color characteristics in both PPL and RL (the two kinds of maps used to calculate modes in this

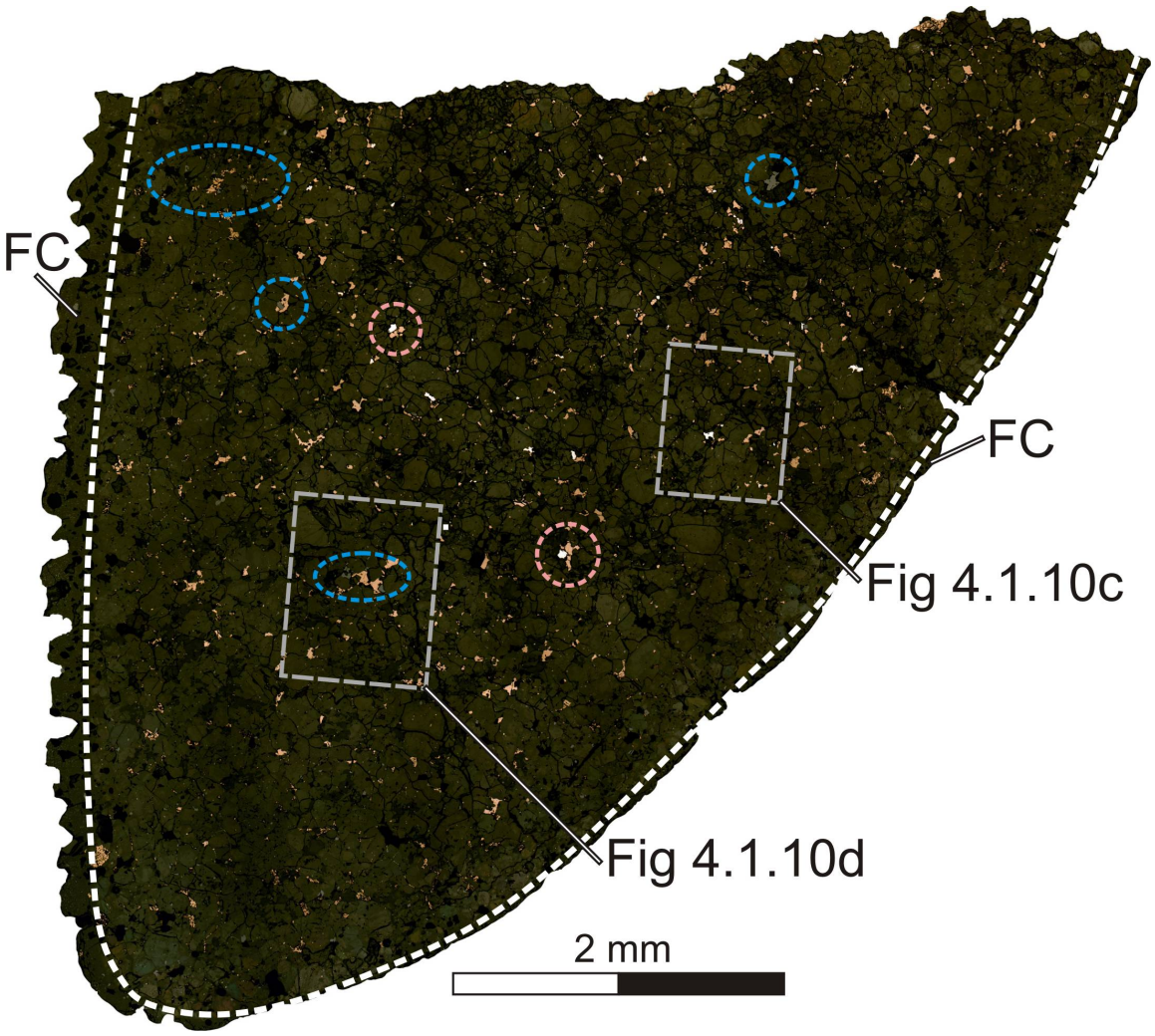

Figure 4.1.9: Reflected light map of LEW 88763, 14. Grains of FeS are visible (gold-brown grains) as well as FeNi grains (white) that are fewer in number. A few notable occurrences of small FeS + FeNi assemblages are circled by pink dashed lines. Chromite grains in LEW 88763 are small, and blue dashed circles and ovals enclose a few chromite grains (which are sometimes accompanied by FeS metal). The meteorite's fusion crust lies outside of the white dashed line and is noted by the abbreviation "FC." Grey dashed rectangles refer to the areas depicted in Figures 4.1.10c and 4.1.10d.

study), modes could not be calculated for LEW 88763 silicate phases. Swindle et al. (1998) found LEW 88763, 11 to contain 71 modal % olivine and 10 modal % plagioclase. LEW 88763 has an overall texture that is less equilibrated than some

brachinites (e.g., ALH 84025, etc.; see above, as well as Mittlefehldt et al. 2003) but similar to less equilibrated textures in others in the group (e.g., Brachina, etc.; Nehru et al. 1983). Its texture also distinctly resembles those of meteorites from other groups, especially some members of the winonaite group (e.g., Mount Morris, Winona, etc.; Benedix et al. 1998).

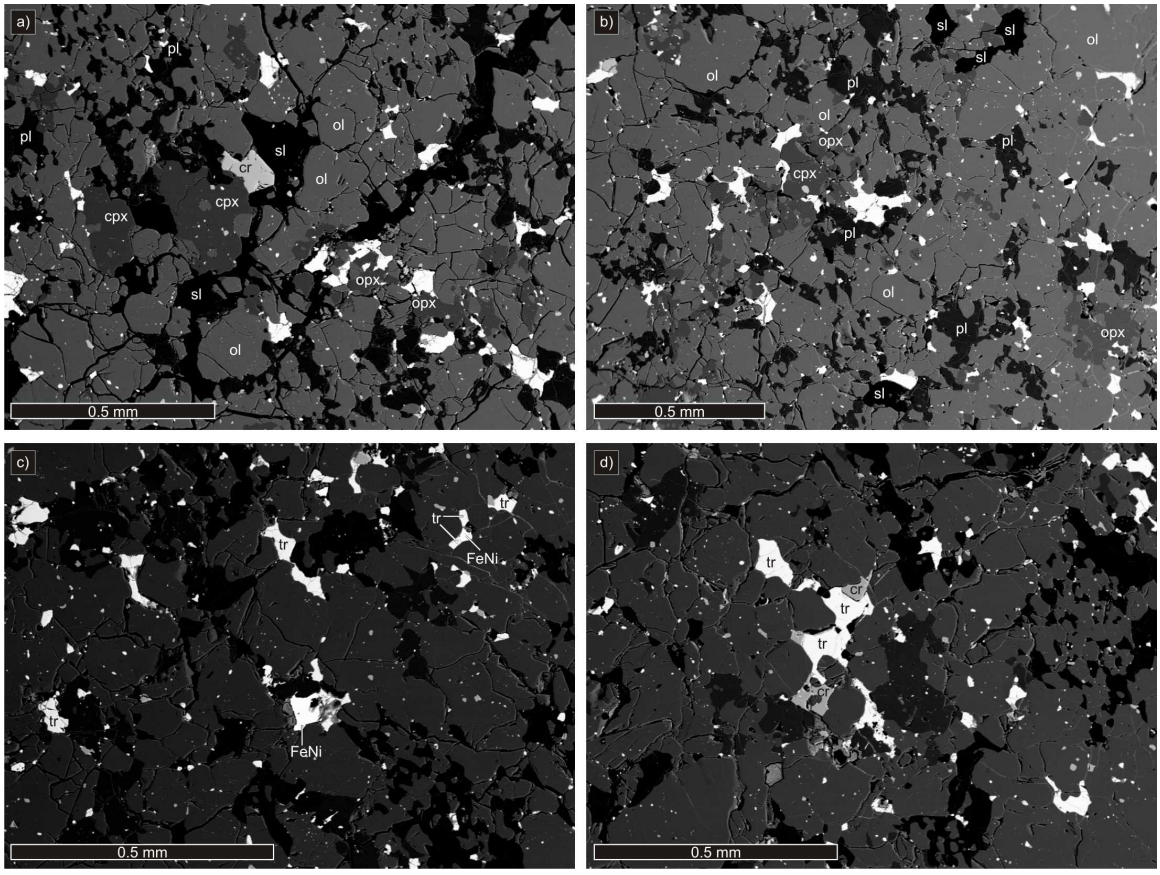

Figure 4.1.10: BSE images of LEW 88763, 14 exhibiting the meteorite's non-equilibrated texture. Abbreviations: pl = plagioclase, cpx = clinopyroxene, opx = orthopyroxene, sl = slide space/no sample, cr = chromite, ol = olivine, FeNi = FeNi metal grains, tr = FeS metal grains (troilite).

MIL 091004 – The MIL 091004 meteorite has previously been described as having an exterior covered in ~95% black/brown fusion crust, with rusty areas, and was classified as a lodranite when first announced in the Antarctic Meteorite Newsletter (Satterwhite and Righter 2012). The polished section that was obtained for this study (,7) contains two distinct regions visible to the naked eye (Figures 4.1.11-4.1.14). The first is the main granoblastic silicate-rich region that makes up 90 area % of the polished thick-section and is predominantly composed of silicate minerals of olivine and high- and low-Ca pyroxene, and its texture is similar to the textures of ureilites described previously (e.g., Goodrich 1992, Goodrich et al. 2004, and Berkley et al. 1980). The major mineral phases present in this region of MIL 091004 are pigeonite, olivine and augite (90 modal %), as well as FeNi, FeS, and schreibersite (2 modal %), with the remainder of the region (8 modal %) containing terrestrial alteration and a small amount of fusion crust. The second region, making up 10 area % of the polished thick-section, has an intergranular texture of numerous lathlike carbon grains (34 modal %) in association with olivine (64 modal %; 21 modal % reduced olivine + 43 modal % non-reduced olivine) and minor FeNi metal (2 modal %). This region is termed the carbon-rich region, and this same region is clearly visible in images of thick-section MIL 091004, 2, used to provisionally describe the meteorite (Satterwhite and Righter 2012). The contact between the two regions is quite sharp. For the entire section pigeonite, olivine, and augite account for 87.2 modal %, FeNi, FeS, and schreibersite account for 1.9 modal %, and carbon accounts for 3.4 modal %. The remainder of the section (7.4 modal %) is comprised of material created through terrestrial weathering (this material occurs along grain

boundaries and within fractures of olivines, likely as iddingsite) and a small amount of crystalline, vesicular fusion crust along the edge of the polished thick-section.

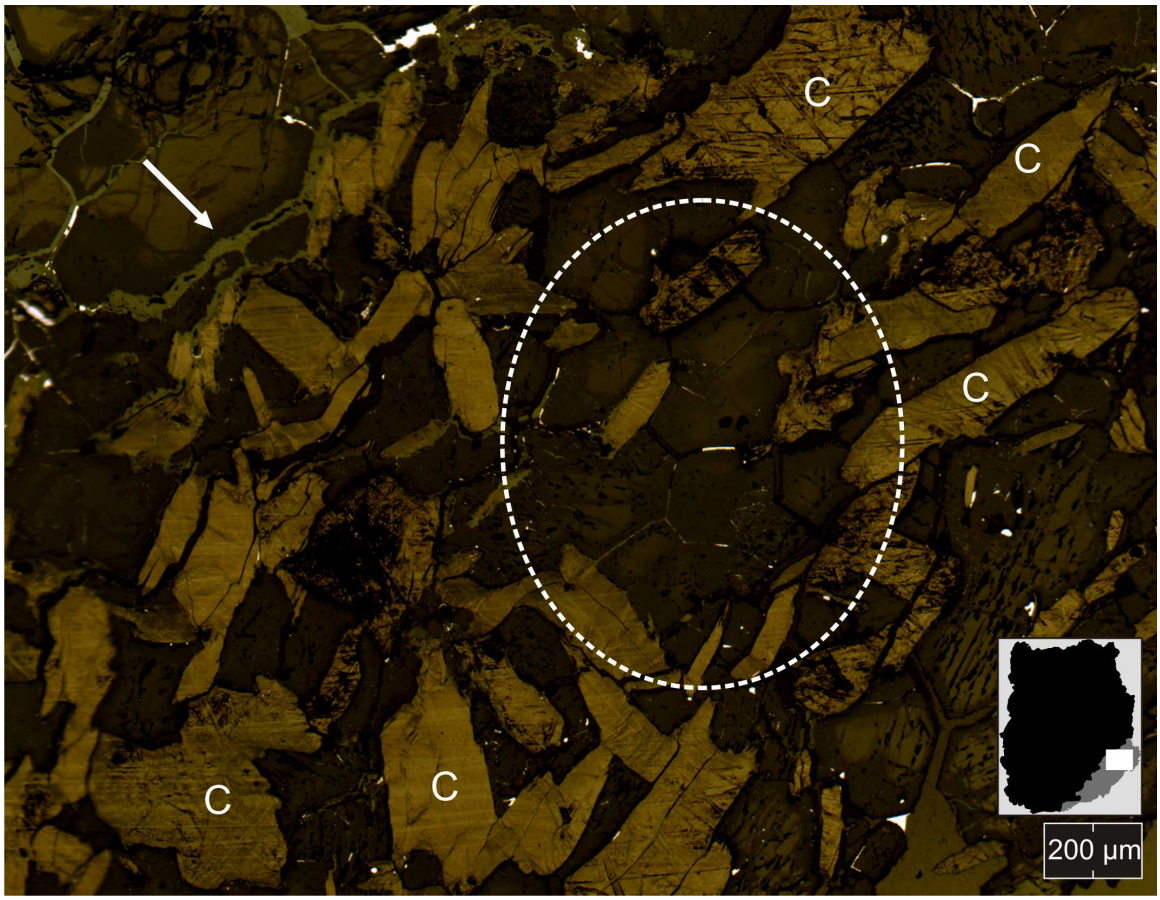

Figure 4.1.11: Reflected light photomicrograph of a portion of the carbon-rich region in MIL 091004, 7. Carbon grains in this region can be identified by their characteristic tan color in reflected light, as well as their tabular morphology and size (>0.5 mm along the long axis). Carbon grains in such high concentration have not previously been observed in ureilites. Also observed are alteration veins from terrestrial weathering (white arrow) and evidence for high-temperature equilibration of olivines in the carbon-rich region from 120˚ triple junctions (white dashed oval). Abbreviations: C = carbon. Inset figure above the scale bar demonstrates the location from which this image was taken (gray area in inset = carbon-rich region, black area in inset = main granoblastic region).

Figure 4.1.12: Composite photomicrograph maps of MIL 091004, 7 in (a) plane-polarized light and (b) reflected light. Carbon grains in the carbon-rich region (outside green dashed lines, labeled *C-rich region*) can be seen in the upper right and right center portions of the reflected light map (light brown, lathlike grains); the same carbon grains are opaque in plane-polarized light. Along the center right edge of the section is a region of vesicular fusion crust (gray dashed lines, labeled *FC*). In (b), veins of highly reflective FeNi, FeS, schreibersite, and products of terrestrial weathering occur between silicate grains.

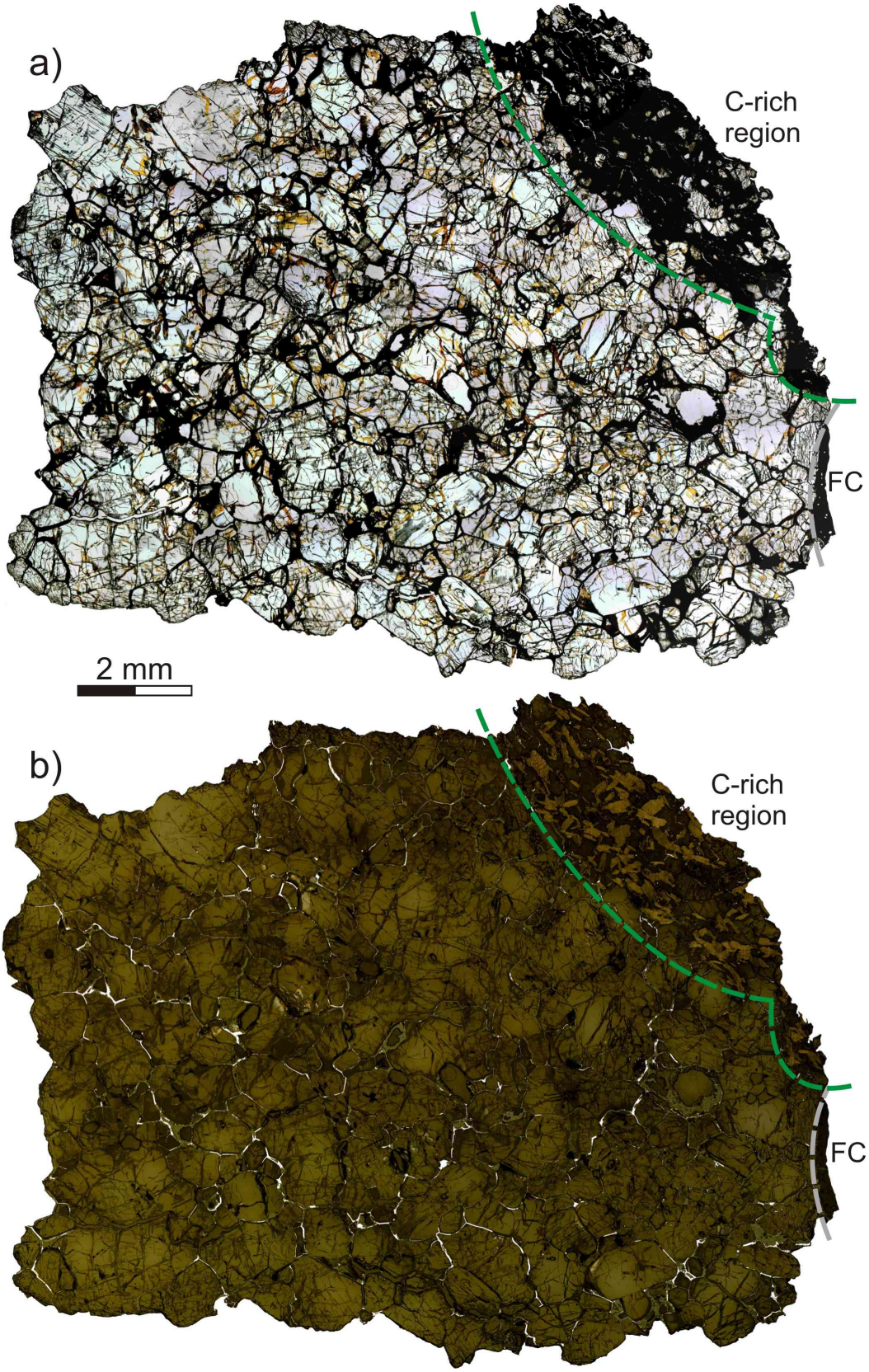
a)
C-rich
region
FC
2 mm
b)
C-rich
region
FC

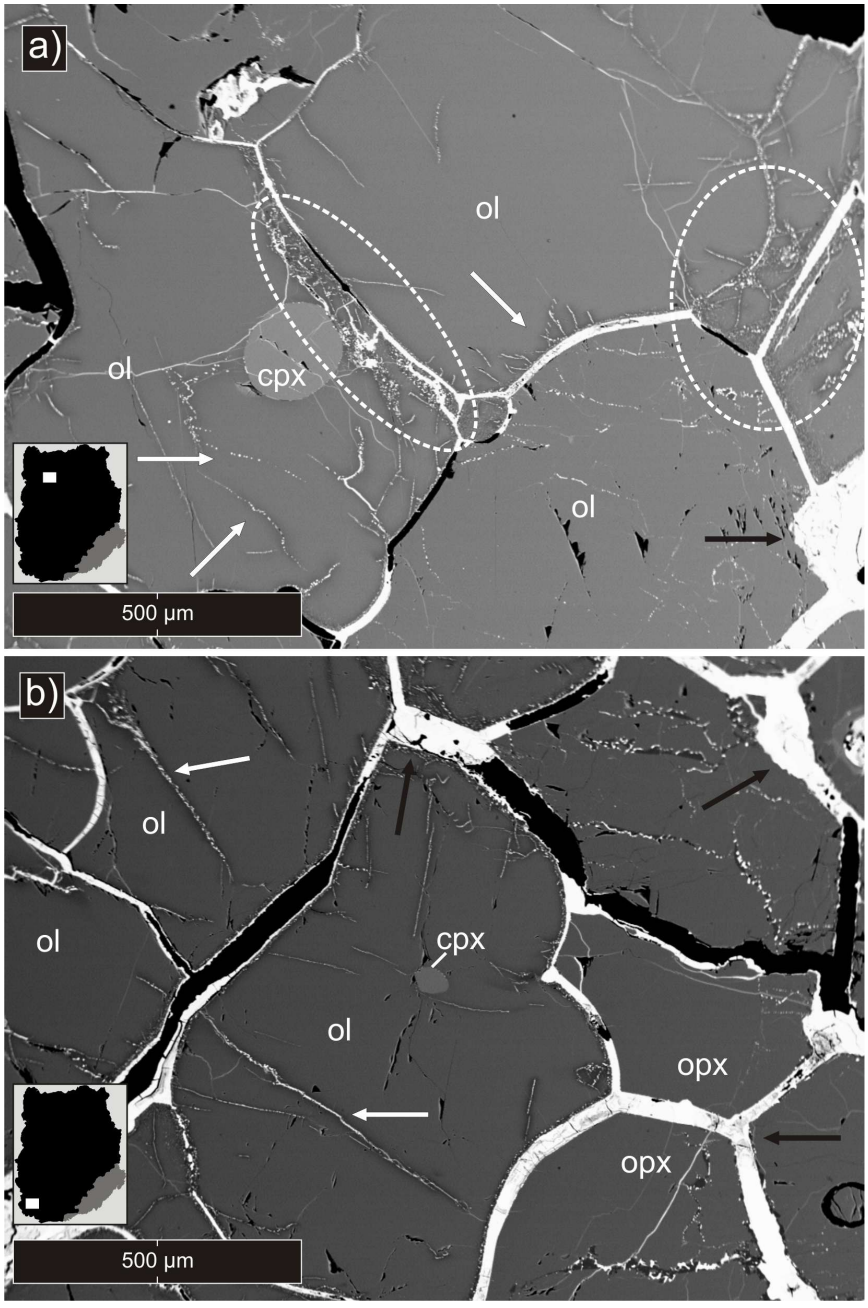

Figure 4.1.13: BSE images of two different areas within the main granoblastic region. Differences in brightness in these two images reflect different BSE settings, not markedly different mineralogies. (a) cpx in olivine, black = gaps in section, white arrows = stringers of FeNi blebs, black arrow = alteration, white dashed ovals = intense alteration (b) cpx in olivine, black = gaps in section, black arrows = alteration, white arrows = stringers of FeNi blebs. Abbreviations: ol = olivine; cpx = clinopyroxene; opx = orthopyroxene. Inset figures above the scale bars demonstrate the location from which each image was taken (gray area in inset = carbon-rich region, black area in inset = main granoblastic region).

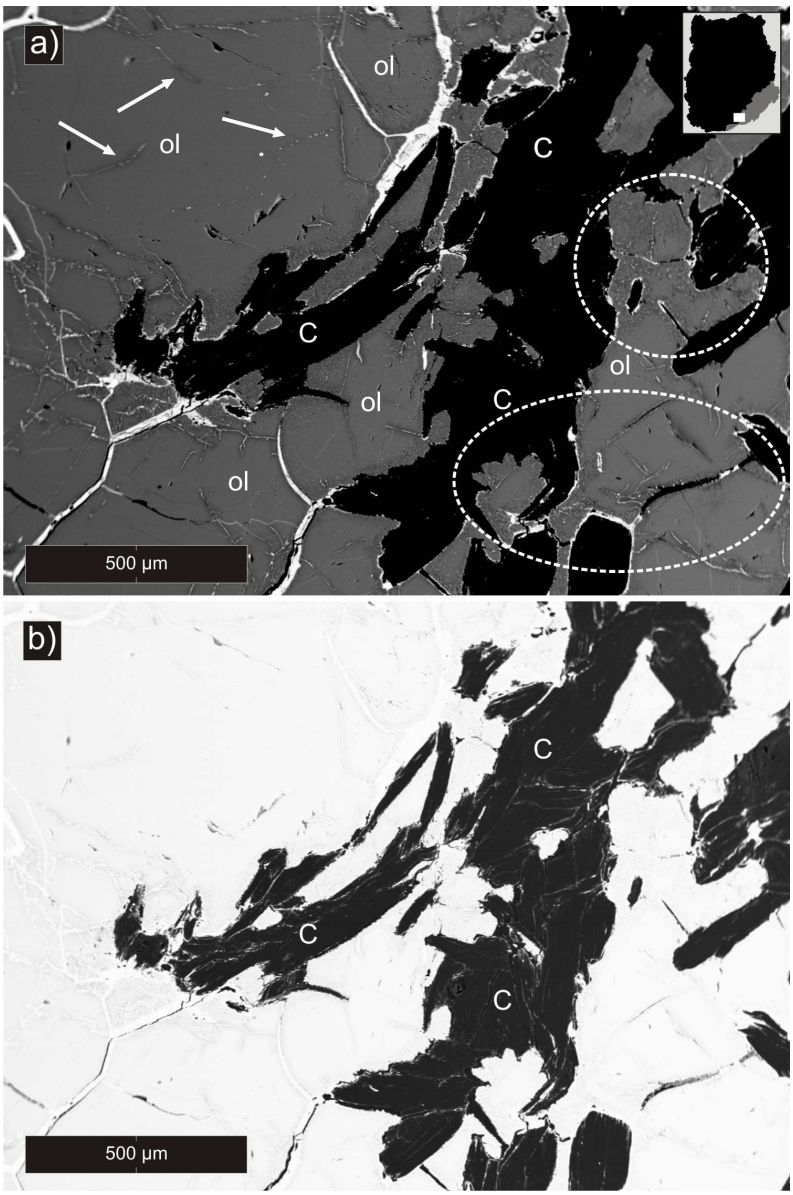

Figure 4.1.14: (a) Backscattered electron (BSE) image of a portion of the boundary between the carbon-rich region and the granoblastic silicate-rich main region. Black areas in the BSE image are large carbon grains. White arrows in the top left of (a) indicate regions of olivine reduction within the silicate-rich main region resulting in high-Mg olivine and exsolved <10 µm FeNi metal. Also highlighted in (a) are areas of intense reduction within the carbon-rich region (white dashed ovals) where high Mg/Fe olivine grains (up to $Fo_{98.5}$; dark grey) and FeNi (bright regions) occur, giving a mottled appearance. Reduction in the carbon-rich region is often associated with fractures in olivine. (b) BSE image of the same region with different grayscale values reveals the shape of the carbon laths. Abbreviations: ol = olivine; C = carbon. Inset figure in upper right of (a) demonstrates the location from which this image was taken (gray area in inset = carbon-rich region, black area in inset = main granoblastic region).

4.2 Major- and minor-element mineral chemistry

More detailed features of the mineral chemistries described below are found in Tables 4.2.1-4.2.11, as well as Figures 4.2.1 and 4.2.2. During analysis of samples with the electron microprobe, measures were taken to identify any faint mineral zoning features in silicates. No zoning was found and silicates in general had notably homogeneous chemical compositions. The only inter-mineral chemistry variation was found in portions of olivines in MIL 091004 that were associated with FeNi metals (which also have variable compositions, see Tables 4.2.2 and 4.2.9). This variation was caused by reduction (see Discussion), and is not considered mineral zonation. In the following described mineral chemistries, variation is listed as 1σ deviation.

Acapulcoites and lodranites – For each phase analyzed within each of the acapulcoite-lodranites in this study, mineral chemistries are consistent with most, if not all, of the observed grains exhibiting no zoning. Considered as a group, our five acapulcoite-lodranites also exhibit a relatively consistent mineral chemistry. As the archetype of the acapulcoite group, the Acapulco meteorite contains olivines of $Fo_{88.4\pm0.1}$ (n=12), feldspars of $An_{15.7\pm0.4}Ab_{80.5\pm0.3}$ (n=13), low-Ca pyroxenes of $Wo_{1.7\pm0.3}En_{86.9\pm1.2}$ (n=13), and high-Ca pyroxenes of $Wo_{44.8\pm1.1}En_{50.5\pm0.6}$ (n=5). The same sample also contains chromites with Cr# (where Cr# = Cr/(Cr+Al)*100) of 87.8±0.5 (n=16), FeNi metals with 87.3±6.1 wt. % Fe (n=24, Table 4.2.7), and FeS metals with 36.7±0.4 wt. % S (n=12). Published data for the Acapulco meteorite (Palme et al. 1981 and Zipfel et al. 1995) agrees well with our data.

Acapulcoite ALH 81187, 7 contains olivines of $Fo_{95.8\pm0.1}$ (n=7), feldspars of $An_{19.4\pm0.7}Ab_{79.0\pm0.7}$ (n=6), low-Ca pyroxenes of $Wo_{3.1\pm0.5}En_{90.5\pm1.3}$ (n=10), and high-Ca

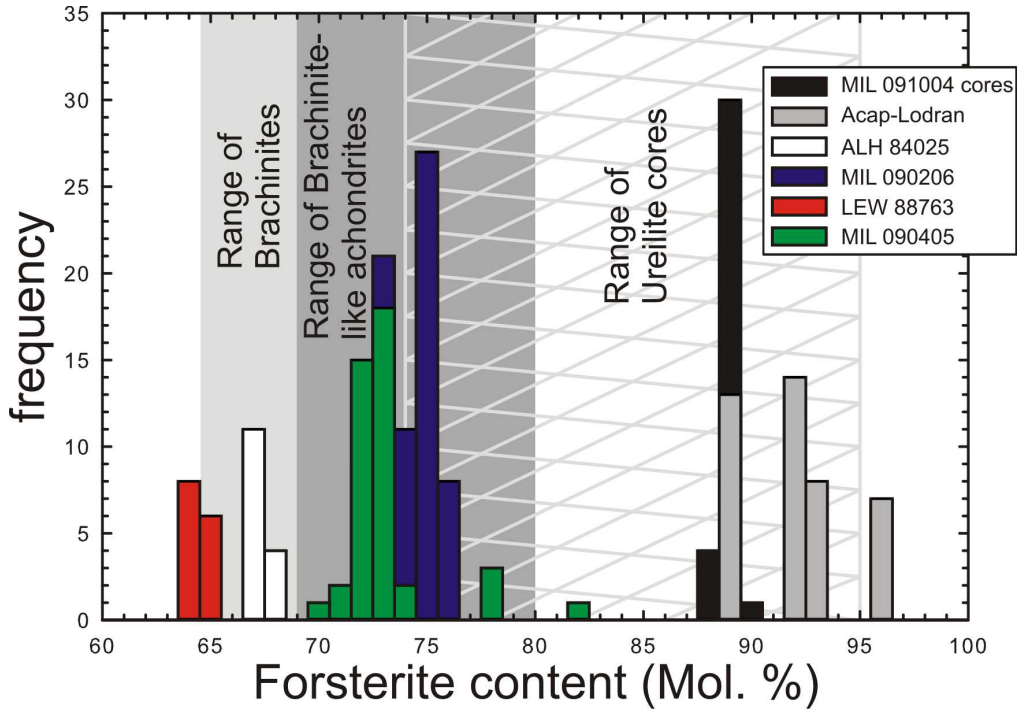

Figure 4.2.1: Frequency plot of forsterite content in olivines in the sample set. Ranges for brachinites and brachinite-like achondrites from Day et al. (2012) and range for ureilite cores from Mittlefehldt (2007).

pyroxenes of $Wo_{43.1\pm0.9}En_{54.1\pm0.6}$ (n=6). Allan Hills 81187 also contains chromites with Cr# of 87.2±1.8 (n=5), FeNi metals with 93.0±0.5 wt. % Fe (n=18), FeS metals with 37.2±0.4 wt. % S (n=6), and schreibersites with 43.1±6.0 wt. % Fe (n=7). Mittlefehldt et al. (1996) and McCoy et al. (1996) published mineral chemistry data for ALHA 81187, and our data agrees with their studies.

The relatively texturally equilibrated acapulcoite MET 01195, 33 contains olivines of $Fo_{91.3\pm0.1}$ (n=7), feldspars of $An_{16.9\pm0.6}Ab_{79.9\pm0.4}$ (n=8), low-Ca pyroxenes of $Wo_{1.7\pm0.4}En_{89.5\pm0.5}$ (n=7), and high-Ca pyroxenes of $Wo_{43.6\pm0.9}En_{52.4\pm0.8}$ (n=8). Meteorite Hills 01195 also contains chromites with Cr# of 86.3±0.2 (n=9), FeNi metals with

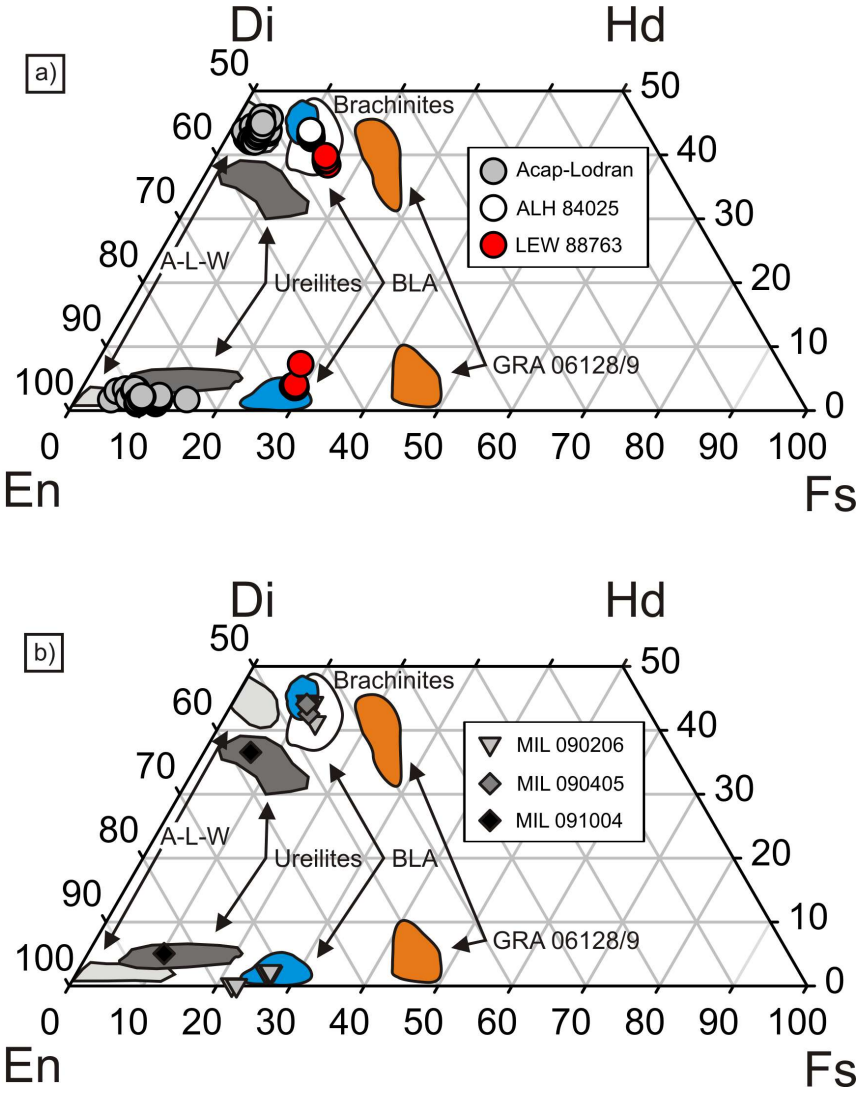

Figure 4.2.2: Pyroxene quadrilaterals for a) acapulcoite-lodranites, ALH 84025, and LEW 88763 and b) MIL samples from 2009 Antarctic collection season. Fields for the meteorite groups and GRA 06128/9 are from Day et al. (2012). Abbreviations: BLA = brachinite-like achondrites, A-L-W = acapulcoites, lodranites, and winonaites.

87.6±6.0 wt. % Fe (n=13, Table 4.2.8), FeS metals with 36.6±0.2 wt. % S (n=12), and schreibersites with 35.5±1.0 wt. % Fe (n=5). Rubin (2007) reported data for MET 01195 olivines, low-Ca pyroxenes, and chromites and our data agrees for the same mineral phases.

The transitional acapulcoite-lodranite EET 84302, 28 contains olivines of $Fo_{91.7\pm0.1}$ (n=7), feldspars of $An_{23.8\pm0.9}Ab_{74.4\pm0.7}$ (n=9), low-Ca pyroxenes of $Wo_{1.8\pm0.3}En_{90.0\pm0.4}$ (n=7), and high-Ca pyroxenes of $Wo_{44.3\pm1.3}En_{52.2\pm1.2}$ (n=7). It also contains FeNi metals with 92.7±0.4 wt. % Fe (n=9), FeS metals with 36.5±0.1 wt. % S (n=6), and schreibersites with 53.7±3.9 wt. % Fe (n=6). Mittlefehldt et al. (1996) reported data for EET 84302 olivines, low-and high-Ca pyroxenes, and feldspars and McCoy et al. (1997a) reported data for olivines and low- and high-Ca pyroxenes. Our data agrees well with both published studies.

The lodranite GRA 95209, 218 contains olivines of $Fo_{92.9\pm0.1}$ (n=8), feldspars of $An_{18.7\pm0.8}Ab_{79.5\pm0.8}$ (n=8), low-Ca pyroxenes of $Wo_{3.1\pm0.5}En_{89.6\pm0.6}$ (n=8), and high-Ca pyroxenes of $Wo_{42.2\pm0.2}En_{54.1\pm0.2}$ (n=7). Graves Nunataks 95209 also contains chromites with Cr# of 91.7±1.3 (n=13), FeNi metals with 92.0±0.6 wt. % Fe (n=9), and FeS metals with 36.7±0.8 wt. % S (n=11). As with the other acapulcoite-lodranites, previously published data for GRA 95209 (Mittlefehldt and Lindstrom 1998 and McCoy et al. 2006) agrees well with our new data.

ALH 84025, MIL 090206, and MIL 090405 – Allan Hills 84025, 6 – the only confirmed brachinite in the sample set – contains olivines of $Fo_{66.8\pm0.2}$ (n=15), high-Ca pyroxenes of $Wo_{43.3\pm0.4}En_{45.6\pm0.2}$ (n=18), chromites with Cr# of 84.5±0.2 (n=15), FeNi metals with 66.9±1.3 wt. % Fe (n=14), and FeS metals with 36.5±1.1 wt. % S (n=20). Our data agrees well with the data collected by Warren and Kallemeyn (1989) for ALH 84025.

The two ungrouped achondrites studied – MIL 090206 and MIL 090405 – both have chemistries that are similar to or within the ranges for brachinites and brachinite-

like achondrites. Miller Range 090206, 10 contains olivines of $Fo_{73.6\pm1.2}$ (n=76), low-Ca pyroxenes of $Wo_{2.1\pm0.3}En_{72.0\pm1.2}$ (n=58), high-Ca pyroxenes of $Wo_{43.8\pm0.5}En_{45.5\pm0.2}$ (n=40), chromites with Cr# of 84.5±0.2 (n=27), FeNi metals with 93.4±0.5 wt. % Fe (n=28), and FeS metals with 36.2±0.6 wt. % S (n=34).

Miller Range 090405, 7 contains olivines of $Fo_{72.4\pm21.7}$ (n=41), high-Ca pyroxenes of $Wo_{43.6\pm0.3}En_{45.7\pm0.2}$ (n=38), chromites with Cr# of 84.3±0.2 (n=17), FeNi metals with 94.8±0.5 wt. % Fe (n=18), and FeS metals with 36.3±0.3 wt. % S (n=14).

Major-element mineral chemistry (%Wo, %En, %Fs) of the two MIL ungrouped achondrites agrees well with published data for brachinites and brachinite-like achondrites (Day et al. 2012, Goodrich et al. 2011, Mittlefehldt 2007, Mittlefehldt et al. 2003, and Keil 2014). The two meteorites' FeO/MnO ratios also lie within the range for brachinites (Mittlefehldt et al. 2003 and Mittlefehldt 2007). Olivines in MIL 090405 (Table 4.2.1) contain 'brachinite-like' levels of CaO (Keil 2014, Mittlefehldt et al 2003, and Mittlefehldt 2007).

LEW 88763 – As with its petrography, LEW 88763 mineral compositions obtained for this study agree well with previously published data for the meteorite (Swindle et al., 1998). Lewis Cliff 88763 contains olivines of $Fo_{64.0\pm0.2}$ (n=14), feldspars of $An_{30.1\pm6.2}Ab_{66.5\pm5.4}$ (n=15), low-Ca pyroxenes of $Wo_{4.3\pm1.3}En_{67.2\pm1.0}$ (n=7), high-Ca pyroxenes of $Wo_{39.0\pm0.5}En_{45.6\pm0.2}$ (n=6), chromites with Cr# of 81.0±0.9 (n=16), FeNi metals with 44.2±1.2 wt. % Fe (n=14), FeS metals with 36.1±0.2 wt. % S (n=15). Although its mineral chemistries agree well with the ranges for brachinites, other chemical characteristics (e.g., oxygen isotopes, noble gases, etc.; see below and Swindle et al. 1998) of LEW 88763 suggest it is not a typical brachinite, or not a brachinite at all.

MIL 091004 – Miller Range 091004, 7 contains olivines of $Fo_{89.5\pm3.1}$ (n=43, Table 4.2.2), low-Ca pyroxenes of $Wo_{5.0\pm0.1}En_{84.7\pm0.1}$ (n=30), high-Ca pyroxenes of $Wo_{36.7\pm0.2}En_{56.9\pm0.2}$ (n=11), FeNi metals with 93.2±3.7 wt. % Fe (n=25, Table 4.2.9), FeS metals with 36.5±0.1 wt. % S (n=8), and schreibersites with 82.1±0.3 wt. % Fe (n=8). Ureilite-like features of MIL 091004 include relatively high CaO (~0.3 wt. %, Table 4.2.2) and Cr_2O_3 (~0.5 wt. %, Table 4.2.2) contents in olivines as well as relatively high Cr_2O_3 (~1 wt. %, Table 4.2.3) contents in pyroxenes. Both major- and minor-element mineral chemistries of the meteorite support its classification as a ureilite, instead of its original classification as a lodranite. Data for other ureilites is available in Goodrich 1992, Warren 2006, Mittlefehldt 2007 and references therein.

Table 4.2.1: Average major- and minor-element composition (in wt. %) of olivines (MIL 091004 is omitted).

Sample	Met. type[1]		SiO_2	TiO_2	Al_2O_3	P_2O_5	Cr_2O_3	MgO	CaO	MnO	FeO	NiO	Total	%Fo[2]	FeO/MnO
Acapulco	A	avg.	40.3	<0.03	<0.03	<0.05	<0.05	47.4	<0.03	0.54	11.1	<0.06	99.4	88.4	20.3
n=12		1σ	0.3	-	-	-	-	0.5	-	0.01	0.1	-	0.8	0.1	0.5
ALHA 81187, 7	A	avg.	41.7	<0.03	<0.03	<0.05	<0.05	53.5	<0.03	0.47	4.2	<0.06	100.3	95.8	8.9
n=7		1σ	0.1	-	-	-	-	0.6	-	0.01	0.1	-	0.3	0.1	0.4
MET 01195, 33	A	avg.	41.0	<0.03	<0.03	<0.05	<0.05	49.9	<0.03	0.46	8.5	<0.06	99.9	91.3	18.3
n=7		1σ	0.1	-	-	-	-	0.1	-	0.01	0.1	-	0.2	0.1	0.5
EET 84302, 28	A-L	avg.	40.9	<0.03	<0.03	<0.05	<0.05	50.3	<0.03	0.46	8.1	<0.06	99.8	91.7	17.5
n=7		1σ	0.2	-	-	-	-	0.2	-	0.01	0.1	-	0.3	0.1	0.4
GRA 95209, 218	L	avg.	41.1	<0.03	<0.03	<0.05	<0.05	51.5	<0.03	0.47	7.0	<0.06	100.2	92.9	15.1
n=8		1σ	0.1	-	-	-	-	0.1	-	0.02	0.1	-	0.2	0.1	0.7
ALH 84025, 6	B	avg.	36.7	<0.03	<0.03	<0.05	<0.05	33.4	0.09	0.43	29.6	<0.06	100.3	66.8	69.2
n=15		1σ	0.1	-	-	-	-	0.2	0.01	0.02	0.2	-	0.2	0.2	2.4
LEW 88763, 14	B-like/an	avg.	36.1	<0.03	<0.03	<0.05	<0.05	31.6	0.13	0.40	31.6	<0.06	100.1	64.0	80.1
n=14		1σ	0.2	-	-	-	-	0.1	0.02	0.01	0.1	-	0.2	0.2	2.5
MIL 090206, 10	B/B-like	avg.	38.0	<0.03	<0.03	<0.05	<0.05	37.8	<0.03	0.44	24.1	<0.06	100.5	73.6	54.7
n=76		1σ	0.2	-	-	-	-	0.8	-	0.02	1.0	-	0.3	1.2	2.6
MIL 090405, 7	B/B-like	avg.	37.8	<0.03	<0.03	<0.05	<0.05	36.7	0.07	0.44	24.9	<0.06	100.2	72.4	56.5
n=41		1σ	0.3	-	-	-	-	1.1	0.02	0.03	1.4	-	0.6	1.7	1.8

[1]Abbreviations: A = acapulcoite, L = lodranite, B = brachinite, B-like = brachinite-like, an = anomalous

[2]%Fo = Mg/(Mg+Fe)*100

Table 4.2.2: Average major- and minor-element composition (in wt. %) of olivines in MIL 091004, 7. Compositions can differ significantly between the two major regions of the sample (main granoblastic and carbon-rich), as well as within a single grain due to reduction (e.g., rims and cores).

			SiO_2	TiO_2	$Al2O_3$	Cr_2O_3	MgO	CaO	MnO	P_2O_5	FeO	NiO	Total	%Fo[1]
Entire Sample	All analyses (n=43)	avg.	40.7	<0.03	0.04	0.51	48.1	0.30	0.54	<0.05	10.0	<0.06	100.1	89.5
		1σ	0.6	-	0.01	0.04	2.3	0.01	0.03	-	2.9	-	0.4	3.1
	All cores (n=35)	avg.	40.5	<0.03	0.04	0.52	47.0	0.30	0.53	<0.05	11.2	<0.06	100.1	88.2
		1σ	0.1	-	0.01	0.02	0.3	0.01	0.01	-	0.2	-	0.3	0.2
	All reduced (n=8)	avg.	41.8	<0.03	0.04	0.47	52.5	0.31	0.58	<0.05	4.53	<0.06	100.2	95.3
		1σ	0.5	-	0.01	0.1	2.2	0.02	0.03	-	2.8	-	0.4	2.9
Main granoblastic region	Cores (n=28)	avg.	40.4	<0.03	0.04	0.52	47.0	0.30	0.53	<0.05	11.3	<0.06	100.1	88.2
		1σ	0.2	-	0.01	0.02	0.3	0.01	0.01	-	0.2	-	0.4	0.2
	Reduced (n=2)	avg.	41.4	<0.03	<0.03	0.50	50.4	0.28	0.57	<0.05	7.1	<0.06	100.3	92.7
		1σ	0.2	-	-	0.01	0.9	0.02	0.02	-	0.6	-	0.5	0.7
Carbon-rich region	Cores (n=7)	avg.	40.6	<0.03	0.04	0.51	47.2	0.30	0.53	<0.05	11.08	<0.06	100.2	88.4
		1σ	0.1	-	0.01	0.02	0.2	0.01	0.01	-	0.31	-	0.2	0.3
	Reduced (n=6)	avg.	41.9	<0.03	0.04	0.46	53.2	0.31	0.59	<0.05	3.7	<0.06	100.1	96.2
		1σ	0.5	-	0.01	0.08	2.1	0.01	0.03	-	2.7	-	0.4	2.8

[1]%Fo = Mg/(Mg+Fe)*100

Table 4.2.3: Average major- and minor-element composition (in wt. %) of low- and high-Ca pyroxenes in all samples that contain them.

	Sample	Met. type[1]		SiO_2	TiO_2	Al_2O_3	Cr_2O_3	MgO	CaO	MnO	FeO	Na_2O	K_2O[2]	Total	Wo[3]	En[3]	Mg#[3]
Low-Ca pyroxenes	Acapulco	A	avg.	56.8	0.21	0.30	0.28	32.9	0.92	0.63	7.7	<0.03	<0.04	99.8	1.7	86.9	88.4
	n=13		1σ	0.8	0.02	0.04	0.04	0.3	0.18	0.02	0.8	-	-	0.5	0.3	1.2	1.2
	ALHA 81187, 7	A	avg.	57.5	0.18	0.45	0.91	34.6	1.6	0.59	4.4	0.11	<0.04	100.4	3.1	90.5	93.4
	n=10		1σ	0.3	0.01	0.05	0.13	0.7	0.3	0.02	0.6	0.03	-	0.3	0.5	1.3	0.9
	MET 01195, 33	A	avg.	57.2	0.22	0.32	0.32	34.4	0.93	0.52	6.0	<0.03	<0.04	99.8	1.7	89.5	91.1
	n=7		1σ	0.2	0.01	0.03	0.06	0.3	0.22	0.02	0.1	-	-	0.2	0.4	0.5	0.2
	EET 84302, 28	A-L	avg.	57.2	0.22	0.47	0.42	34.6	1.0	0.51	5.6	<0.03	<0.04	100.0	1.8	90.0	91.6
	n=7		1σ	0.2	0.01	0.05	0.05	0.3	0.2	0.02	0.1	-	-	0.4	0.3	0.4	0.2
	GRA 95209, 218	L	avg.	57.2	0.19	0.37	0.84	34.3	1.6	0.56	5.0	0.10	<0.04	100.2	3.1	89.6	92.4
	n=8		1σ	0.2	0.02	0.05	0.14	0.4	0.3	0.02	0.1	0.01	-	0.5	0.5	0.6	0.2
	LEW 88763, 14	B-like/an	avg.	53.2	0.28	0.52	0.41	24.4	2.2	0.36	18.5	0.06	<0.04	99.8	4.3	67.2	70.2
	n=7		1σ	0.2	0.03	0.04	0.07	0.4	0.7	0.01	0.3	0.02	-	0.1	1.3	1.0	0.2
	MIL 090206, 10	B/B-like	avg.	54.6	0.10	0.26	0.21	26.5	1.1	0.40	17.0	<0.03	n.a.	100.2	2.1	72.0	73.6
	n=58		1σ	0.3	0.06	0.25	0.08	0.6	0.2	0.02	0.5	-	-	0.4	0.3	1.2	1.0
	MIL 091004, 7	U	avg.	56.3	0.10	1.3	0.98	31.5	2.6	0.52	6.8	<0.03	n.a.	100.1	5.0	84.7	89.1
	n=30		1σ	0.2	0.01	0.0	0.02	0.1	0.0	0.01	0.1	-	-	0.3	0.1	0.1	0.1
High-Ca pyroxenes	Acapulco	A	avg.	53.5	0.51	0.74	1.3	17.3	21.4	0.35	2.9	0.68	<0.04	98.6	44.8	50.5	91.5
	n=5		1σ	0.2	0.02	0.14	0.2	0.2	0.6	0.04	0.3	0.04	-	0.4	1.1	0.6	0.7
	ALHA 81187, 7	A	avg.	53.8	0.55	1.1	1.7	18.7	20.7	0.34	1.7	0.84	<0.04	99.4	43.1	54.1	95.1
	n=6		1σ	0.4	0.03	0.1	0.2	0.3	0.4	0.03	0.3	0.06	-	0.5	0.9	0.6	0.9
	MET 01195, 33	A	avg.	53.9	0.60	0.93	1.6	18.0	20.9	0.32	2.5	0.74	<0.04	99.5	43.6	52.4	92.9
	n=8		1σ	0.1	0.02	0.02	0.1	0.3	0.4	0.02	0.1	0.02	-	0.2	0.9	0.8	0.2
	EET 84302, 28	A-L	avg.	53.9	0.53	1.0	1.5	18.1	21.4	0.30	2.2	0.69	<0.04	99.6	44.3	52.2	93.6
	n=7		1σ	0.2	0.07	0.2	0.2	0.4	0.7	0.03	0.1	0.07	-	0.2	1.3	1.2	0.3
	GRA 95209, 218	L	avg.	53.9	0.58	0.98	1.7	18.7	20.3	0.33	2.2	0.82	<0.04	99.6	42.2	54.1	93.7
	n=7		1σ	0.2	0.03	0.03	0.0	0.1	0.1	0.03	0.2	0.03	-	0.4	0.2	0.2	0.4
	ALH 84025, 6	B	avg.	53.1	0.16	0.63	0.84	16.0	21.2	0.21	7.0	0.49	<0.04	99.6	43.3	45.6	80.4
	n=18		1σ	0.2	0.01	0.07	0.05	0.0	0.3	0.02	0.1	0.04	-	0.2	0.4	0.2	0.3
	LEW 88763, 14	B-like/an	avg.	52.1	0.55	1.02	0.95	15.8	18.8	0.25	9.5	0.49	<0.04	99.5	39.0	45.6	74.9
	n=6		1σ	0.1	0.04	0.04	0.05	0.1	0.2	0.01	0.2	0.02	-	0.3	0.5	0.2	0.4
	MIL 090206, 10	B/B-like	avg.	53.6	0.23	0.59	0.78	16.0	21.4	0.20	6.8	0.47	n.a.	100.1	43.8	45.5	80.9
	n=40		1σ	0.5	0.11	0.03	0.06	0.1	0.3	0.01	0.3	0.02	-	0.4	0.5	0.2	0.6
	MIL 090405, 7	B/B-like	avg.	53.5	0.28	0.63	0.80	15.8	21.1	0.21	6.60	0.48	n.a.	99.4	43.6	45.7	81.1
	n=38		1σ	0.2	0.02	0.04	0.05	0.1	0.2	0.01	0.12	0.03	-	0.3	0.3	0.2	0.3
	MIL 091004, 7	U	avg.	53.7	0.18	2.0	1.2	20.1	18.1	0.40	4.0	0.13	n.a.	99.8	36.7	56.9	89.9
	n=11		1σ	0.2	0.01	0.0	0.0	0.1	0.1	0.01	0.1	0.01	-	0.2	0.2	0.2	0.1

[1]Abbreviations: A = acapulcoite, L = lodranite, B = brachinite, B-like = brachinite-like, an = anomalous, U = ureilite

[2]Abbreviation: n.a. = not analyzed

[3]Wo = Ca/(Ca+Mg+Fe)*100, En = Mg/(Ca+Mg+Fe)*100, Mg# = Mg/(Mg+Fe)*100

Table 4.2.4: Average major- and minor-element composition (in wt. %) of feldspars in all samples that contain them. LEW 88763 contains feldspars with Ca contents that are notably different that the acapulcoites and lodranites. Although LEW 88763 has been classified as a brachinite in the past, many brachinites do not contain feldspars.

Sample	Met. type[1]		SiO_2	Al_2O_3	MgO	CaO	FeO	BaO	Na_2O	K_2O	Total	An[2]	Ab[2]
Acapulco	A	avg.	64.0	22.0	<0.03	3.3	0.19	<0.1	9.2	0.66	99.3	15.7	80.5
n=13		1σ	0.3	0.1	-	0.1	0.07	-	0.1	0.07	0.4	0.4	0.3
ALHA 81187, 7	A	avg.	62.9	22.3	<0.03	4.0	0.18	<0.1	9.2	0.29	98.9	19.4	79.0
n=6		1σ	0.2	0.2	-	0.1	0.05	-	0.1	0.04	0.3	0.7	0.7
MET 01195, 33	A	avg.	63.5	22.1	<0.03	3.5	0.22	<0.1	9.1	0.56	99.0	16.9	79.9
n=8		1σ	0.3	0.2	-	0.1	0.07	-	0.1	0.04	0.3	0.6	0.4
EET 84302, 28	A-L	avg.	62.2	23.2	<0.03	4.9	0.08	<0.1	8.6	0.33	99.4	# 23.8	74.4
n=9		1σ	0.3	0.2	-	0.2	0.04	-	0.1	0.10	0.3	# 0.9	0.7
GRA 95209, 218	L	avg.	63.4	22.1	<0.03	3.9	0.26	<0.1	9.3	0.32	99.2	18.7	79.5
n=8		1σ	0.3	0.3	-	0.1	0.12	-	0.1	0.05	0.4	0.8	0.8
LEW 88763, 14	B-like/an	avg.	60.4	24.1	<0.03	6.2	0.47	<0.1	7.8	0.60	99.6	30.1	66.5
n=15		1σ	1.6	1.1	-	1.3	0.13	-	0.7	0.16	0.2	6.2	5.4

[1]Abbreviations: A = acapulcoite, L = lodranite, B-like = brachinite-like, an = anomalous

[2]An = Ca/(Ca+Na+K)*100, Ab = Na/(Ca+Na+K)*100

Table 4.2.5: Average major- and minor-element composition (in wt. %) of chromites in all samples that contain them. The acapulcoite-lodranite chromites have relatively consistent Cr# values but can range in Mg#.

Sample	Met. type[1]		SiO_2	TiO_2	Al_2O_3	V_2O_3	Cr_2O_3	MgO	CaO	MnO	FeO	NiO[2]	Total	Cr#[3]	Mg#[3]
Acapulco	A	avg.	0.07	1.2	5.8	0.57	62.7	6.5	<0.03	1.3	21.2	<0.06	99.5	87.8	35.4
n=16		1σ	0.02	0.0	0.3	0.03	0.5	0.6	-	0.2	0.6	-	0.6	0.5	2.7
ALHA 81187, 7	A	avg.	0.07	0.64	6.4	0.54	64.8	9.6	<0.03	2.9	15.1	<0.06	100.0	87.2	52.9
n=5		1σ	0.01	0.26	1.0	0.08	0.7	1.1	-	0.8	1.0	-	0.3	1.8	4.5
MET 01195, 33	A	avg.	0.07	1.1	6.8	0.53	63.5	8.6	<0.03	1.3	18.0	<0.06	99.8	86.3	45.9
n=9		1σ	0.01	0.0	0.1	0.02	0.4	0.3	-	0.3	0.5	-	0.3	0.2	1.6
GRA 95209, 218	L	avg.	0.06	1.0	3.8	0.53	62.8	1.7	<0.03	1.4	26.5	<0.06	97.8	91.7	10.1
n=13		1σ	0.01	0.1	0.6	0.07	0.6	0.8	-	0.3	1.0	-	0.3	1.3	4.4
ALH 84025, 6	B	avg.	0.07	1.3	7.3	0.70	59.0	3.9	<0.03	0.34	27.9	<0.06	100.5	84.5	20.0
n=15		1σ	0.02	0.0	0.1	0.03	0.4	0.1	-	0.02	0.2	-	0.4	0.2	0.7
LEW 88763, 14	B-like/an	avg.	0.09	5.1	7.9	0.53	50.1	3.2	<0.03	0.36	33.1	<0.06	100.4	81.0	14.6
n=16		1σ	0.01	0.2	0.5	0.03	0.3	0.3	-	0.02	0.6	-	0.5	0.9	1.4
MIL 090206, 10	B/B-like	avg.	0.07	2.3	7.1	0.68	57.8	5.0	<0.03	0.46	27.1	<0.06	100.5	84.5	24.7
n=27		1σ	0.01	0.1	0.1	0.03	0.3	0.5	-	0.03	0.8	-	0.3	0.2	2.5
MIL 090405, 7	B/B-like	avg.	0.07	2.4	7.1	0.67	56.6	4.7	<0.03	0.44	27.6	n.a.	99.4	84.3	23.3
n=17		1σ	0.01	0.0	0.1	0.03	0.3	0.2	-	0.02	0.3	-	0.4	0.2	0.8

[1]Abbreviations: A = acapulcoite, L = lodranite, B = brachinite, B-like = brachinite-like, an = anomalous

[2]Abbreviation: n.a. = not analyzed

[3]Cr# = Cr/(Cr+Al)*100, Mg# = Mg/(Mg+Fe)*100

Table 4.2.6: Average major- and minor-element composition (in wt. %) of FeNi metals in all meteorites where FeNi compositions are consistent throughout the sample.

Sample	Met. type[1]		Fe	Ni	S	Co	P	Si	Mn[2]	Mg	Al	Ti	Total	Ni/Co
ALHA 81187	A	avg.	93.0	5.76	<0.04	0.48	<0.03	<0.03	<0.04	<0.03	<0.03	<0.03	99.3	12.0
n=18		1σ	0.5	0.23	-	0.02	-	-	-	-	-	-	0.4	
EET 84302	A-L	avg.	92.7	5.66	<0.04	0.46	0.08	<0.03	<0.04	<0.03	<0.03	<0.03	99.0	12.3
n=9		1σ	0.4	0.35	-	0.03	0.04	-	-	-	-	-	0.5	
GRA 95209	L	avg.	92.0	6.11	<0.04	0.43	<0.03	<0.03	<0.04	<0.03	<0.03	<0.03	98.6	14.3
n=9		1σ	0.6	0.12	-	0.02	-	-	-	-	-	-	0.5	
ALH 84025	B	avg.	66.9	30.97	<0.04	1.57	<0.03	<0.03	<0.04	<0.03	<0.03	<0.03	99.6	19.8
n=14		1σ	1.3	1.11	-	0.07	-	-	-	-	-	-	0.4	
LEW 88763	B=like/an	avg.	44.2	53.14	<0.04	1.79	<0.03	<0.03	<0.04	<0.03	0.17	<0.03	99.4	29.7
n=14		1σ	1.2	0.79	-	0.05	-	-	-	-	0.10	-	0.7	
MIL 090206	B/B-like	avg.	93.4	5.43	<0.04	0.50	<0.03	<0.03	<0.04	<0.03	<0.03	<0.03	99.5	10.8
n=28		1σ	0.5	0.42	-	0.06	-	-	-	-	-	-	0.4	
MIL 090405	B/B-like	avg.	94.8	4.00	<0.04	0.40	<0.03	<0.03	n.a.	<0.03	<0.03	<0.03	99.3	10.1
n=18		1σ	0.5	0.65	-	0.02	-	-	-	-	-	-	0.4	

Note: samples with variable Fe and Ni wt. % listed in subsequent tables

[1]Abbreviations: A = acapulcoite, L = lodranite, B = brachinite, B-like = brachinite-like, an = anomalous, U = ureilite

[2]Abbreviation: n.a. = not analyzed

Table 4.2.7: Major- and minor-element composition (in wt. %) of FeNi metals in Acapulco (n=24). One feature to note is the relatively stable Co contents as Fe and Ni contents vary.

Point[1]	Fe	Ni	S	Co	P	Si	Mn	Mg	Al	Ti	Total	Ni/Co
Aca_51	92.7	6.7	<0.04	0.63	0.09	<0.03	<0.04	<0.03	<0.03	<0.03	100.2	10.7
Aca_49	91.8	6.9	<0.04	0.50	0.09	<0.03	<0.04	<0.03	<0.03	<0.03	99.3	13.8
Aca_36	91.7	6.5	<0.04	0.62	0.05	<0.03	<0.04	<0.03	<0.03	<0.03	98.9	10.5
Aca_32	91.7	6.9	<0.04	0.58	0.08	<0.03	<0.04	<0.03	<0.03	<0.03	99.2	11.9
Aca_53	91.6	7.2	<0.04	0.52	0.03	<0.03	<0.04	<0.03	<0.03	<0.03	99.4	13.8
Aca_37	91.5	6.9	<0.04	0.59	0.08	<0.03	<0.04	<0.03	<0.03	<0.03	99.1	11.7
Aca_34	91.3	6.9	<0.04	0.57	0.07	<0.03	<0.04	<0.03	<0.03	<0.03	98.9	12.2
Aca_50	91.2	6.9	<0.04	0.57	0.08	<0.03	<0.04	<0.03	<0.03	<0.03	98.7	12.0
Aca_33	91.2	7.0	<0.04	0.59	0.08	<0.03	<0.04	<0.03	<0.03	<0.03	98.9	11.8
Aca_35	91.0	6.9	<0.04	0.62	0.05	<0.03	<0.04	<0.03	<0.03	<0.03	98.6	11.2
Aca_21	90.8	6.4	<0.04	1.1	<0.03	0.03	<0.04	<0.03	0.05	<0.03	98.4	6.0
Aca_31	90.3	6.9	<0.04	0.57	0.08	<0.03	<0.04	<0.03	<0.03	<0.03	98.0	12.2
Aca_39	89.4	9.6	<0.04	0.47	<0.03	<0.03	<0.04	<0.03	<0.03	<0.03	99.5	20.3
Aca_46	88.8	9.7	<0.04	0.51	<0.03	<0.03	<0.04	<0.03	<0.03	<0.03	99.1	19.1
Aca_45	88.5	10.2	<0.04	0.44	<0.03	<0.03	<0.04	<0.03	<0.03	<0.03	99.1	23.2
Aca_38	88.1	9.6	<0.04	0.47	<0.03	<0.03	<0.04	<0.03	<0.03	<0.03	98.1	20.3
Aca_47	87.2	11.4	<0.04	0.38	0.04	<0.03	<0.04	<0.03	<0.03	<0.03	99.1	29.9
Aca_48	87.1	11.3	<0.04	0.43	<0.03	<0.03	<0.04	<0.03	<0.03	<0.03	98.8	26.4
Aca_43	83.7	15.1	<0.04	0.35	<0.03	<0.03	<0.04	<0.03	0.06	<0.03	99.3	43.4
Aca_41	82.1	15.7	<0.04	0.32	<0.03	<0.03	<0.04	<0.03	<0.03	<0.03	98.2	48.5
Aca_44	80.8	18.1	<0.04	0.30	<0.03	<0.03	<0.04	<0.03	<0.03	<0.03	99.2	60.8
Aca_42	80.1	17.9	<0.04	0.28	0.03	0.04	<0.04	<0.03	<0.03	<0.03	98.5	63.4
Aca_40	72.9	25.8	<0.04	0.28	<0.03	<0.03	<0.04	<0.03	<0.03	<0.03	99.0	91.0
Aca_52	70.2	28.0	<0.04	0.29	<0.03	<0.03	<0.04	<0.03	<0.03	<0.03	98.6	98.2
avg.	87.3	11.0	-	0.5	-	-	-	-	-	-	98.9	28.4
1σ	6.1	6.1	-	0.2	-	-	-	-	-	-	0.5	25.9

[1]"Point" column contains labeling information specific to the author, but is included here in order to distinguish individual points

Table 4.2.8: Major- and minor-element composition (in wt. %) of FeNi metals in MET 01195, 33 (n=13). As in Acapulco, Co contents remain relatively stable as Fe and Ni contents vary.

Point[1]	Fe	Ni	S	Co	P	Si	Mn	Mg	Al	Ti	Total	Ni/Co
MET01195_38	92.2	6.7	<0.04	0.49	0.14	<0.03	<0.04	<0.03	<0.03	<0.03	99.5	13.6
MET01195_41	92.1	7.0	<0.04	0.39	0.04	<0.03	<0.04	<0.03	<0.03	<0.03	99.5	18.0
MET01195_36	91.2	6.8	<0.04	0.44	0.13	<0.03	<0.04	<0.03	<0.03	<0.03	98.6	15.7
MET01195_22	91.1	6.9	<0.04	0.43	0.03	<0.03	<0.04	<0.03	<0.03	<0.03	98.5	16.2
MET01195_1	90.9	6.7	<0.04	0.53	<0.03	<0.03	<0.04	<0.03	<0.03	<0.03	98.2	12.7
MET01195_35	90.9	6.8	<0.04	0.48	0.15	<0.03	<0.04	<0.03	<0.03	<0.03	98.3	14.2
MET01195_3	90.8	6.8	<0.04	0.49	<0.03	<0.03	<0.04	<0.03	<0.03	<0.03	98.2	13.8
MET01195_24	90.8	7.1	<0.04	0.45	0.06	<0.03	<0.04	<0.03	<0.03	<0.03	98.4	15.9
MET01195_23	90.6	7.2	<0.04	0.49	0.07	<0.03	<0.04	<0.03	<0.03	<0.03	98.5	14.7
MET01195_40	83.2	15.7	<0.04	0.3	<0.03	<0.03	<0.04	<0.03	<0.03	<0.03	99.1	56.9
MET01195_39	82.1	16.4	<0.04	0.30	<0.03	<0.03	<0.04	<0.03	<0.03	<0.03	98.9	54.6
MET01195_20	76.7	22.0	<0.04	0.22	<0.03	<0.03	<0.04	<0.03	<0.03	<0.03	99.1	100.3
MET01195_21	75.7	23.2	<0.04	0.20	<0.03	<0.03	<0.04	<0.03	<0.03	<0.03	99.1	117.5
avg.	87.6	10.7	-	0.4	-	-	-	-	-	-	98.8	35.7
1σ	6.0	6.3	-	0.1	-	-	-	-	-	-	0.5	36.0

[1]"Point" column contains labeling information specific to the author, but is included here in order to distinguish individual points

Table 4.2.9: Major- and minor-element composition (in wt. %) of FeNi metals in MIL 091004, 7 (n=25). Metals have been organized into group based on their Si contents. Among these groups Fe and Ni contents remain stable. Throughout the sample, Co contents remain stable as Fe and Ni contents vary with Si content.

	Point[1]	Si	Fe	Ni	S	Co	P	Mg	Al	Ti	Total	Ni/Co	D from C-rich region (mm)[2]
~11.0% Si group	M_118	11.2	84.9	1.9	<0.04	0.1	0.2	<0.03	<0.03	<0.03	98.3	13.8	0
	M_117	11.2	85.2	1.9	<0.04	0.1	0.1	<0.03	<0.03	<0.03	98.6	14.7	0
	M_108	11.2	85.4	1.9	<0.04	0.1	0.2	<0.03	<0.03	<0.03	98.7	14.8	0
	M_119	11.1	85.5	1.8	<0.04	0.1	0.2	<0.03	<0.03	<0.03	98.8	15.7	0
	avg.	11.2	85.2	1.9	-	0.1	0.2	-	-	-	98.6	14.7	-
	1σ	0.02	0.2	0.03	-	0.01	0.03	-	-	-	0.2	0.8	-
~3.5% Si group	L_103	4.1	93.2	1.9	<0.04	0.1	0.5	<0.03	<0.03	<0.03	99.8	14.4	0
	L_104	3.8	93.2	2.2	<0.04	0.1	0.4	<0.03	<0.03	<0.03	99.8	16.4	0
	M_107	3.8	93.3	2.1	<0.04	0.2	0.4	<0.03	<0.03	<0.03	99.8	13.4	0
	L_101	3.7	93.2	1.9	<0.04	0.1	0.4	<0.03	<0.03	<0.03	99.4	15.8	0
	L_100	3.7	93.4	2.0	<0.04	0.1	0.3	<0.03	<0.03	<0.03	99.5	14.2	0
	L_102	3.6	94.2	1.9	<0.04	0.2	0.4	<0.03	<0.03	<0.03	100.4	12.2	0
	M_105	3.6	93.9	2.3	<0.04	0.1	0.4	<0.03	<0.03	<0.03	100.4	17.4	0
	M_106	3.5	93.9	2.1	<0.04	0.1	0.4	<0.03	<0.03	<0.03	100.1	14.7	0
	avg.	3.7	93.5	2.1	-	0.1	0.4	-	-	-	99.9	14.8	-
	1σ	0.2	0.4	0.1	-	0.01	0.1	-	-	-	0.4	1.7	-
~1.5% Si group	D_5	1.8	95.0	2.0	<0.04	0.1	0.9	<0.03	<0.03	<0.03	99.7	14.3	5.79
	D_4	1.8	94.8	1.9	<0.04	0.2	0.8	<0.03	<0.03	<0.03	99.5	12.3	5.81
	D_3	1.8	95.6	1.9	<0.04	0.2	0.8	<0.03	<0.03	<0.03	100.3	11.6	5.87
	B_85	1.5	95.2	2.0	<0.04	0.2	0.9	<0.03	<0.03	<0.03	99.9	12.2	8.08
	A_6	1.5	96.0	1.9	<0.04	0.2	0.7	<0.03	<0.03	<0.03	100.2	11.9	6.92
	B_90	1.5	95.1	2.0	<0.04	0.2	0.9	<0.03	<0.03	<0.03	99.7	12.7	8.22
	A_7	1.5	95.2	1.9	<0.04	0.1	0.7	<0.03	<0.03	<0.03	99.4	12.6	6.84
	B_86	1.4	94.9	2.0	<0.04	0.2	1.1	<0.03	<0.03	<0.03	99.5	12.3	8.24
	C_14	1.4	95.9	2.0	<0.04	0.2	1.0	<0.03	<0.03	<0.03	100.4	12.6	7.64
	A_8	1.4	95.5	1.9	<0.04	0.1	0.8	<0.03	<0.03	<0.03	99.8	15.0	6.74
	C_16	1.4	95.9	2.0	<0.04	0.1	0.9	<0.03	<0.03	<0.03	100.4	13.5	7.69
	A_9	1.3	95.5	2.0	<0.04	0.1	1.0	<0.03	<0.03	<0.03	99.9	14.5	7.00
	C_15	1.3	96.2	2.0	<0.04	0.2	1.0	<0.03	<0.03	<0.03	100.7	12.7	7.62
	avg.	1.5	95.4	2.0	-	0.2	0.9	-	-	-	100.0	12.9	7.1
	1σ	0.2	0.5	0.04	-	0.01	0.1	-	-	-	0.4	1.1	0.9

[1]"Point" column contains labeling information specific to the author, but is included here in order to distinguish individual points

[2]Distance from carbon-rich region was measured using *Microsoft Photoshop*. The distance from each analysis spot to the nearest point in an outline of the carbon-rich region was calculated.

Table 4.2.10: Average major- and minor-element composition (in wt. %) of FeS metals.

Sample	Met. type[1]		S	Fe	Co	Ni	P	Si	Mn[2]	Mg	Al	Ti	Cr[2]	Total
Acapulco	A	avg.	36.7	62.4	<0.05	<0.05	<0.03	<0.03	<0.04	<0.03	<0.03	<0.03	n.a.	99.2
n=12		1σ	0.4	0.3	-	-	-	-	-	-	-	-	-	0.5
ALHA 81187, 7	A	avg.	37.2	62.7	<0.05	<0.05	<0.03	<0.03	<0.04	<0.03	<0.03	<0.03	n.a.	99.9
n=6		1σ	0.4	0.3	-	-	-	-	-	-	-	-	-	0.3
MET 01195, 33	A	avg.	36.6	62.5	<0.05	<0.05	<0.03	<0.03	<0.04	<0.03	<0.03	<0.03	n.a.	99.1
n=12		1σ	0.2	0.1	-	-	-	-	-	-	-	-	-	0.3
EET 84302, 28	A-L	avg.	36.5	62.3	<0.05	<0.05	<0.03	<0.03	<0.04	<0.03	<0.03	<0.03	n.a.	98.9
n=6		1σ	0.1	0.1	-	-	-	-	-	-	-	-	-	0.1
GRA 95209, 218	L	avg.	36.7	62.7	<0.05	<0.05	<0.03	<0.03	<0.04	<0.03	<0.03	<0.03	n.a.	99.4
n=11		1σ	0.8	0.3	-	-	-	-	-	-	-	-	-	0.9
ALH 84025, 6	B	avg.	36.5	60.2	<0.05	<0.05	<0.03	<0.03	<0.04	<0.03	<0.03	<0.03	n.a.	99.4
n=20		1σ	1.1	6.6	-	-	-	-	-	-	-	-	-	0.7
LEW 88763, 14	B-like/an	avg.	36.1	62.1	0.14	0.90	<0.03	<0.03	<0.04	<0.03	<0.03	<0.03	n.a.	99.2
n=15		1σ	0.2	0.6	0.06	0.57	-	-	-	-	-	-	-	0.4
MIL 090206, 10	B/B-like	avg.	36.2	63.1	<0.05	<0.05	<0.03	<0.03	<0.04	<0.03	<0.03	<0.03	n.a.	99.4
n=34		1σ	0.6	0.5	-	-	-	-	-	-	-	-	-	0.8
MIL 090405, 7	B/B-like	avg.	36.3	62.9	<0.05	<0.05	<0.03	<0.03	n.a.	<0.03	<0.03	<0.03	n.a.	99.3
n=14		1σ	0.3	0.3	-	-	-	-	-	-	-	-	-	0.5
MIL 091004, 7	U	avg.	36.5	55.7	<0.05	<0.05	<0.03	<0.03	0.26	<0.03	<0.03	0.11	6.0	98.7
n=8		1σ	0.1	0.6	-	-	-	-	0.06	-	-	0.03	0.5	0.2

[1]Abbreviations: A = acapulcoite, L = lodranite, B = brachinite, B-like = brachinite-like, an = anomalous, U = ureilite

[2]Abbreviation: n.a. = not analyzed

Table 4.2.11: Average major- and minor-element composition (in wt. %) of schreibersites in all samples that contain them.

Sample	Met. type[1]		Fe	Ni	P	S	Co	Si	Mn[2]	Mg	Al	Ti	Total
ALHA 81187, 7	A	avg.	43.1	41.6	15.2	<0.04	0.08	<0.03	<0.04	<0.03	<0.03	<0.03	100.0
n=7		1σ	6.0	5.9	0.1	-	0.02	-	-	-	-	-	0.4
MET 01195, 33	A	avg.	35.5	49.5	15.2	<0.04	<0.05	<0.03	<0.04	<0.03	<0.03	<0.03	100.4
n=5		1σ	1.0	0.9	0.1	-	-	-	-	-	-	-	0.2
EET 84302, 28	A-L	avg.	53.7	31.1	15.4	<0.04	0.12	<0.03	<0.04	<0.03	<0.03	<0.03	100.4
n=6		1σ	3.9	3.8	0.0	-	0.01	-	-	-	-	-	0.1
MIL 091004, 7	U	avg.	82.1	2.4	15.1	0.21	0.11	0.13	n.a.	<0.03	<0.03	<0.03	100.1
n=8		1σ	0.3	0.0	0.1	0.03	0.02	0.02	-	-	-	-	0.2

[1]Abbreviations: A = acapulcoite, L = lodranite, U = ureilite

[2]Abbreviation: n.a. = not analyzed

4.3 Whole-rock major- and trace-element chemistry

Acapulcoites and lodranites – Trace-element abundances were analyzed in eight different acapulcoite-lodranites (two separates of NWA 2871 gave nine total acapulcoite-lodranite analyses) and values are exceptionally unfractionated when normalized to data for chondrite Ivuna (McDonough and Sun 1995). When comparing multi-element trace element plots for acapulcoite-lodranites (Figure 4.3.2) and ordinary and carbonaceous chondrites measured in this study (Figure 4.3.1), similar flat patterns are observed. There are also a number of similar element anomalies (negative Cs, occasional positive Ba, and occasional positive U). Rare earth element abundances are particularly chondrite-like with chondrite Ivuna normalized values ranging between 0.3 and 2.6, and La/Yb ratios ranging from 0.656 (NWA 2871, smaller mass) to 4.039 (NWA 4833). Eight out of the nine analyses display at least a small positive Eu anomaly (Eu/Sm ratios between 1.0 and 2.2), which is consistent with previous studies' reports of samples in the group containing plagioclase. MET 01195, the single acapulcoite-lodranite with a negative Eu anomaly, has a Eu/Sm ratio of 0.880. The desert meteorite NWA 4875 displays interesting negative Zr and Hf anomalies more pronounced than the rest of the acapulcoite-lodranites. The Zr/Hf ratio of the meteorite is positive, whereas the rest of the group displays negative Zr/Hf.

ALH 84025, MIL 090206, and MIL 090405 – In the following descriptions of trace element abundances for ALH 84025, MIL 090206, and MIL 090405, data and ranges for "brachinites and brachinite-like achondrites" are taken from Day et al. 2012.

The meteorite ALH 84025 is trace element depleted relative to chondrite Ivuna. Its multi-element plot (Figure 4.3.3) lies within ranges for previously analyzed

brachinites and brachinite-like achondrites and displays marked positive Sc and Ta anomalies. Only Sc and Ta abundances are above those of Ivuna's. ALH 84025's depleted REE pattern (La/Yb = 0.076) also lies within ranges for brachinites and brachinite-like achondrites and displays a negative Eu anomaly (Eu/Sm = 0.435). All REE normalized values lie between 0.1 and 1, except for Ta, which has a value of 0.069.

Two separate powder masses of MIL 090206 were analyzed (38.90 and 20.75 mg) and trace element abundances agree very well with each other (Table 4.3.3 and Figure 4.3.3) attesting to possible homogeneity in the meteorite. Abundances also agree well with previously published values for brachinites and brachinite-like achondrites. A multi-element plot of MIL 090206 shows significant anomalies, the most pronounced being positive Nb, Ta and Ti, and negative Sr and Eu. These anomalies largely mirror the anomalies seen in plots of the ungrouped brachinite-like pair GRA 06128/9. The same large negative Eu anomaly (Eu/Sm = 0.368 and 0.322) is observed in the REE plot for MIL 090206. The meteorite's REEs plot towards the more depleted side of the range for brachinite and brachinite-like achondrites with La/Yb ratios of 0.054 and 0.125. The higher of the two La/Yb ratios is somewhat deceiving as a measure of depletion in that a positive La anomaly masks the extent of depletion in the rest of the REEs.

Two analyses of MIL 090405 powder (38.32 and 40.47 mg) produced depleted trace element abundances very similar to each other, attesting to homogeneity in the measured meteorite fragment. Abundances lie within the range for brachinites and brachinite-like achondrites and are also similar to the abundances for ALH 84025, except with slightly differing significant anomalies in a multi-element plot (positive Ba, Nb, and Ta for MIL 090405). The two MIL 090405 REE plots show depleted patterns (La/Yb =

0.110 and 0.120) and are also very similar to ALH 84025's REE plot, except with less negative Eu anomalies (Eu/Sm = 0.895 and 0.867). MIL 090405 REEs plot well within the range for brachinites and brachinite-like achondrites.

LEW 88763 – Trace element abundances in LEW 88763 are chondrite-like. The meteorite's multi trace-element plot (Figure 4.3.3) is remarkably similar to acapulcoite-lodranites (Figure 4.3.2) as well as chondrites (Figure 4.3.1) with the same negative Cs anomaly. LEW 88763 also has a slight positive U anomaly (normalized U = 2.969). Although LEW 88763 has been previously classified as a brachinite, its slightly enriched trace element abundances are distinct from many members of the group (although meteorite Brachina also has a chondritic pattern). Relative to chondrite Ivuna, the brachinite ALH 84025 and the ungrouped achondrites MIL 090206 and MIL 090405 (which are likely brachinites) are generally depleted in most trace elements, whereas LEW 88763 is enriched in every trace element except for Rb and Cs. The REE pattern for LEW 88763 is similarly unfractionated and chondritic. Normalized values for REEs remain between 1.3 and 1.6, with a La/Yb ratio of 1.003. Lewis Cliff 88763 contains ~10 % plagioclase (Swindle et al. 1998), yet the REE pattern reported here shows only a small positive Eu anomaly (Eu/Sm ratio = 1.059). Swindle et al. (1998) analyzed three splits of LEW 88763 for a number of trace elements, including some of the REEs. An average of the three splits produce a La/Yb ratio (1.097) that is similar to our value, and a Eu/Sm ratio (1.736) that is distinctively different than ours. The difference in the Eu/Sm is likely explained by higher sampling of plagioclase in the study by Swindle et al. – their study analyzed a total of 208.63 mg of material over the three splits, whereas we analyzed 15.77 mg of material.

MIL 091004 – Two MIL 091004 whole-rock powder separates (40.82 and 21.03 mg) were analyzed in this study for trace-element abundances. Absolute and relative abundances of trace elements in MIL 091004 are consistent with those reported for ureilites (e.g., Spitz and Boynton 1991). As with other ureilites, the rare earth element (REE) patterns for MIL 091004 are depleted relative to chondrite Ivuna, which is consistent with the meteorite representing a residue after partial melting (La/Yb ratios are 0.011 and 0.059 for the 21.03 and 40.82 mg separates, respectively). Each separate displayed a small negative Eu anomaly and a small positive Sm anomaly. The 40.82 mg powder separate (as well as ureilites with previously published data) showed enrichments in the light REEs (LREEs), suggesting later melt infiltration (c.f., auto-fertilization).

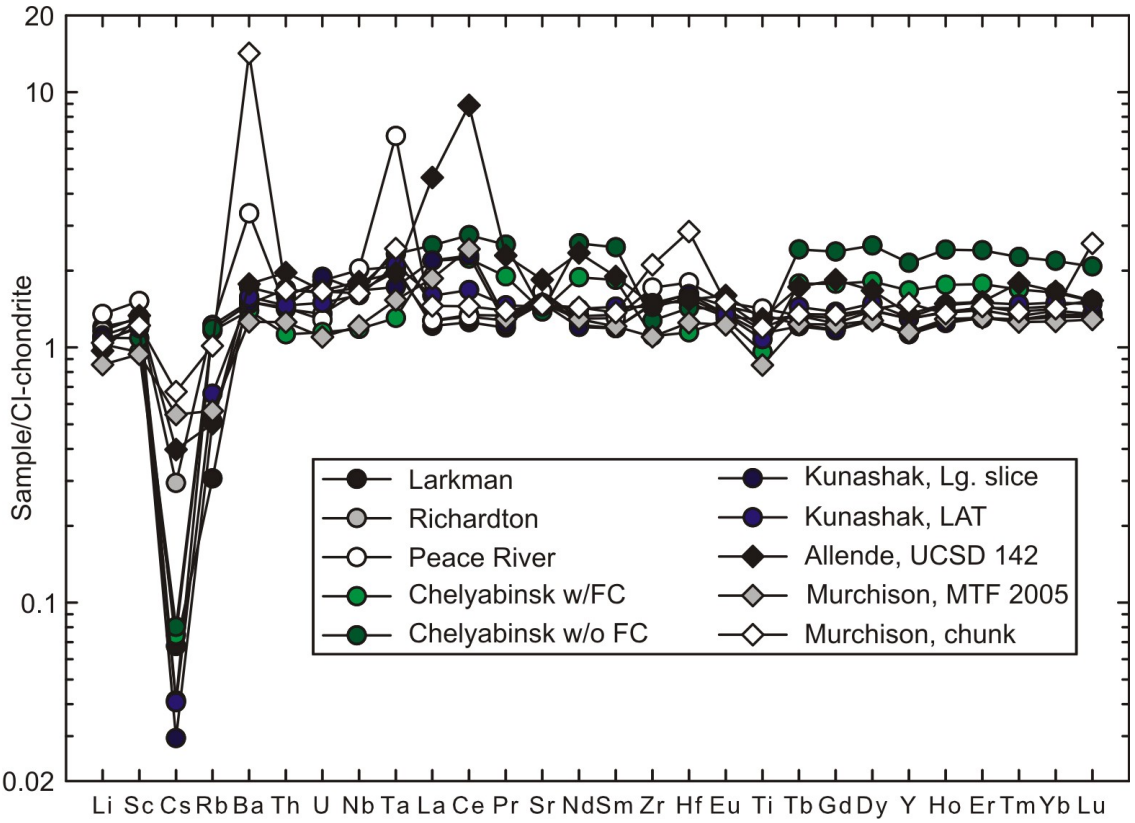

Figure 4.3.1: Trace multi-element plot for ordinary (circles) and carbonaceous (diamonds) chondrites normalized to CI-chondrite Ivuna. All data (except for chondrite Ivuna data from McDonough and Sun, 1995) are from this study.

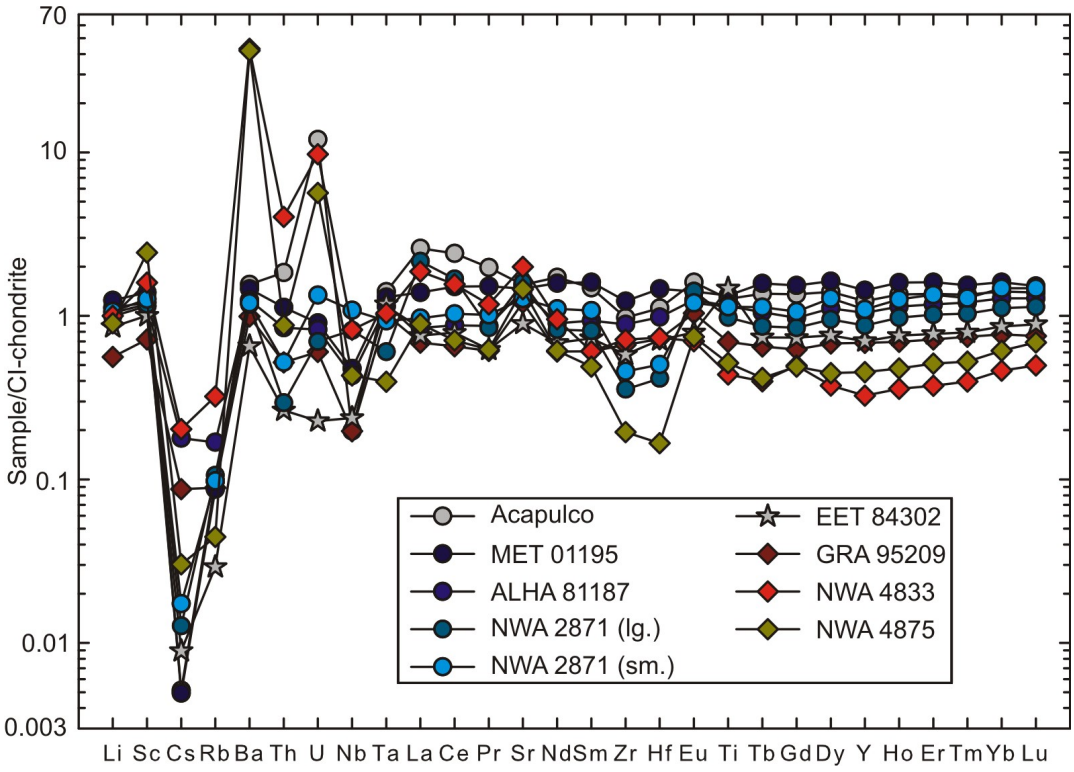

Figure 4.3.2: Trace multi-element plot for acapulcoite-lodranites normalized to CI-chondrite Ivuna. Samples plotted with circles are acapulcoites, samples plotted with diamonds are lodranites, and EET 84302 – a transitional acapulcoite-lodranite – is plotted with stars. All data (except for chondrite Ivuna data from McDonough and Sun, 1995) are from this study.

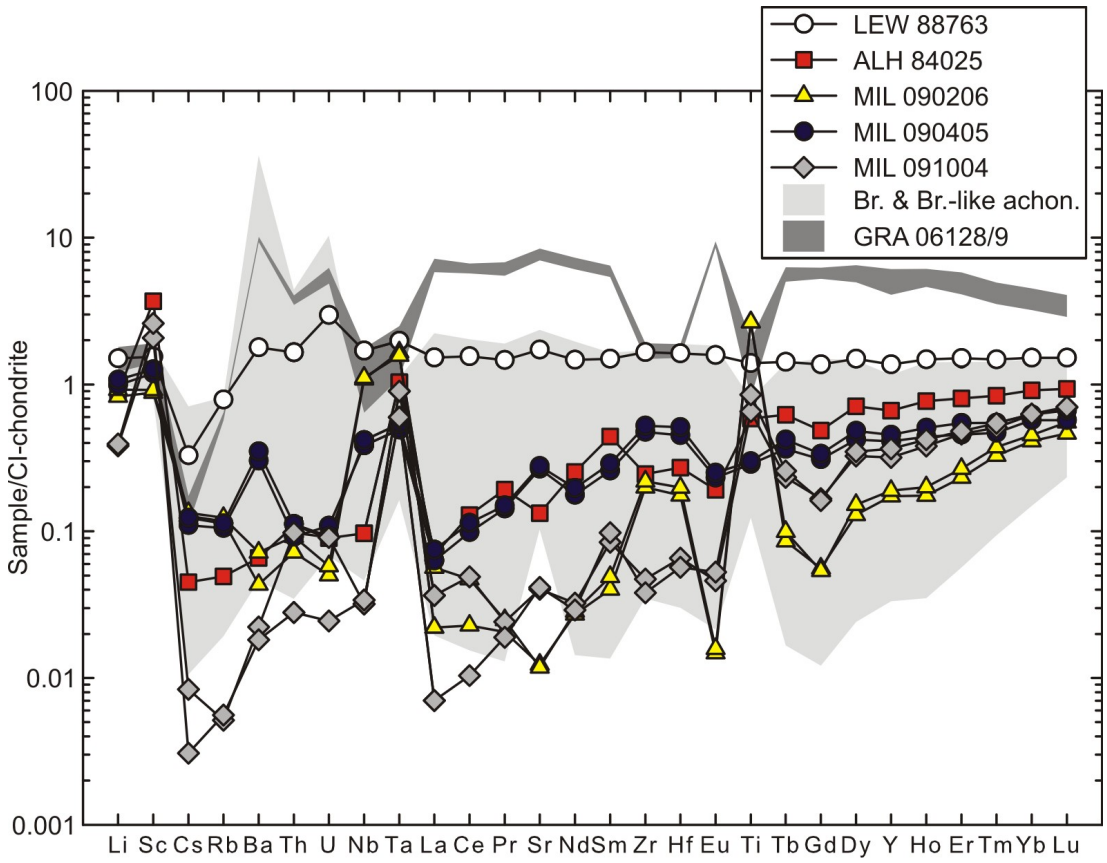

Figure 4.3.3: Trace multi-element plot for LEW 88763, ALH 84025, MIL 090206, MIL 090405, and MIL 091004 with fields for GRA 06128/9 and brachinites and brachinite-like achondrites. Data for all plots are from this study, and data for fields are from Day et al. 2012.

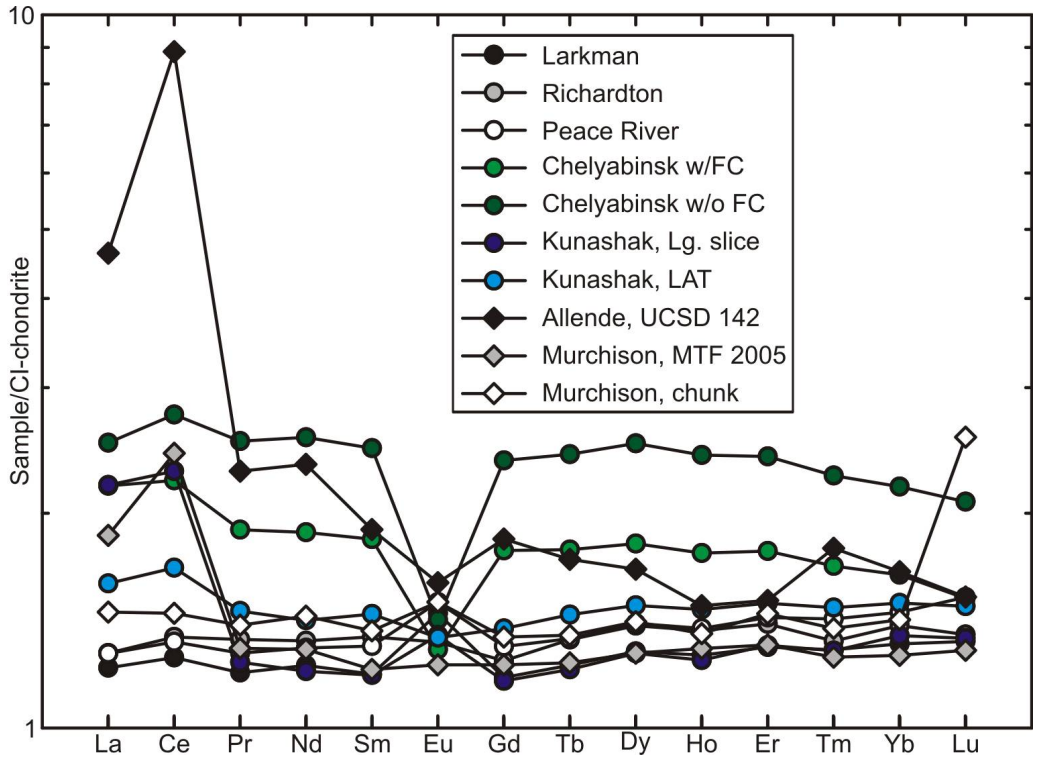

Figure 4.3.4: Rare earth element abundances of ordinary (circles) and carbonaceous (diamonds) chondrites normalized to CI-chondrite Ivuna. All data (except for chondrite Ivuna data from McDonough and Sun, 1995) are from this study.

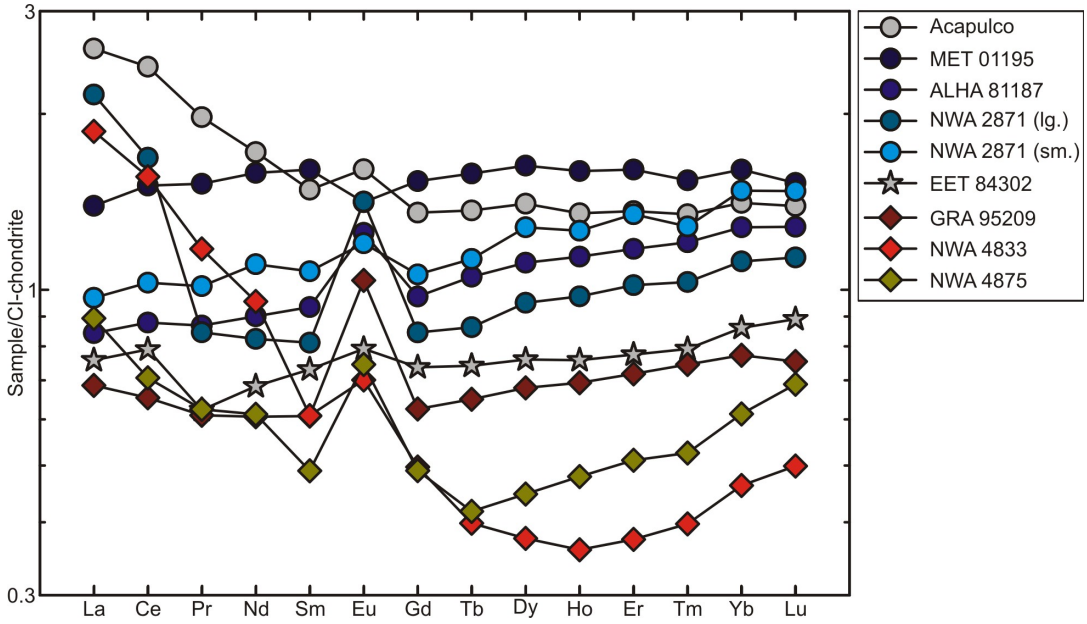

Figure 4.3.5: Rare earth element abundances of acapulcoite-lodranites normalized to CI-chondrite Ivuna. Acapulcoite-lodranite meteorites have largely chondritic REE patterns, with varying degrees of slight overall depletion or enrichment, as well as varying degrees of both positive and negative Eu anomalies. Samples plotted with circles are acapulcoites, samples plotted with diamonds are lodranites, and EET 84302 – a transitional acapulcoite-lodranite – is plotted with stars. All data (except for chondrite Ivuna data from McDonough and Sun, 1995) are from this study.

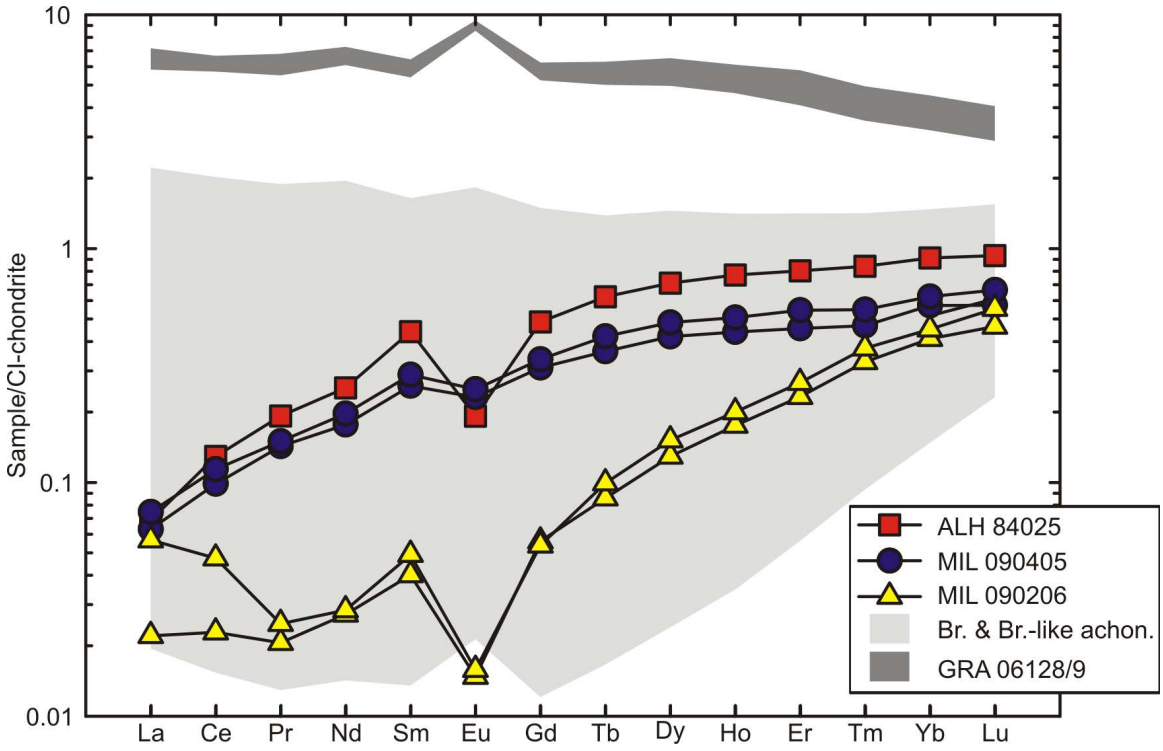

Figure 4.3.6: Rare earth element abundances of brachinites, brachinite-like achondrites, and ungrouped achondrites (likely to be classified as brachinites in future) normalized to chondrite Ivuna. The abbreviation "Br. & Br.-like achon." labels the range of values of brachinites and brachinite-like achondrites studied by Day et al. (2012). The field for GRA (Graves Nunataks) 06128/9 is also taken from data found in Day et al. (2012). Data for ALH 84025 and MIL samples are from this study and data for chondrite Ivuna used to normalize is from McDonough and Sun (1995).

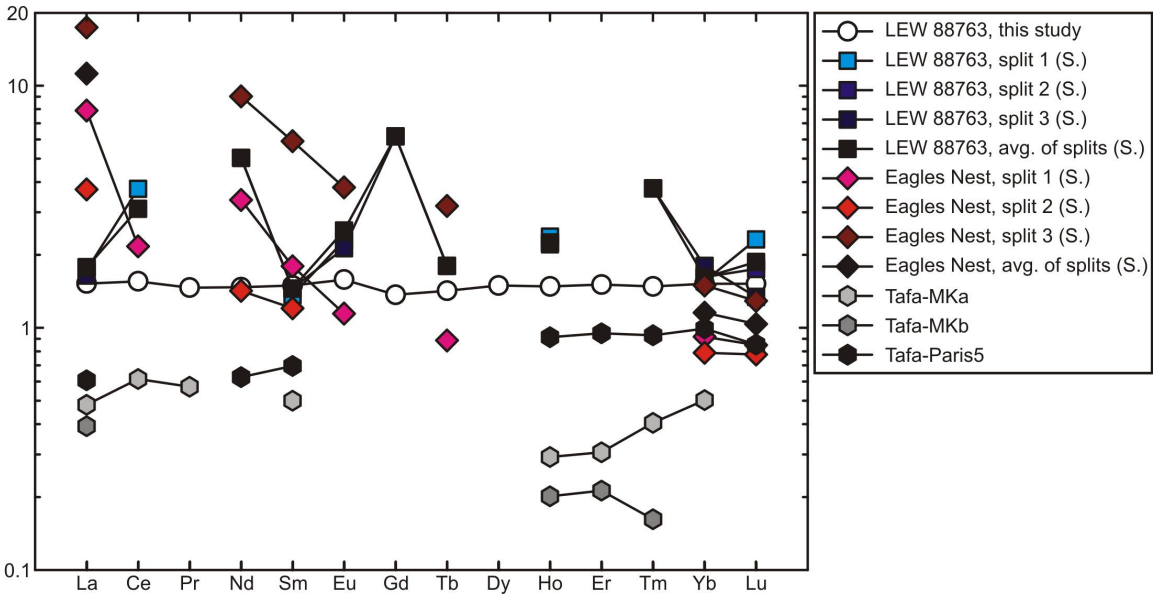

Figure 4.3.7: Rare earth element abundances of LEW 88763 (this study and Swindle et al. 1998), Eagles Nest (Swindle et al. 1998), and Tafassasset (Gardner-Vandy et al. 2012) normalized to chondrite Ivuna. The analysis of LEW 88763 reported in this study (white circles) produced unfractionated chondrite-like values. LEW 88763 has been compared to Eagles Nest and Tafassasset, but scarcity of data make comparisons using REE abundances difficult.

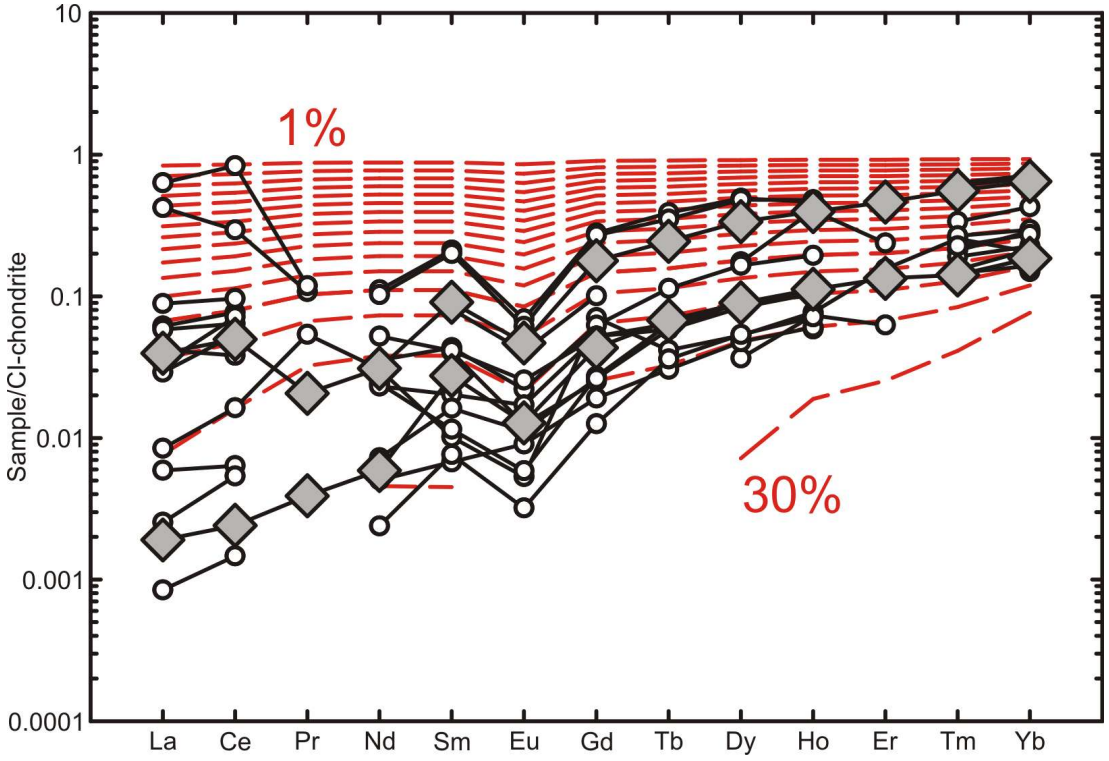

Figure 4.3.8: Chondrite Ivuna normalized rare Earth element patterns for MIL 091004, 4 (gray diamonds) versus published ureilite data (unfilled circles, Spitz and Boynton 1991) showing a residue depletion model (dashed red lines) assuming 70 % olivine, 25 % orthopyroxene, 5 % clinopyroxene and melting proportions 0.2/0.3/0.5. Residues after 1-30 % partial melting are shown.

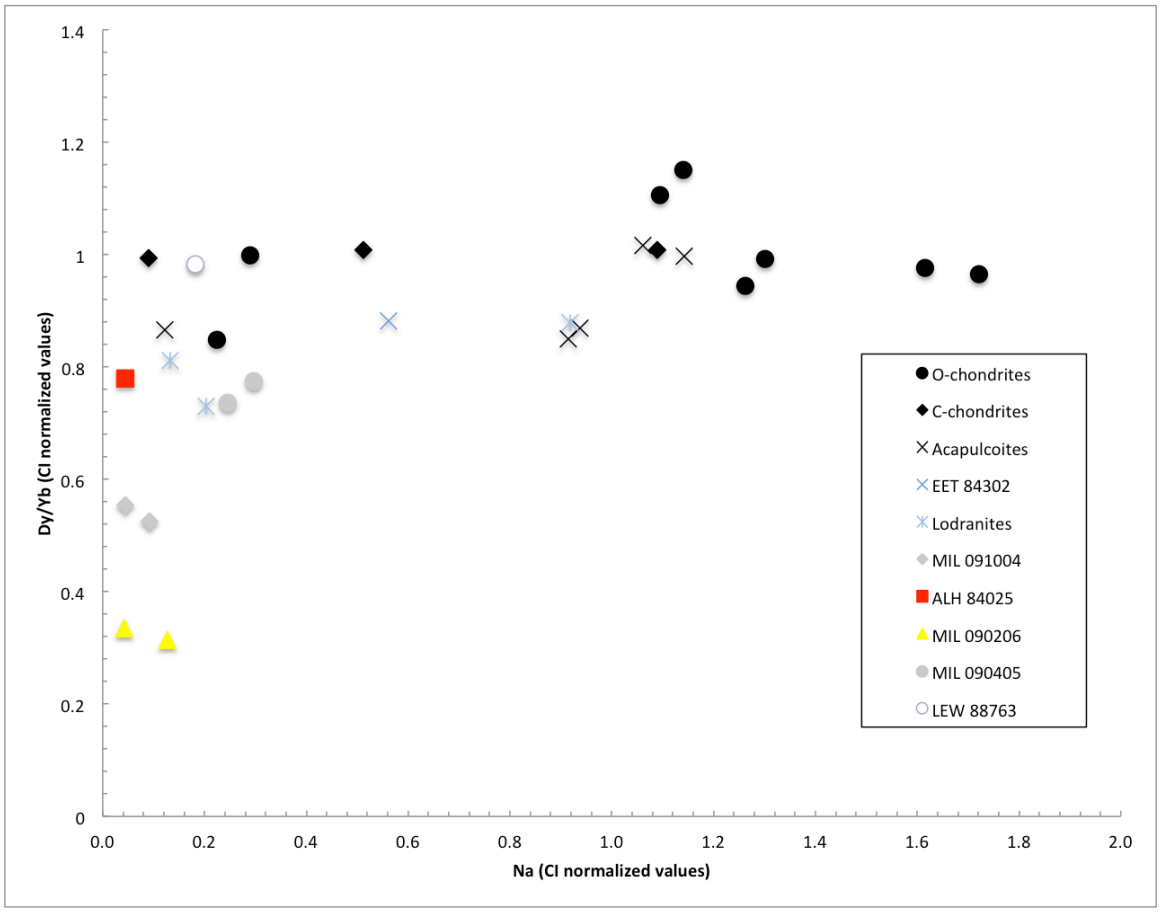

Figure 4.3.9: Whole-rock Na compositions plotted against whole-rock Dy/Yb ratios. Abbreviations: O-chondrites = ordinary chondrites, C-chondrites = carbonaceous chondrites. All data are from this study.

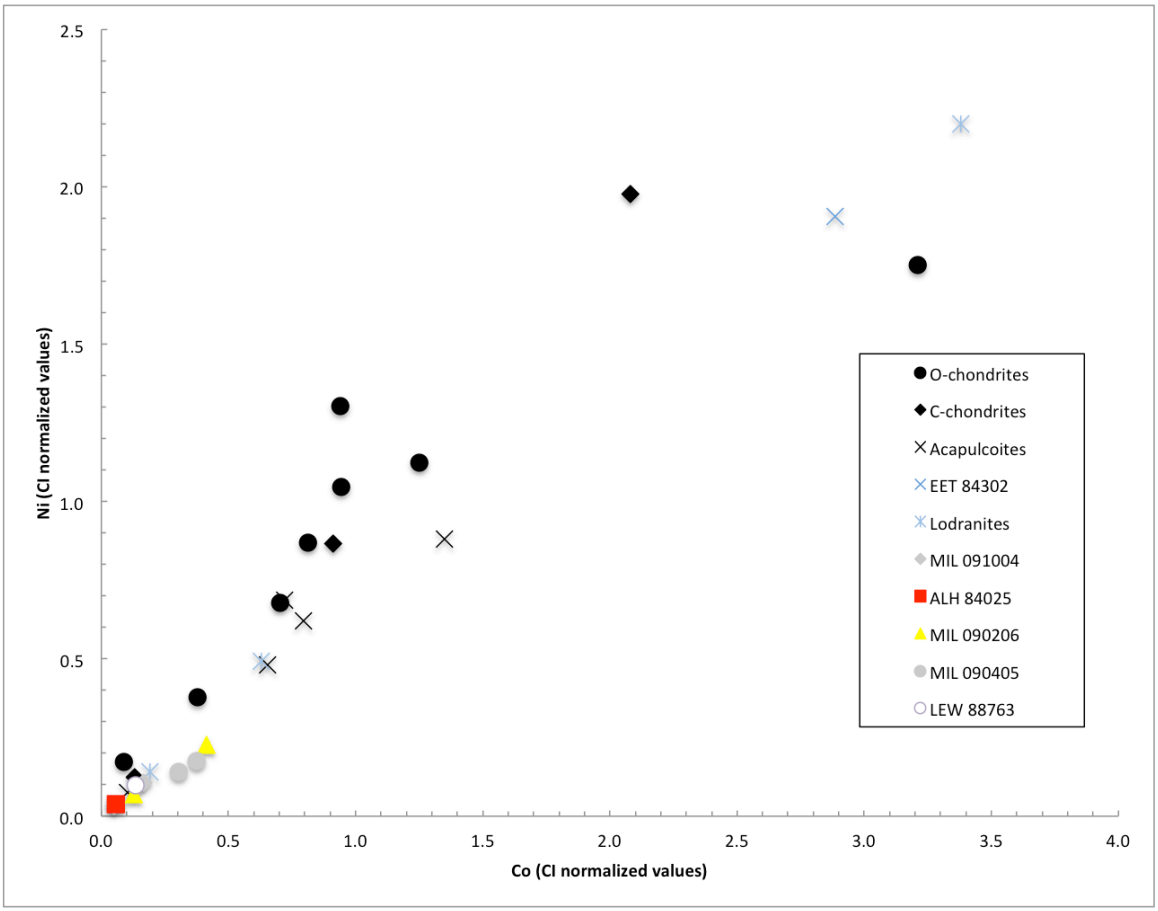

Figure 4.3.10: Whole-rock Co vs. Ni plot. Abbreviations: O-chondrites = ordinary chondrites, C-chondrites = carbonaceous chondrites. All data are from this study.

Table 4.3.1: Whole-rock trace-element abundances in chondrite meteorite samples and BHVO-2 standard (in μg g^{-1}).

Sample ID	Allende UCSD 142	Murchison chunk	Murchison MTF 2005, vlc	Chelyabinsk w/FC	Chelyabinsk w/o FC	Kunashak LAT	Kunashak slice	Peace River chunk	Larkman 3 fragments	NWA 869 chunk	Richardton chunk	BHVO-2[2] *(n=4)*	BHVO-2 Stdev[2] *1σ*
Met. Type[1]	CV3	CM2	CM2	O - LL5	O - LL5	O - L6	O - L6	O - L6	O	O - L3-6	O - H5	-	-
Li	1.46	1.56	1.28	1.54	1.64	1.60	1.67	2.03	1.81	3.57	1.74	4.75	0.128
P	937	992	739	1128	1440	932	825	839	912	950	1083	1180	33
Sc	7.9	7.2	5.6	5.7	6.4	7.0	7.4	9.0	7.6	8.2	7.8	32	1.1
Ti	570	530	380	420	510	470	500	620	591	530	560	16500	799
V	59	70	42	57	52	54	56	68.6	64	60	69	320	16
Cr	2700	2800	1900	3200	2700	2700	2800	3200	3300	2800	3700	310	15
Ni	7600	7500	5300	13400	8723.4	5400	4400	6100	6600	7917.5	12900	120	6
Cu	89	115	82	110	86	54	52	55	73	102	100	130	6
Zn	75	152	116	47	38	29	29	52	36	45	68	105	4.4
Ga	4.8	8.0	6.0	5.0	4.4	4.5	4.5	4.9	4.7	5.2	6.8	22	1
Ge	5.7	8.9	6.6	9	5.0	3.6	3.3	4.1	4.9	4.1	6.4	1.7	0.08
Rb	1.16	2.33	1.30	2.67	2.72	1.51	1.18	2.79	0.70	2.71	2.81	10.0	0.30
Sr	13.4	10.6	10.8	10.1	10.0	10.5	10.8	12.0	11.9	65	10.8	410	10
Y	2.12	2.34	1.80	2.62	3.36	2.06	1.76	2.03	1.78	1.47	2.04	26.0	0.65
Zr	5.6	8.1	4.2	4.22	4.9	5.5	5.7	6.5	5.6	6.2	5.8	171	4.8
Nb	0.43	0.39	0.29	0.28	0.41	0.38	0.40	0.49	0.48	0.38	0.40	18.1	0.39
Cs	0.076	0.128	0.104	0.0142	0.0152	0.0077	0.0056	0.0078	0.0128	0.0098	0.056	0.100	0.0039
Ba	4.27	34.2	3.03	3.36	3.56	3.79	3.63	8.07	4.14	205	3.64	139	2.2
La	1.10	0.345	0.441	0.52	0.60	0.378	0.52	0.301	0.288	0.267	0.302	15.1	0.33
Ce	5.44	0.89	1.49	1.36	1.69	1.03	1.40	0.81	0.77	0.67	0.82	37.1	0.70
Pr	0.213	0.129	0.120	0.176	0.234	0.135	0.115	0.118	0.111	0.095	0.123	5.3	0.12
Nd	1.07	0.66	0.59	0.86	1.17	0.65	0.55	0.59	0.56	0.467	0.61	24.3	0.54
Sm	0.281	0.203	0.179	0.272	0.365	0.214	0.176	0.193	0.176	0.158	0.199	6.0	0.16
Eu	0.090	0.085	0.069	0.073	0.080	0.075	0.076	0.084	0.082	0.132	0.074	2.05	0.047
Gd	0.366	0.267	0.244	0.353	0.47	0.274	0.232	0.259	0.234	0.200	0.247	6.2	0.13
Tb	0.062	0.049	0.045	0.064	0.087	0.052	0.044	0.048	0.044	0.0367	0.048	0.91	0.021
Dy	0.41	0.347	0.313	0.45	0.62	0.365	0.313	0.345	0.315	0.253	0.342	5.3	0.12
Ho	0.081	0.074	0.071	0.096	0.132	0.080	0.068	0.075	0.069	0.056	0.075	0.97	0.024
Er	0.241	0.231	0.209	0.283	0.38	0.239	0.209	0.229	0.208	0.164	0.224	2.52	0.064
Tm	0.044	0.034	0.0310	0.042	0.056	0.036	0.0317	0.035	0.0318	0.0266	0.033	0.33	0.009
Yb	0.267	0.228	0.203	0.264	0.351	0.241	0.217	0.234	0.211	0.195	0.224	1.97	0.056
Lu	0.038	0.063	0.0316	0.037	0.051	0.036	0.0329	0.038	0.0325	0.0282	0.0332	0.271	0.0073
Hf	0.158	0.29	0.129	0.118	0.147	0.160	0.166	0.185	0.166	0.188	0.154	4.3	0.10
Ta	0.027	0.033	0.0208	0.0177	0.032	0.029	0.0234	0.091	0.028	0.031	0.027	1.12	0.024
Th	0.057	0.048	0.036	0.033	0.049	0.042	0.042	0.042	0.046	0.044	0.041	1.21	0.057
U	0.123	0.123	0.081	0.085	0.121	0.111	0.140	0.095	0.135	0.93	0.100	4.0	0.12

[1]Meteorite type abbreviations: C=carbonaceous chondrite, V=Vigarano type, M=Mighei type, O=ordinary chondrite, LL=low-iron, low-metal, L=low-iron, H=high-iron, numbers 2-6=petrologic type

[2]Data for BHVO-2 standard applicable to trace-element data in Tables 4.3.2 and 4.3.3

Table 4.3.2: Whole-rock trace-element abundances in grouped achondrite meteorite samples (in μg g^{-1}).

	Acapulco	MET 01195	ALHA 81187	NWA 2871	NWA 2871	EET 84302	GRA 95209	NWA 4833	NWA 4875	ALH 84025	LEW 88763	Norton County	Norton County
Sample ID	-	,30	,41	larger mass	smaller mass	,47	,258	-	-	,31	,20	5081	MTF536, N-184
Met. Type[1]	A	A	A	A	A	A-L	L	L	L	B	An	Aub	Aub
Li	1.68	1.87	1.50	1.57	1.59	1.29	0.84	1.50	1.36	1.31	2.26	0.174	0.488
P	1970	1035	1086	809	2200	1810	3033	528	517	148	1018	26.1	44.3
Sc	7.1	8.2	6.8	7.0	7.5	5.9	4.2	9.5	14.4	22	9.1	4.7	2.2
Ti	560	590	510	430	500	640	305.5	190	220	260	620	200	220
V	71	80	59	56	90	150	33.0	90	115	120	77	6.8	8.9
Cr	4900	5200	3700	2300	5800	16000	1580.5	4100	4100	3600	3800	630	160
Ni	5000	4700	6400	3400	3800	14700	18030.0	3500	1020	2060	4600	150	13
Cu	72.5	46	20	49	56	37	37.9	38	18	39	80	12	2.0
Zn	180	172	102	11.8	21	220	40.4	110	105	140	65	1.8	2.9
Ga	4.5	6.5	6.3	4.6	6.5	15	8.2	3.6	1.5	2.4	6.0	0.128	0.33
Ge	3.7	8	12	7	11.1	32	40.2	7	2.3	4.5	2.4	0.16	0.048
Rb	0.224	0.200	0.39	0.244	0.225	0.067	0.205	0.74	0.103	0.113	1.81	0.084	2.40
Sr	11.2	10.6	10.4	11.6	9.3	6.5	8.7	14.4	10.5	0.96	12.5	0.251	6.7
Y	1.93	2.25	1.64	1.37	1.72	1.10	1.07	0.51	0.71	1.04	2.15	1.63	0.75
Zr	3.7	4.7	3.4	1.36	1.75	2.2	2.5	2.7	0.75	0.94	6.3	1.13	12.4
Nb	0.047	0.114	0.104	0.196	0.26	0.057	0.047	0.197	0.104	0.0233	0.41	0.0156	0.38
Cs	0.0010	0.0009	0.034	0.0024	0.0033	0.0017	0.0166	0.039	0.0058	0.0086	0.062	0.0068	0.106
Ba	3.75	3.52	3.01	2.83	2.89	1.57	2.39	104	101	0.159	4.30	0.196	14.7
La	0.613	0.330	0.200	0.51	0.230	0.180	0.163	0.443	0.212	0.0163	0.361	0.457	0.81
Ce	1.48	0.92	0.54	1.03	0.63	0.48	0.401	0.96	0.43	0.079	0.95	1.60	1.74
Pr	0.183	0.141	0.081	0.078	0.094	0.058	0.057	0.109	0.058	0.0178	0.136	0.220	0.208
Nd	0.79	0.72	0.412	0.377	0.51	0.312	0.277	0.436	0.280	0.116	0.67	0.97	0.77
Sm	0.220	0.238	0.138	0.120	0.159	0.108	0.090	0.090	0.073	0.065	0.221	0.229	0.140
Eu	0.091	0.080	0.070	0.080	0.068	0.045	0.058	0.0394	0.0420	0.0108	0.089	0.0332	0.0312
Gd	0.270	0.305	0.194	0.168	0.211	0.147	0.124	0.099	0.098	0.097	0.272	0.228	0.132
Tb	0.049	0.057	0.038	0.0312	0.041	0.0267	0.0235	0.0144	0.0151	0.0224	0.051	0.039	0.0176
Dy	0.345	0.40	0.274	0.234	0.315	0.187	0.167	0.092	0.110	0.175	0.368	0.267	0.106
Ho	0.074	0.087	0.062	0.053	0.069	0.041	0.038	0.0196	0.0261	0.042	0.081	0.060	0.0234
Er	0.218	0.257	0.188	0.163	0.215	0.124	0.115	0.060	0.082	0.129	0.241	0.189	0.077
Tm	0.033	0.038	0.0298	0.0255	0.0317	0.0196	0.0184	0.0098	0.0130	0.0207	0.037	0.0297	0.0132
Yb	0.227	0.259	0.206	0.180	0.238	0.139	0.124	0.074	0.099	0.147	0.245	0.222	0.095
Lu	0.034	0.037	0.0315	0.0279	0.036	0.0219	0.0185	0.0123	0.0170	0.0229	0.037	0.0317	0.0146
Hf	0.115	0.151	0.101	0.043	0.052	0.073	0.074	0.076	0.0172	0.028	0.168	0.0171	0.29
Ta	0.0191	0.0177	0.0156	0.0082	0.0127	0.0160	0.0139	0.0142	0.0054	0.0141	0.027	0.0086	0.0258
Th	0.053	0.033	0.025	0.0085	0.0151	0.0077	0.0151	0.117	0.025	0.0032	0.048	0.0086	0.201
U	0.89	0.067	0.061	0.052	0.099	0.0168	0.045	0.72	0.42	0.0067	0.220	0.097	0.83

[1]Meteorite type abbreviations: A=acapulcoite, L=lodranite, B=brachinite, An=anomolous, Aub=aubrite

Table 4.3.3: Whole-rock trace-element abundances in ungrouped achondrite meteorite samples (in μg g^{-1}).

	MIL 090206	MIL 090206	MIL 090405	MIL 090405	MIL 091004	MIL 091004
Sample ID	,8	,8	,5	,5	,4	,4
Powder mass (mg)	38.90	20.75	38.32	40.47	40.82	21.03
Met. Type[1]	UA	UA	UA	UA	Ur	Ur
Li	1.24	1.38	1.48	1.61	0.57	0.59
P	90.1	110.8	118	132	1573	1860
Sc	5.2	5.4	7.0	7.5	12.3	15.4
Ti	1170	1170	126	130	290	370
V	370	370	40	43	69	90
Cr	29000	28000	1230	1290	3600	4700
Ni	1800	1800	1200	1200	670	830
Cu	19	18	14	15	4.6	5.7
Zn	73	73	6.8	7.3	87	108
Ga	9.5	9.5	1.6	1.7	3.5	4.2
Ge	14	14	13	12.9	1.8	2.2
Rb	0.269	0.284	0.242	0.259	0.0119	0.0129
Sr	0.090	0.086	1.93	2.01	0.29	0.30
Y	0.272	0.297	0.64	0.71	0.50	0.57
Zr	0.76	0.84	1.81	2.00	0.180	0.145
Nb	0.26	0.27	0.092	0.100	0.0077	0.0082
Cs	0.0242	0.0254	0.0209	0.0235	0.0016	0.0006
Ba	0.104	0.173	0.73	0.84	0.054	0.0438
La	0.0052	0.0134	0.0149	0.0177	0.0087	0.0017
Ce	0.0140	0.0290	0.060	0.070	0.0301	0.0064
Pr	0.0019	0.0023	0.0132	0.0139	0.0022	0.0018
Nd	0.0124	0.0130	0.081	0.090	0.0148	0.0133
Sm	0.0059	0.0073	0.0383	0.043	0.0125	0.0145
Eu	0.0008	0.0009	0.0130	0.0141	0.0026	0.0030
Gd	0.0111	0.0107	0.062	0.067	0.0331	0.0322
Tb	0.0031	0.0036	0.0131	0.0152	0.0084	0.0093
Dy	0.0318	0.0373	0.103	0.119	0.080	0.086
Ho	0.0096	0.0109	0.0240	0.0277	0.0208	0.0230
Er	0.037	0.043	0.073	0.087	0.074	0.077
Tm	0.0081	0.0093	0.0116	0.0135	0.0125	0.0134
Yb	0.066	0.073	0.092	0.100	0.100	0.101
Lu	0.0114	0.0136	0.0141	0.0164	0.0172	0.0173
Hf	0.0181	0.0204	0.046	0.053	0.0068	0.0059
Ta	0.0226	0.0214	0.0067	0.0073	0.0123	0.0081
Th	0.0021	0.0027	0.0027	0.0032	0.0028	0.0008
U	0.0037	0.0043	0.0080	0.0068	0.0067	0.0018

[1]Meteorite type abbreviations: UA=ungrouped achondrite, Ur=ureilite

Table 4.3.4: Whole-rock Dy/Yb ratios for meteorites in the sample set. Dy/Yb ratios can be used to quantify approximations of trace-element (REE) depletion or enrichment in samples.

Sample	Met. Type[1]	Dy/Yb
Larkman	O	0.976
Richardton, chunk	O - H5	0.999
Peace River, chunk	O - L6	0.965
Chelyabinsk w/FC	O - LL5	1.106
Chelyabinsk, no FC	O - LL5	1.150
Kunashak, Lg. slice	O - L6	0.944
Kunashak, LAT	O - L6	0.993
Allende, UCSD 142	CV3	1.008
Murchison, MTF 2005	CM2	1.007
Murchison, chunk	CM2	0.994
Acapulco	Acapulcoite	0.997
GRA 95209	Lodranite (t)	0.879
MET 01195	Acapulcoite	1.016
ALHA 81187	Acapulcoite	0.869
EET 84302	A-Lo	0.883
NWA 2871 (larger)	Acapulcoite	0.850
NWA 2871 (smaller)	Acapulcoite	0.866
NWA 869, chunk	L3-6	0.848
NWA 4833	Lodranite	0.812
NWA 4875	Lodranite	0.729
MIL 091004	Ureilite	0.524
MIL 091004	Ureilite	0.555
ALH 84025	Brachinite	0.780
MIL 090206	BLA	0.314
MIL 090206	BLA	0.335
MIL 090405	BLA	0.737
MIL 090405	BLA	0.775
LEW 88763	BLA-Anom	0.983
Norton County, 5081	Aubrite	0.785
Norton County, MTF536, N-184	Aubrite	0.732

[1]Meteorite type abbreviations: O=ordinary chondrite, H= high-iron, L=low-iron, LL=low-iron, low-metal, C= carbonaceous chondrite, V=Vigarano type, M=Mighei type, numbers 2-6= petrologic type, (t)=transitional, BLA= brachinite-like achondrite, Anom=anomalous

Table 4.3.5: Whole-rock major-element abundances in chondrite meteorite samples (in μg g^{-1}).

	Allende	Murchison	Murchison	Chelyabinsk	Chelyabinsk	Kunashak	Kunashak	Peace River	Larkman	NWA 869	Richardton
Sample ID	UCSD 142	chunk	MTF 2005, vlc	w/FC	w/o FC	LAT	slice	chunk	3 fragments	chunk	chunk
Met. Type[1]	CV3	CM2	CM2	O - LL5	O - LL5	O - L6	O - L6	O - L6	O	O - L3-6	O - H5
Na	3118	4092	2462	5984	5978	6171	6341	7218	6866	7416	6710
Mg	122865	115235	95844	119124	123269	126688	128720	149069	134221	138022	140582
Al	13627	12329	9215	9560	9476	10125	10347	12349	11820	12873	10917
P	842	3316	998	1135	1159	1033	1041	1077	1137	2806	2368
Ca	14684	14944	11450	10688	12879	12588	13275	14470	12871	17693	12924
Ti	745	1351	605	488	710	683	697	880	885	1251	1070
Cr	2928	2959	2123	3343	2979	2975	3111	3256	3433	2803	3560
Mn	1254	1701	1264	2045	2234	2280	2300	2653	2399	2404	2276
Fe	203759	221844	161608	224585	168198	164993	163706	174150	197066	191361	274223
Co	583	582	430	1722	483	378	346	387	521	283	857
Ni	11650	11738	8567	19717	14043	8501	7023	9046	9823	11681	18061

[1]Meteorite type abbreviations: C=carbonaceous chondrite, V=Vigarano type, M=Mighei type, O=ordinary chondrite, LL=low-iron, low-metal, L=low-iron, H=high-iron, numbers 2-6=petrologic type

Table 4.3.6: Whole-rock major-element abundances in grouped achondrite meteorite samples (in μg g^{-1}).

	Acapulco	MET 01195	ALHA 81187	NWA 2871	NWA 2871	EET 84302	GRA 95209	NWA 4833	NWA 4875	ALH 84025	LEW 88763	Norton County	Norton County
Sample ID	-	,30	,41	larger mass	smaller mass	,47	,258	-	-	,31	,20	5081	MTF536, N-184
Met. Type[1]	A	A	A	A	A	A-L	L	L	L	B	An	Aub	Aub
Na	5990	5907	4845	4760	4505	3065	5005	684	1076	1777	5988	421	673
Mg	130071	132169	130564	123015	137894	118041	76239	179647	177916	150457	146898	206888	170254
Al	10880	10620	9368	9785	7781	8020	7892	1695	1605	1245	12849	324	1665
P	1329	1178	1171	1121	3202	1399	1553	1157	1174	2897	2810	1018	989
Ca	11456	14076	11076	10230	12065	8259	7519	14728	28840	36195	16197	5014	5577
Ti	925	985	816	671	1057	1013	629	537	512	1320	1525	421	327
Cr	5081	5282	3782	2368	6033	16411	1587	4179	4244	3645	3704	574	144
Mn	2856	2313	2389	2283	2551	2248	1867	2649	2693	2486	2394	1069	529
Fe	154815	152555	163367	131427	154184	353215	413747	157149	102880	212404	225428	11947	5680
Co	370	434	683	333	380	1545	1806	319	100	222	430	8	1
Ni	7422	7121	9367	5161	5737	21452	24693	5264	1526	3035	6660	210	21

[1]Meteorite type abbreviations: A=acapulcoite, L=lodranite, B=brachinite, An=anomolous, Aub=aubrite

Table 4.3.7: Whole-rock major-element abundances in ungrouped achondrite samples (in µg g^{-1}).

	MIL 090206	MIL 090206	MIL 090405	MIL 090405	MIL 091004	MIL 091004
Sample ID	,8	,8	,5	,5	,4	,4
Powder mass (mg)	38.90	20.75	38.32	40.47	40.82	21.03
Met. Type[1]	UA	UA	UA	UA	Ur	Ur
Na	688	796	1362	1477	454	814
Mg	134016	157882	149247	166631	161616	184018
Al	3405	3729	1841	2085	4281	4917
P	990	1981	1012	1018	1149	2273
Ca	3063	3945	8025	8911	11635	13971
Ti	1487	1637	473	246	444	581
Cr	27209	30096	1153	1356	4055	4756
Mn	2494	2840	2479	2779	3060	3555
Fe	181179	207550	183824	205181	97501	115686
Co	219	238	166	183	79	90
Ni	2525	2769	1625	1792	1084	1231

[1]Meteorite type abbreviations: UA=ungrouped achondrite, Ur=ureilite

4.4 Oxygen isotope data

When reporting the following oxygen isotope data, variation is listed as 2σ standard deviation.

Acapulcoites and lodranites – The oxygen isotope data obtained for the primitive acapulcoite-lodranite meteorites studied here agree well with data previously published for the meteorite groups, although oxygen in some of the meteorites in the sample set have never before been analyzed (SEE TABLE). Although the non-magnetic fractions of acapulcoites and lodranites we analyzed produced $\delta^{17}O$ and $\delta^{18}O$ values that reflected the presence of an overall lighter oxygen signature (lower $\delta^{17}O$ and $\delta^{18}O$ values) than acapulcoites and lodranite analyses from previous studies, deviation from the terrestrial fractionation line (average $\Delta^{17}O$ = -1.07 ± 0.25 ‰, n=18) is consistent with deviation averaged from previous studies (average $\Delta^{17}O$ = -1.09 ± 0.35 ‰, n=67; Greenwood et al. 2012, Clayton and Mayeda 1996).

ALH 84025, MIL 090206, and MIL 090405 – Oxygen isotopes in the meteorite Allan Hills 84025 have been studied previously (Warren and Kallemeyn 1989, Clayton and Mayeda 1996, and Greenwood et al. 2012) and average values compiled from those studies (n=4) are $\delta^{17}O$ = 1.97 ± 0.61 ‰, $\delta^{18}O$ = 4.32 ± 1.15 ‰, and $\Delta^{17}O$ = -0.30 ± 0.03 ‰. During our study, two analyses of ALH 84025 indicated homogeneous oxygen isotopic values within our sample ($\delta^{17}O$ = 1.87, 1.88 ‰, $\delta^{18}O$ = 4.10, 4.14 ‰, and $\Delta^{17}O$ = -0.28, -0.28 ‰). These values agree well with previously published values for ALH 84025, as well as data published for the entire brachinite group ($\Delta^{17}O$ = -0.21 ± 0.23 ‰, n=64; data from this study, Keil 2014, Greenwood et al. 2012, Clayton and Mayeda 1996).

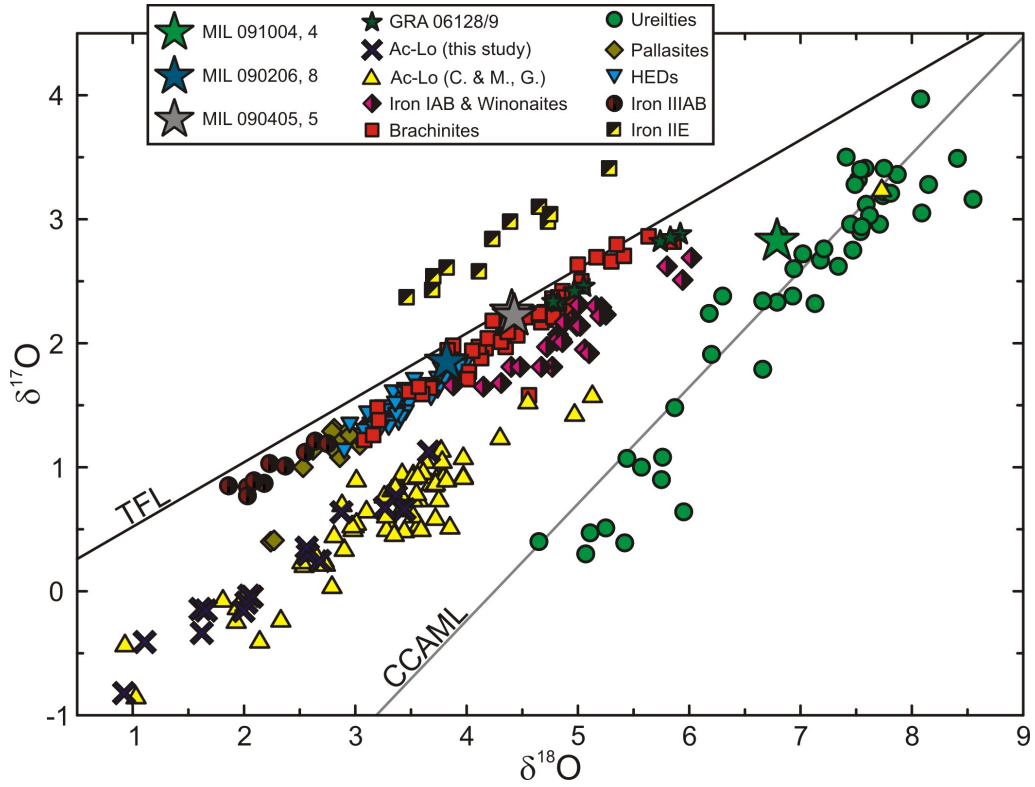

Figure 4.4.1: Oxygen three-isotope plot with ungrouped MIL samples as well as acapulcoite-lodranites from this study plotted among previously published oxygen isotope data. Oxygen isotope values for MIL 091004, 4 lie within published oxygen isotope data for ureilites and values for MIL 090206, 8 and MIL 090405, 5 lie within published data for brachinites. Note that data for some meteorite groups (aubrites, angrites, etc.) has been omitted from this plot for increased clarity. Abbreviations: TFL = terrestrial fractionation line, CCAML = carbonaceous chondrite anhydrous mineral line, C. & M. = Clayton and Mayeda 1996, and G. = Greenwood et al. 2012. $\delta^{17}O$ and $\delta^{18}O$ values are expressed in per mille (‰). Published data is from Day et al. 2009, Shearer et al. 2010, Clayton and Mayeda 1996, Greenwood et al. 2012, and Keil 2014.

The ungrouped achondrites MIL 090206 and MIL 090405 have oxygen isotope signatures that lie within the ranges for brachinites. One analysis of MIL 090206 oxygen isotopes produced values of $\delta^{17}O$ = 1.85 ‰, $\delta^{18}O$ = 3.82 ‰, and $\Delta^{17}O$ = -0.15 ‰. Two analyses of MIL 090405 oxygen isotopes produced values of $\delta^{17}O$ = 2.25, 2.22 ‰, $\delta^{18}O$ = 4.41, 4.43 ‰, and $\Delta^{17}O$ = -0.05, -0.10 ‰.

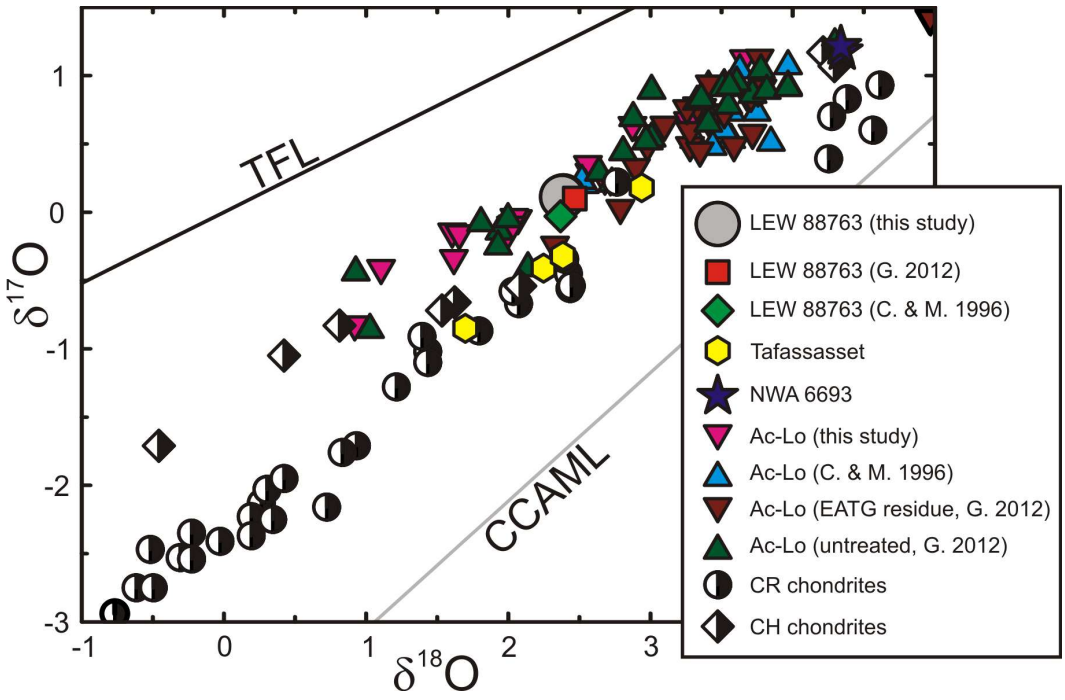

Figure 4.4.2: Oxygen three-isotope plot with LEW 88763 (data from this study as well as previously published studies) and meteorites with similar oxygen isotope signatures. Abbreviations: TFL = terrestrial fractionation line, CCAML = carbonaceous chondrite anhydrous mineral line, G. 2012 = Greenwood et al. 2012, and C. & M. 1996 = Clayton and Mayeda 1996. $\delta^{17}O$ and $\delta^{18}O$ values are expressed in per mille (‰). Published data is from Greenwood et al. 2012, Clayton and Mayeda 1996, Clayton and Mayeda 1999, Gardner-Vandy et al. 2012, Warren et al. 2013, Schrader et al. 2011, and Ivanova et al. 2006.

LEW 88763 – Two separate analyses of LEW 88763 oxygen isotopes were conducted. The average of the two analyses produced $\delta^{17}O = 0.11 \pm 0.01$ ‰, $\delta^{18}O = 2.38 \pm 0.01$ ‰, and $\Delta^{17}O = -1.14 \pm 0.001$ ‰. These values agree well with previously published LEW 88763 oxygen isotope data (Greenwood et al. 2012: $\delta^{17}O = 0.10$ ‰, $\delta^{18}O = 2.47$ ‰, and $\Delta^{17}O = -1.19$ ‰; and Clayton and Mayeda 1996: $\delta^{17}O = -0.03$ ‰, $\delta^{18}O = 2.37$ ‰, and $\Delta^{17}O = -1.26$ ‰).

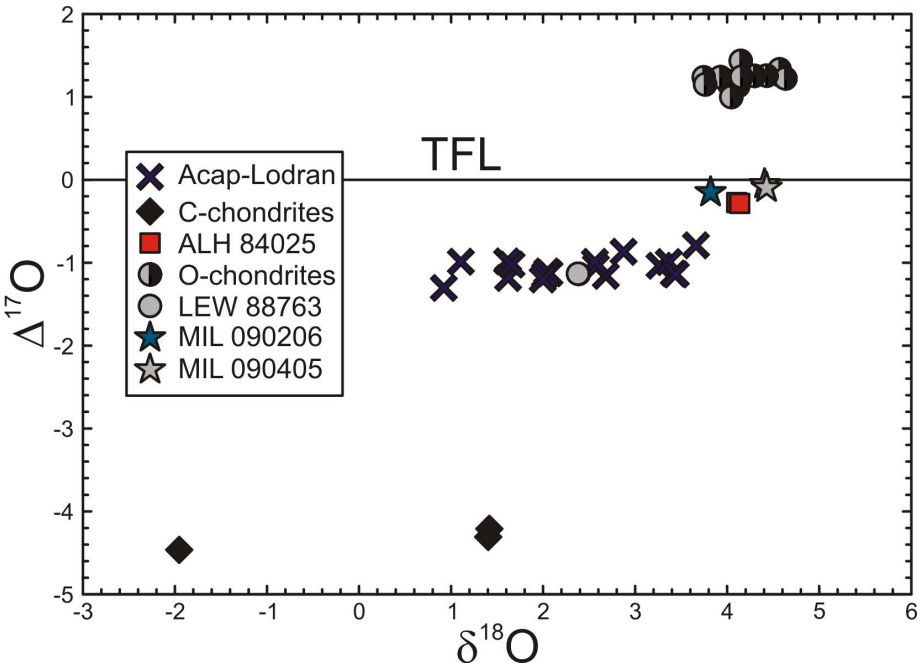

Figure 4.4.3: Oxygen isotope plot ($\delta^{18}O$ vs. $\Delta^{17}O$) with meteorites analyzed in this study. Abbreviations: TFL = terrestrial fractionation line, Acap-Lodran = acapulcoite-lodranites, C-chondrites = carbonaceous chondrites, O-chondrites = ordinary chondrites. $\delta^{17}O$ and $\delta^{18}O$ values are expressed in per mille (‰). All data are from this study.

Although LEW 88763 is classified in the Meteoritical Database (at the time of this publication) as a brachinite, its oxygen isotope signature is not consistent with the brachinite group ($\Delta^{17}O$ = -0.21 ± 0.23 ‰, n=64; data from this study, Keil 2014, Greenwood et al. 2012, Clayton and Mayeda 1996). Its values are much closer to the relatively well-established oxygen isotope signature of the acapulcoite-lodranite group ($\Delta^{17}O$ = -1.09 ± 0.33 ‰, n=85). This anomalous meteorite also plots near some CR ($\Delta^{17}O$ = -2.01 ± 0.93 ‰, n=39) and CH ($\Delta^{17}O$ = -1.38 ± 0.39 ‰, n=9) chondrites, as well as the meteorites Tafassasset ($\Delta^{17}O$ = -1.56 ± 0.31 ‰, n=4) and NWA 6693 ($\Delta^{17}O$ = -1.08 ± 0.06 ‰, n=2). See Table 4.3.10 for references as well as values for $\delta^{17}O$ and $\delta^{18}O$.

MIL 091004 – Analysis of MIL 091004 oxygen isotopes gave a $\Delta^{17}O$ value of -0.727 ‰ ($\delta^{17}O$ = 2.825 ‰ and $\delta^{18}O$ = 6.789 ‰). Although the ureilite group has a wide range of $\Delta^{17}O$ values suggesting a primitive origin (-0.23 ‰ to -2.45 ‰, from Clayton and Mayeda 1996), in an oxygen three-isotope plot the ureilite field is roughly constrained along the carbonaceous chondrite anhydrous mineral line (CCAML), which is defined by analysis of minerals separated from Allende CAIs (Clayton et al. 1977, and Clayton and Mayeda 1999). The O-isotope systematics of MIL 091004 are consistent with it being a ureilite.

Table 4.3.8: Oxygen isotopes for the sample set.

Sample	Sample ID	Met. Type[1]	$\delta^{17}O$	$\delta^{18}O$	$\Delta^{17}O$
Allende	UCSD 142	CV3	-5.49	-1.95	-4.47
Murchison	chunk	CM2	-3.47	1.42	-4.21
			-3.57	1.40	-4.31
Chelyabinsk	JD + LAT (w/FC)	O - LL5	3.65	4.59	1.25
			3.72	4.57	1.33
			3.65	4.63	1.22
Chelyabinsk	JD + LAT (w/o FC)	O - LL5	3.57	4.43	1.25
Kunashak	LAT	O - L6	3.29	4.12	1.13
Kunashak	slice	O - L6	2.52	3.75	0.56
			2.52	3.79	0.54
			3.29	4.01	1.19
			3.26	4.02	1.15
Larkman	3 fragments	O	3.29	3.93	1.24
			3.20	3.75	1.24
			3.12	3.76	1.15
Peace River	chunk	O - L6	3.50	4.29	1.25
			3.60	4.15	1.43
			3.42	4.15	1.24
Richardton	chunk	O - H5	3.11	4.04	1.00
Acapulco	-	A	1.13	3.66	-0.79
ALHA 81187	,41	A	-0.14	1.61	-0.99
			-0.41	1.11	-0.99
MET 01195	,30	A	0.29	2.57	-1.05
			0.35	2.56	-0.99
NWA 2871	larger mass	A	0.66	3.42	-1.13
			0.77	3.37	-0.99
			0.66	3.44	-1.14
NWA 2871	smaller mass	A	0.67	3.27	-1.04
EET 84302	,47	A-L	0.64	2.88	-0.87
			0.24	2.68	-1.16
GRA 95209	,258	L	-0.82	0.92	-1.31
NWA 4833	-	L	-0.05	2.07	-1.13
			-0.04	2.05	-1.11
			-0.09	2.02	-1.15
			-0.34	1.62	-1.19
NWA 4875	-	L	-0.16	2.00	-1.20
			-0.16	1.66	-1.02
Norton County	5081	Aub	2.94	5.26	0.19
			2.92	5.31	0.14
			2.87	5.40	0.04
Norton County	MTF536, N-184	Aub	2.65	5.05	0.00
ALH 84025	,31	B	1.87	4.10	-0.28
			1.88	4.14	-0.28
LEW 88763	,20	B-like/an	0.12	2.39	-1.14
			0.11	2.38	-1.14
MIL 090206	,8	B/B-like	1.85	3.82	-0.15
MIL 090405	,5	B/B-like	2.25	4.41	-0.05
			2.22	4.43	-0.10
MIL 091004	,4	U	2.83	6.79	-0.73

[1]Abbreviations: A = acapulcoite, L = lodranite, Aub = Aubrite, B = brachinite, B-like = Brachinite-like, an = anomalous, U = ureilite

Table 4.3.9: Oxygen isotope data for acapulcoites and lodranites in this study, as well as previously published data. Although averages of $\delta^{17}O$ and $\delta^{18}O$ can vary from study to study, as a whole the acapulcoite-lodranites have well-defined oxygen isotope ranges, including that for $\Delta^{17}O$.

Meteorite Group	Source		$\delta^{17}O$	$\delta^{18}O$	$\Delta^{17}O$
Acapulcoites and lodranites	This study	avg.	0.18	2.38	-1.07
n=18		1σ	0.50	0.84	0.12
Acapulcoites and lodranites	Clayton and Mayeda 1996	avg.	0.67	3.42	-1.11
n=16		1σ	0.26	0.42	0.18
Acapulcoites and lodranites (untreated)[1]	Greenwood et al. 2012	avg.	0.65	3.24	-1.05
n=30		1σ	0.76	1.29	0.17
Acapulcoites and lodranites (EATG residue)[1]	Greenwood et al. 2012	avg.	0.64	3.39	-1.14
n=21		1σ	0.37	0.54	0.18
Acapulcoites and lodranites	Clayton and Mayeda 1996 &	avg.	0.65	3.33	-1.09
n=67	Greenwood et al. 2012	1σ	0.56	0.93	0.18
Acapulcoites and lodranites	All studies above	avg.	0.55	3.13	-1.09
n=85		1σ	0.58	0.99	0.17

[1]Note: "Untreated" and "EATG residue" refer to analytical methods used in Greenwood et al. 2012 in which terrestrial weathering was removed from some samples with an ethanolamine thioglycollate (EATG) solution

Table 4.3.10: Oxygen isotope data for LEW 88763 compared to selected meteorites. LEW 88763 oxygen is most similar to oxygen measurements from acapulcoite-lodranites and CH chondrites.

Sample/Meteorite Group		$\delta^{17}O$	$\delta^{18}O$	$\Delta^{17}O$
LEW 88763[1]	avg.	0.07	2.40	-1.18
n=4	1σ	0.07	0.05	0.06
Brachinites[2]	avg.	2.11	4.42	-0.21
n=64	1σ	0.36	0.58	0.12
Acapulcoite-lodranites[1]	avg.	0.55	3.13	-1.09
n=85	1σ	0.58	0.99	0.17
CR chondrites[3]	avg.	-1.21	1.53	-2.01
n=39	1σ	1.70	2.46	0.47
CH chondrites[4]	avg.	-0.22	2.22	-1.38
n=9	1σ	1.10	2.00	0.20
Tafassasset[5]	avg.	2.32	-0.35	-1.56
n=4	1σ	0.51	0.42	0.16
NWA 6693[6]	avg.	1.19	4.32	-1.08
n=2	1σ	0.03	0.01	0.03

[1]Data from this study, Greenwood et al. 2012, and Clayton and Mayeda 1996
[2]Data from this study, Keil 2014, Greenwood et al. 2012, Clayton and Mayeda 1996
[3]Data from Schrader et al. 2011 and Clayton and Mayeda 1999
[4]Data from Ivanova 2006 and Clayton and Mayeda 1999
[5]Data from Gardner-Vandy et al. 2012, Bourot-Denise et al. 2002, and Russell et al. 2002
[6]Data from Warren et al. 2013

4.5 Raman spectroscopy of MIL 091004

The carbon grains in MIL 091004 are large in size and number, and were originally identified by petrography. One grain was analyzed, and the Raman spectrum (Figure 4.4.4c) of the analyzed grain shows distinguishing disordered (D, ~1350 cm^{-1}) and ordered (G, ~1600 cm^{-1}) Raman peaks of graphitic carbon, as well as a distinguishing second-order band (2D, ~2700 cm^{-1}). Because all other mineral phases in MIL 091004 have petrographic characteristics that are clearly dissimilar to the carbon laths, Raman analysis was only necessary to identify one carbon grain. Petrographic comparison of this grain to other grains was used to identify other carbon in the section.

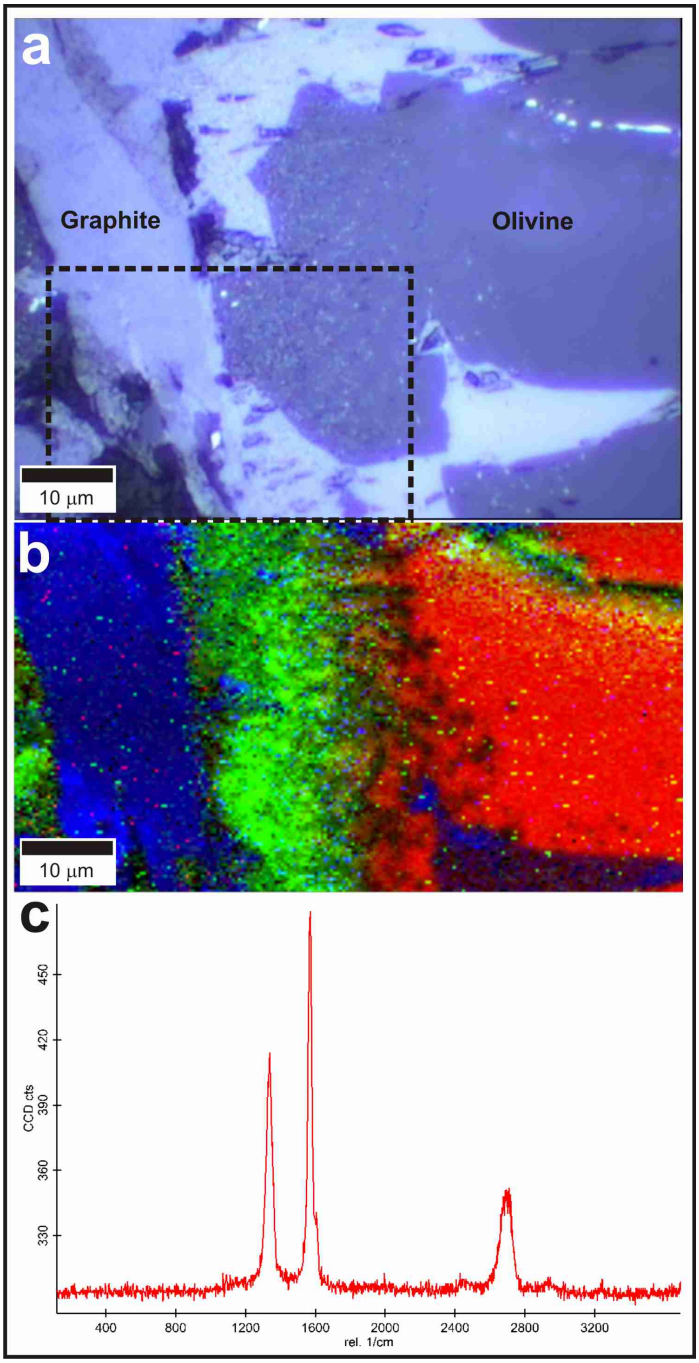

Figure 4.4.4: Panel a) displays an overview image of the area of interest in MIL 091004, 7 that was targeted for Raman spectroscopy, with the black dashed rectangle highlighting the scan area. Panel b) displays roughly the same area in RGB colors with red depicting olivine, blue depicting graphite, and green depicting high background fluorescence which is likely a combination of both graphite and olivine. Brightness of each color scales with intensity of signal. Panel c) displays a spectra from the blue area in b) showing peaks corresponding to highly crystalline graphite.

5. Discussion

5.1 Acapulcoites and lodranites

Acapulcoites and lodranites have essentially identical oxygen isotope compositions (Table 4.3.9) and similar mineralogy, mineral compositions, thermal histories and exposure ages, indicating their genesis on the same parent body (McCoy et al. 1996; Mittlefehldt et al. 1996) under low to moderate degrees of partial melting (<1-20 %; McCoy et al. 1997b). Cessation of melting in acapulcoite-lodranites cannot reasonably be associated with loss of Al-rich melts, as has been suggested for brachinites (Day et al. 2012). Instead the young ages of acapulcoite-lodranites (4563 ± 1 Ma; Touboul et al. 2009) may point to accretion of their parent body after burn-out of ^{26}Al. Rubin (2007) also made an argument to suggest acapulcoite-lodranites relate to impact generated melting. Regardless of the cause of melting on the acapulcoite-lodranite parent body, it is clear that the two sub-groups have experienced slightly different degrees of melting, and the acapulcoite-lodranites as a whole (<1-20 % partial melting) have experienced less melting than other achondrite groups (e.g., >10-30 % partial melting in brachinites). Acapulcoites have experienced temperatures high enough to partially melt FeNi metals and FeS (~950-1050 °C peak temperatures; McCoy et al. 1996) while lodranites have experienced Fe,Ni-FeS and silicate partial melting (~1100-1250 °C peak temperatures; McCoy et al. 1997a; also see this study's Figure 5.1.1). The lodranites' loss of a silicate partial melt is readily observable in lower modal abundances of plagioclase. Recent geophysical modeling (Golabek et al. 2014) has also produced different formation depths for acapulcoites (9-19 km) and lodranites (14-25 km) when constraining the two groups to the same parent body (in this case a body of radius 25-65 km). Acapulcoite-

lodranites therefore form a continuum with other primitive achondrites, as well as a bridge between chondrites and non-primitive achondrites, revealing the nature of planetary differentiation in the early Solar System.

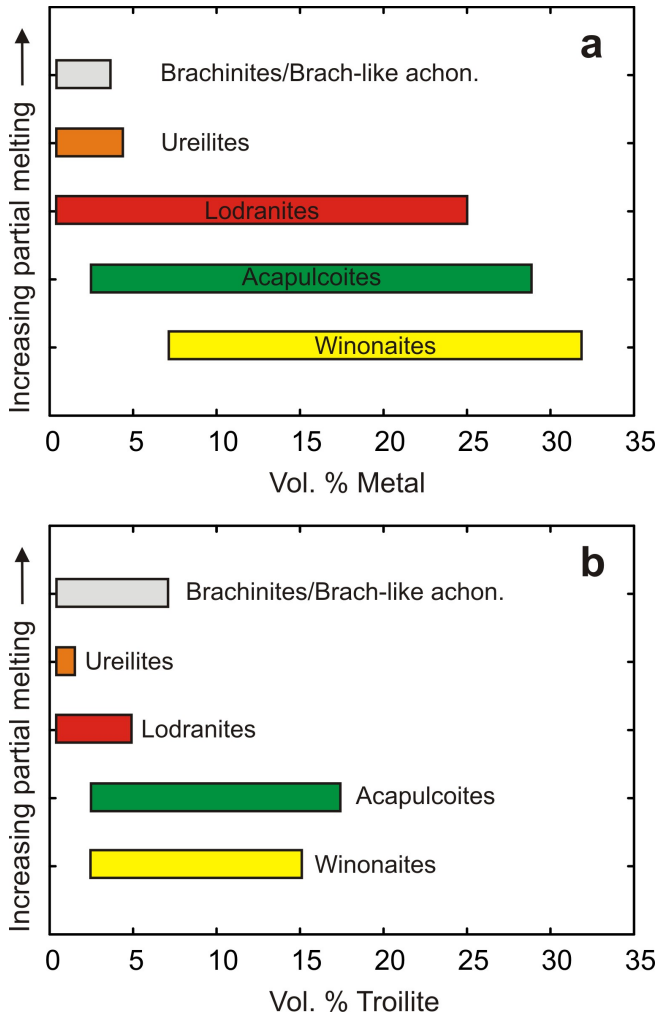

Figure 5.1.1: Plots of a) ranges of FeNi abundances and b) ranges of FeS abundances observed in achondrite meteorite groups plotted against degree of partial melting. Especially in FeNi, increased partial melting correlates very well with lower abundances of FeNi and FeS (brachinites and brachinite-like achondrites display an exception in FeS, with abundances that range higher than ureilites).

Rare earth element patterns in the acapulcoite-lodranites are chondrite-like, and in this study do not vary outside 0.3-3× CI-chondrite values (Figures 4.3.4 and 4.3.5). The acapulcoites that were measured for trace-elements in this study (Acapulco, MET 01195, ALHA 81187, NWA 2871) in general have higher CI-chondrite normalized REE values than the lodranites measured (GRA 95209, NWA 4833, NWA 4875). Most of the acapulcoites are slightly enriched relative to CI-chondrite and most of the lodranites are slightly depleted. The only meteorite in the study classified as a "transitional" acapulcoite-lodranite – EET 84302 – has REE values that more or less lie between acapulcoites and lodranites. These REE behaviors are especially visible in the elements Gd through Lu. If attention is focused on these elements, EET 84302 stands out as lying between the acapulcoites and lodranites. As an extension of this feature, the acapulcoites are completely separated from the lodranites among these elements. Moreover, all of the normalized Gd through Lu values for lodranites are depleted relative to CI-chondrite, and nearly all of the same values for acapulcoites are enriched (all except for the slightly depleted Gd and Tb values for NWA 2871 "larger mass"). The segregation of the acapulcoite and lodranite REE patterns (especially in the elements Gd through Lu) strongly supports the observation that acapulcoites experienced partial melting at lower temperatures than did the lodranites.

With the above REE behaviors in mind, it is worthwhile to mention metal grain morphology in the transitional EET 84302. The polished thick section of this meteorite contains very large FeNi grains that seem to have "pooled" together – grains are reminiscent of liquid puddles and are often connected to each other by small metallic arms. This morphology is consistent with its REE patterns – the same partial melting that

caused metal migration and pooling in the meteorite caused slight REE depletion. The lodranite GRA 95209 and the acapulcoite MET 01195 also both display some pooling metal, but not to the extent found in EET 84302. Because MET 01195 is considered an acapulcoite (evident in its REE pattern, Figure 4.3.5) but it petrographically presents metal migration, it may be worthwhile to investigate it as being more closely related to transitional acapulcoite-lodranites than acapulcoites. Even though EET 84302 displays metal migration that is more severe than the more-REE-depleted lodranite GRA 95209, it still displays much more metal migration than the three acapulcoites for which sections were obtained.

Whole-rock major-element abundances of the elements Fe, Ni, and Co reveal interesting features of the acapulcoites and lodranites. When compared to the chondrites in the sample set, acapulcoites have whole-rock Fe, Ni, and Co abundances that are either slightly depleted or within the ranges for the chondrites (Tables 4.3.5 and 4.3.6). For a quick comparison, the range of Fe abundances (powder weight corrected) in acapulcoites is 131,427-163,367 ppm and the range in chondrites is 161,608-274,223 ppm. Nickel abundances in acapulcoites range 5,161-9,367 ppm and in chondrites range 7,023-19,717 ppm (7,023-18,061 ppm if the Chelyabinsk sample with fusion crust is not included). Cobalt, which has relatively low abundances in both acapulcoites and chondrites, ranges 333-683 ppm in acapulcoites and 346-1,722 ppm in chondrites (346-857 ppm if the Chelyabinsk sample with fusion crust is not included here as well). With even a cursory inspection it is apparent that if acapulcoites are derived from chondritic material, then they have seen slight loss of some major siderophile elements which is evidence

supporting the notion that the acapulcoites experienced limited partial melting during their lives, and furthermore, they have likely lost a small portion of that melt.

The lodranites and the single transitional acapulcoite-lodranite have a more complicated relationship to the chondrites in the sample set. Two meteorites – GRA 95209 (lodranite) and EET 84302 (acapulcoite-lodranite) – have Fe and Ni abundances that are significantly higher than the values for chondrites (Tables 4.3.5 and 4.3.6). The two meteorites also have Co abundances that lie within the range for chondrites (or are significantly higher than the range that does not include the Chelyabinsk sample without fusion crust). In contrast the two hot desert lodranites NWA 4833 and NWA 4875 have Fe, Ni, and Co abundances that all lie significantly below the ranges for chondrites. This diversity in the lodranites (as well as the acapulcoite-lodranite) reveals that some lodranites have experienced FeNi and FeS melt removal, whereas other lodranites (and the transitional EET 84302) can be considered a metal cumulate of sorts. This notion is also supported by recent highly siderophile element abundance analyses (Dhaliwal et al. 2015). Although polished sections were not obtained for NWA 4833 and NWA 4875, this observation is also supported by the appearance of GRA 95209 (Figure 4.1.2) and EET 84302 (Figure 4.1.3) in reflected light. In these meteorites, a high modal percentage of FeNi metal is visible (especially in GRA 95209) supporting their metal cumulate melting histories.

It is again worthwhile to mention the metallic pooling most visible in EET 84302 in relation to recent geophysical modeling. Gobalek et al. (2014) used modeling to conclude that the best fit to acapulcoite-lodranite geochemical data and observations gives the acapulcoites and lodranites formation depths of 9-19 km and 14-25 km,

respectively (on a parent body of 25-65 km radius). This conclusion is consistent with a modal increase of FeNi metal, as well as the pooling features in lodranites. If some lodranites are in fact metal cumulates, they would form closer to the interior of their parent body than the lithologies that lost the metal phases that the lodranites gained. Although the acapulcoite-lodranite parent body was likely very small compared to the differentiated rocky planets in the Solar System, as well as the tiny differentiated asteroidal body Vesta, it still may have experienced "preliminary" or "weakened" differentiation in which heavy metal phases migrated towards the interior but never accreted into a full-fledged core.

Another notable feature of the trace-element patterns in some of the acapulcoite-lodranites are small negative Zr and Hf anomalies. Noticeable negative Zr and Hf anomalies exist in Acapulco (acapulcoite), EET 84302 (acapulcoite-lodranite), both splits of NWA 2871 (acapulcoite), and the most pronounced anomaly is observed in NWA 4875 (lodranite). Because Zr and Hf is often associated with the mineral zircon, these anomalies suggest that zircon may exist (or did exist) in petrologically significant levels in these particular meteorites. Moreover, because the anomaly is negative, at some point in their petrogenesis these meteorites may have experienced the extremely high temperatures necessary to melt zircon and subsequently lost a partial melt component that included the melted zircon. The petrography conducted for this study focused on the more prominent silicates and zircons were not targeted. It will be worthwhile in future studies to determine if zircon exists in these samples in petrographically and furthermore in petrologically significant levels.

5.2 Brachinites and brachinite-like achondrites

ALH 84025, the only confirmed brachinite in the sample set, has been well studied and our results confirm those of previous studies (see Results, above). For this study, ALH 84025 will serve primarily as a representative of the brachinite group with which we compare the ungrouped MIL samples. MIL 090206 and MIL 090405 were provisionally classified as being similar to ureilites; however, recent work has shown that they have closer affinities to brachinites, and should likely be classified as brachinite-like achondrites (Goodrich et al. 2010, Satterwhite and Righter 2011b, Day et al. 2012).

The olivine dominated, sulfide rich petrography of MIL 090206 is the first line of evidence suggesting the meteorite's relationship to the brachinites (compared to brachinite petrography in Day et al. 2012, Mittlefehldt et al. 2003, Mittlefehldt 2003, etc.). The new oxygen isotope data for MIL 090206 lie within the field for brachinites on oxygen three-isotope plots (Figures 4.4.1 and 4.4.3) and mineral (olivine and pyroxene) major-element compositions lie within the fields for brachinite-like achondrites (Figures 4.2.1 and 4.2.2). Whole-rock trace-element abundances (including the REEs) in MIL 090206 lie within the ranges for brachinites and brachinite-like achondrites with exceptions in only a few elements' abundances (Ta, Sr, Eu, and Ti). We find MIL 090206 to be most similar to NWA 5400 or NWA 6077 (Day et al. 2012) and classify it as a brachinite-like achondrite, a classification that has also been suggested by Goodrich et al. (2012) by comparing the meteorite to NWA 595.

The whole-rock trace-element patterns produced by MIL 090206 deserve a special note. When plotted with ranges for the meteorite GRA 06128/9 (Figures 4.3.3 and 4.3.6), MIL 090206 creates nearly an exactly complementary pattern to the felsic GRA

06128/9, suggesting that the two meteorites could be residue/melt products from the same parent rock. This differentiation process in which both GRA 06128/9 and the complementary brachinites and brachinite-like achondrites derived from volatile-rich and oxidized chondritic material (possibly from the same parent body) was suggested by Day et al. (2012), and MIL 090206 may exhibit the best trace-element evidence in support of the process. The oxygen isotope data for MIL 090206 ($\Delta^{17}O$ = -0.15) is consistent with it deriving from the same parent body as GRA 06128 ($\Delta^{17}O$ = -0.208; Day et al. 2012), GRA 06129 ($\Delta^{17}O$ = -0.186; Day et al. 2012) as well as the brachinites ($\Delta^{17}O$ = -0.21 ± 0.23 ‰, n=64; data from this study, Keil 2014, Greenwood et al. 2012, Clayton and Mayeda 1996). If MIL 090206 is a brachinite, it may serve as further evidence that GRA 06128/9 is related to the brachinites as a felsic complementary. In any case, MIL 090206 is at least superficially related to the GRA 06128/9 stones.

The meteorite MIL 090405 lacks low-Ca pyroxenes but its overall petrography is still noticeably brachinite-like (compared to brachinite petrography in Day et al. 2012, Mittlefehldt et al. 2003, Mittlefehldt 2003, etc.). The meteorite's olivine compositions lie within the field for brachinite-like achondrites, and its pyroxene compositions lie within the fields for brachinites and brachinite-like achondrites. MIL 090405 also presents oxygen isotopes that are within the ranges and fields (Figures 4.4.1 and 4.4.3) for brachinites. Whole-rock trace-element abundances (including the REEs) lie within the ranges for brachinites and brachinite-like achondrites. Given the current constraints, we consider MIL 090405 to also be a variety of brachinite-like achondrite.

The expanding compositional range of meteorites which exhibit evidence for partial melting processes similar to brachinite-like achondrites suggests that low degree

partial melting was a common process on numerous asteroids and planetesimals in the early Solar System. The preservation of these meteorites and lack of evidence for run-away melting on their parent bodies may owe much to impact disruption or to depletion of ^{26}Al through segregation of Al-rich melts (Day et al. 2012). While this observation may be unsurprising, the large ranges in oxygen isotope composition and Mg/Fe values of silicates suggests that these bodies formed from materials with very different original oxidation and volatile compositions.

5.3 Lewis Cliff 88763

The achondrite Lewis Cliff 88763 was originally described as a Brachina-like olivine rich (Fa_{33}) achondrite (Lindstrom 1991), with a later, more comprehensive study (Swindle et al. 1998) establishing LEW 88763 as a partially melted primitive achondrite with roughly chondritic proportions of major- and highly-siderophile element (HSE: Os, Ir, Ru, Pt, Pd, and Re) abundances. Garnder-Vandy et al. (2012) reported the meteorite Tafassasset and LEW 88763 to be similar based on textures, FeO-rich silicates, and depleted refractory lithophile and siderophile compositions. Likewise, Warren et al. (2013) found similarities between NWA 6693 and LEW 88763 in bulk Na/Al ratios, $\Delta^{17}O$ values, and siderophile and chalcophile/volatile element abundances. A crucial limitation in studying LEW 88763 is in its small initial mass (4.1 g), making comprehensive petrological and geochemical studies challenging.

LEW 88763 has somewhat of a split personality. The oxygen isotope composition of the meteorite ($\Delta^{17}O$ = -1.136 + ± 0.001 ‰) places it within the field for acapulcoite-lodranites (and near NWA 6693), however the modal abundances of FeNi metal (0.5 %)

and troilite (1.3 %) are low compared to acapulcoite-lodranites. The granoblastic-recrystallized texture of the sample is strongly reminiscent of those observed in winonaites (e.g., Mount Morris, Winona, etc.; Benedix et al. 1998). Its bulk-rock Mg# (40) and mafic silicate mineral constituents are ferroan, similar to brachinites, Tafassasset, and NWA 6693. Finally, LEW 88763 has flat, chondrite-relative REE abundances (see data from this study, Figure 4.3.7), which are more consistent with chondrites and acapulcoite-lodranites than with brachinites or other partially melted achondrites (Corder et al. 2014).

Abundances of the REEs (as well as Se, Sr, and Cs) in LEW 88763 (Figures 4.3.7 and 5.3.1) are inconsistent between this study and the study by Swindle et al. (1998). Whereas we observe a strikingly unfractionated near-chondritic REE pattern, data by Swindle et al. (1998) shows elevated values for Ce, Nd, Eu, Gd, Ho, and Tm (the study also did not include measurements for Pr, Dy, and Er). There is good agreement between the three splits that were used in their study, and we are confident in the quality of our trace element analysis procedures and dataset. These conflicting datasets, together with the fact that material chosen for trace element analysis in both studies came from a meteorite with such a small initial mass (i.e., less chance for sampling different lithologies if LEW 88763 was a heterogeneous sample), make it difficult to resolve the discrepancy between some of the REE abundances. Nakamura and Morikawa (1993) also reported a chondritic REE pattern (with no analyses for Pr, Tb, Ho, and Tm) for LEW 88763 (see their Figure 1b), but did not report data. The pattern produced by their study looks much like the REE pattern in ours, but instead with a slight negative Eu anomaly. We have decided to trust the data produced in this study for discussion.

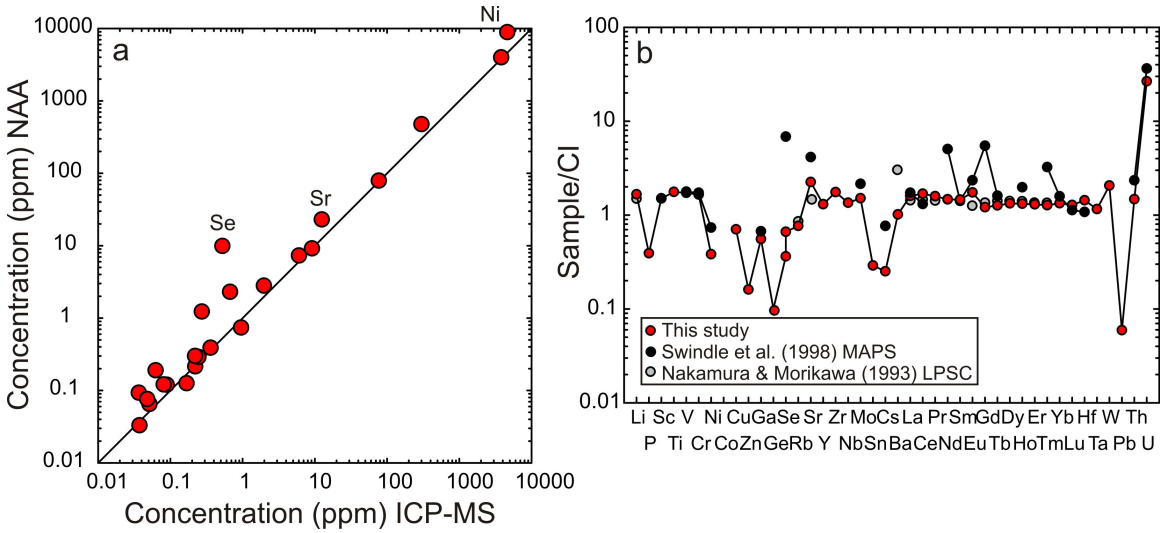

Figure 5.3.1: Panel a) demonstrates differences in LEW 88763 data analyzed by NAA (Swindle et al. 1998) and ID (Nakamura and Morikawa 1993) versus ICP-MS (this study). Panel b) demonstrates same differences except normalized to CI-chondrite. Differences in abundances for elements such as Ni and Se are due to variable metal contents in aliquants from separate studies (i.e., "the mode effect").

While considering the diverse petrological and geochemical characteristics of LEW 88763, we reach the following conclusions. First, the texture and bulk-rock composition of LEW 88763 are consistent with limited partial melting of a FeO-rich parent body that was at least as oxidized as the brachinite- and brachinite-like parent bodies (c.f., Day et al. 2012), although LEW 88763 may not be closely related to the brachinites or brachinite-like achondrites. Secondly, the LEW 88763 parent material is clearly distinct from brachinites, and more similar to acapulcoite-lodranites, CH chondrites, and CR chondrites based on O-isotope composition (Figure 4.4.2). Thirdly, the presence of meteorites such as LEW 88763, NWA 6693, and Tafassasset (as well as meteorites not mentioned here) in the meteorite collection clearly indicates the presence of materials in the early Solar System that underwent similar partial differentiation

processes, but that were strongly oxidized, and possibly came from separate parent bodies. LEW 88763 in particular may point to extreme heterogeneity (e.g., variable degrees of partial melting) on the parent bodies of the meteorite groups it shares characteristics with (acapulcoite-lodranites, brachinites, etc.). Such heterogeneity is evident in ureilites (e.g., ureilite oxygen isotope ranges), most especially Almahata Sitta (Rumble et al. 2010). Lastly, understanding if these oxidized materials were within discrete homogeneous parent bodies or were amalgamated in heterogeneous parent bodies with variable oxidation and melting (and the timing of these processes) is a first order query to be addressed for elucidating asteroidal and planetary formation in the early Solar System.

5.4 Miller Range 091004

The Miller Range 091004 meteorite is undoubtedly an exceptional planetary sample. Its carbon-rich region is one of the most remarkable lithologies found in any known meteorite, and certainly the most remarkable report of carbon within the ureilite group. Although announced as a lodranite, there is ample evidence suggesting this meteorite belongs to the ureilite group (Corder et al., 2014c). The most apparent evidence is the existence of carbon minerals. Although the ureilites can differ widely in their oxygen isotope values, when plotted on a three-isotope diagram populated with other achondrites they exist separate from other meteorite groups. MIL 091004 oxygen isotopes plot within this field (Figure 4.4.1). The main granoblastic region (as well as the carbon-rich region with the exception of the preponderance of carbon laths) displays mineralogy and textures typical of ureilites and MIL 091004 pyroxenes and olivines have

ureilitic major-element compositions (Figures 4.2.1 and 4.2.2). MIL 091004 whole-rock trace-element abundances agree with previously published ureilite data and certain silicate mineral trace elements are consistent with ureilites (~1 % Cr in pyroxenes, ~0.5 % Cr and ~0.3 % Ca in olivines). Silicon has been found in FeNi metal in some ureilites, although usually at lesser abundances than what we have found in some MIL 091004 FeNi grains (up to 11.2% Si; Table 4.2.9). Although FeNi has a relatively low modal abundance in the meteorite, the high silicon content in some FeNi grains could prove important for discussion of smelting processes on the ureilite parent body, especially when coupled with the existence of extensive carbon. Iron-sulfide in MIL 091004 also has appreciable amounts of Cr, which is similar to other ureilites.

The carbon-rich region, with its numerous and densely populated graphite laths, is most likely an intrusion into the main granoblastic MIL 091004 lithology. That there is no observed carbon in the main granoblastic region supports the idea of the carbon-rich region as an intrusion. Further petrographic and chemical evidence exists. Graphite laths in the carbon-rich region are often sidewall oriented, suggesting deposition in a flow regime. Silicates in the region have inherited the silicate textures of the main granoblastic region – grain size remains the same in both regions and a bimodal distribution of silicates is observed in both regions as well (Figure 4.1.11). The contact between the two regions is sharp and silicates at the contact do not display significantly enhanced reduction. The most striking piece of evidence supporting the carbon-rich region as an intrusion is that olivine cores in the region (average = Fo_{88}; n = 7) have compositions identical to olivine cores in the main granoblastic region (average = Fo_{88}; n = 28; Table 4.2.2).

Combining the observation of the intrusive carbon-rich region with data revealing light REE enrichment in some ureilites (including one of the MIL 091004 separates) and variable degrees of melt depletion (Figure 4.3.8), we propose a similar auto-fertilization mechanism to that observed in some terrestrial mantle peridotites (e.g., Niu 2004) for the ureilite parent body. According to Niu, bulk-rock LREE enrichment relative to middle-REEs (MREEs) in terrestrial peridotites reflects post-primary-melting re-fertilization where secondary low degree partial melts with less depleted REE abundances infiltrate peridotites with more depleted REE abundances. This terrestrial re-fertilization model utilizes tectonic spreading processes to produce observed peridotite REE patterns. Asteroidal bodies and protoplanets that cultivate meteorite samples (e.g., the ureilite parent body) likely are not large enough to support tectonic processes, but a similar model for the genesis of MIL 091004 can be applied by using the chronological and degree-of-melting parameters used in the terrestrial model (Figure 5.4.1).

We propose a model in which the main granoblastic region of MIL 091004 is a result of primary differentiation processes and the intrusive carbon-rich region is the petrographic expression of post-primary-melting re-fertilization processes. There is general agreement that ureilites formed as mantle restites in the ureilite parent body (Warren and Kallemeyn 1992, Scott et al. 1993, Singletary and Grove 2003, Goodrich et al. 2004, etc.), and with its mafic igneous mineralogy and depleted REE patterns, MIL 091004 is no exception. After initial melt depletion, some ureilites acted as conduits to melt migration from low degree partial melts from within the parent body. The secondary partial melts could have originated from carbon-rich pockets within the ureilite parent body, and served to enrich some ureilite LREE abundances. In the case of MIL 091004,

the intrusive carbon-rich region represents this secondary melt migration process and the cause of LREE enrichment in some ureilite samples.

An auto-fertilization model has important implications for smelting (Walker and Grove 1993), since it would allow coexistence of high Fe/Mg olivines with C due to a combination of melt depletion at a range of pressures, followed by C-rich melt infiltration. It would also be a more reduced analog to terrestrial peridotite environments where low degree C-rich partial melts are increasingly cited for explaining features of melt processes (e.g., Dasgupta et al. 2013). In the case of low degree partial melts in a reduced ureilite parent body, they would likely need to be CH_4-rich to explain the mineralogy of MIL 091004.

There are two possible mechanisms by which C-rich melt infiltration could have occurred in ureilites. The first is during primary differentiation and the second is through impact processes. It has previously been noted that only the lowest shock ureilites have significant carbon (Warren and Rubin 2010). That the granoblastic region of MIL 091004 is infiltrated by the C-rich region but is also shocked (undulose extinction and shock discoloration of olivine) suggests impact related melting as a possible mechanism for auto-fertilization of ureilites.

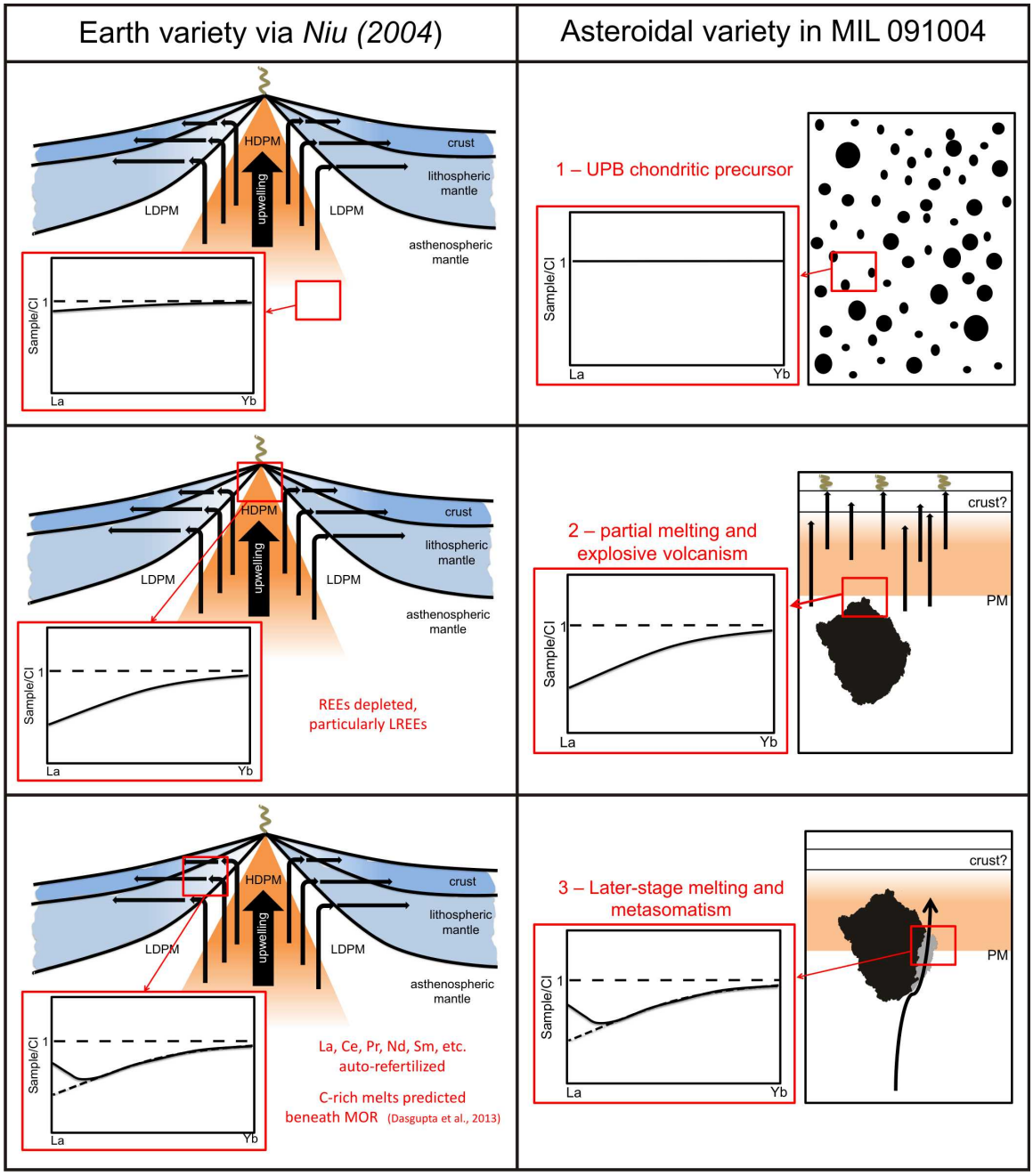

Figure 5.4.1: Schematic diagram illustrating the temporal and degree of melting similarities between lithologies created at terrestrial mid-ocean ridge systems (Earth variety) and those that could have occurred on the ureilite parent body to create the two distinct lithologies in meteorite MIL 091004 (Asteroidal variety). Abbreviations: HDPM = high degree partial melt, LDPM = low degree partial melt, PM = partial melting.

5.5 A note about terrestrial weathering

It is well known that terrestrial processes can have a significant impact on some of the chemical characteristics of meteorites, even in the cases of falls where the meteorite was discovered soon after its impact with Earth's surface. Alteration is especially significant in meteorites that are discovered as finds, the majority of which come from cold (e.g., Antarctica) and hot (e.g., the Sahara) deserts. In these cases it is not often known how long the stone has been exposed to severe conditions that can alter its chemistry. For these reasons, it is necessary to be vigilant in all types of chemical analyses of meteorites. Discussion without assessing the response to terrestrial alteration is cautioned. In this study, it is especially important when discussing whole-rock trace element abundances, with the main culprits often being the elements Sr, Ba, Cs, Ce, and some of the LREE (Crozaz et al. 2003, Floss and Crozaz 1991, Mittlefehldt and Lindstrom 1991).

These cautions are especially important for discussion of REEs in MIL 091004. Because we propose an auto-fertilization model that involves the LREEs (elements susceptible to terrestrial alteration), it is necessary to find further independent evidence that supports the model. In contrast, and although it is an Antarctic find, LEW 88763 seems relatively unaffected by terrestrial alteration. Most of its trace elements (except for Cs, Rb, and U), including all of its REEs, are chondrite-like with very few ambiguous anomalous features, and the above cautions are not as important in the discussion.

5.6 Future work

Further study of the meteorites in the sample set stands to illuminate many details about differentiation processes on asteroidal bodies in the early Solar System. A sensible step in expanding the work conducted here is to simply expand the sample set with both polished sections (for petrography, etc.) and bulk-rock samples (for detailed geochemistry). Although the set is already extensive, increasing the number of each type of meteorite sample would serve the purpose of gaining a more representative picture of each meteorite group. This is particularly important for the acapulcoites and lodranites because of their melting histories that seem to link the chondrites and the differentiated achondrites. If a more coherent picture of planetesimal differentiation is to be created, it would be quite worthwhile to increase the number of acapulcoite-lodranites in this study from its present value of nine. As of 4 January 2015, 123 entries for the acapulcoite-lodranite family exist in the Meteoritical Bulletin Database. This simple expansion of the sample set is worthwhile but less important for the chondrites since a wide body of chondrite data exists already.

A complete set of modal mineralogy data for the ten sections would reinforce the foundation for which more detailed chemical studies build upon. Accurate modes could be calculated by procedures such as point counting or spectroscopy. A simple yet accurate method to obtain accurate modes would be to use the color-contrast methods used in this study, except with sample maps stitched together from detailed BSE images. Another foundational analysis worth undertaking would be dating of the meteorites in the sample set. Further petrographic analysis of the samples for all of the sections in this study would also be a worthwhile endeavor, especially for the ungrouped achondrite

meteorites MIL 090405 and MIL 090206. In these samples, FeS presents itself as numerous tiny grains scattered throughout grain boundaries as well as fractures within silicates. This morphology and the processes that created it have yet to be studied in great detail and could provide interesting insights into the petrogenesis of not only these meteorites, but their various pairs as well.

To further the high precision whole-rock trace- and major-element analysis conducted, a logical next step would be mineral separate trace- and major-element analysis for each of the bulk-rock samples. Because such limited material is usually available for meteorite samples, this may not be a reasonable analysis for much of the sample set. If enough material is available, though, such an analysis would allow a better understanding of the mineralogical controls on fractionation and differentiation in the early Solar System.

For the meteorite MIL 091004, separate trace- and major-element analyses of the main granoblastic region and the carbon-rich region. Similar to mineral separation, it may be difficult to locate and separate the two different regions in the relatively small bulk-rock sample allocation, but if that it is possible, it would allow confirmation of this ureilite's multi-stage melting and re-fertilization history.

Very important analyses for the purposes of this sample set are highly siderophile element abundances and Os isotope measurements. Partial melting causes highly siderophile element fractionation in terrestrial systems (Barnes et al. 1985, Day et al. 2008), on the Moon (Day et al. 2010), and on asteroids (Day et al. 2012, Riches et al. 2012). Because the sample set represents a range of degrees of partial melting on meteorite parent bodies, high-precision HSE abundance measurements will be useful for

making connections between meteorite groups as well as comparing asteroidal partial melting to terrestrial processes.

6. Conclusions

The young acapulcoite-lodranites may have accreted on their parent body after burn-out of ^{26}Al. Acapulcoite-lodranites (<1-20 % partial melting) have experienced less melting than other achondrite groups (e.g., >10-30 % partial melting in brachinites) and acapulcoites (~950-1050 °C peak temperatures) have experienced lower temperatures and less melting than lodranites (~1100-1250 °C peak temperatures). Rare earth element patterns for the acapulcoite-lodranites are markedly chondrite-like, with most of the acapulcoite values are slightly enriched (<3× CI-chondrite) and most of the lodranite values are slightly depleted (>0.3× CI-chondrite). As would be expected, REE values for the transitional acapulcoite-lodranite EET 84302 lie between the acapulcoite values and the lodranite values. "Pooling" of FeNi metal is visible in some of the acapulcoite-lodranites and is most pronounced in EET 84302. This morphology is likely a snapshot of the physical process that caused the chemical differences between acapulcoites and lodranites, as well as chemical differences between chondrites and differentiated achondrites (where acapulcoite-lodranites serve as the connection between the two major meteorite types). Whole-rock major element abundances of Fe, Ni, and Co in the acapulcoites also suggest that acapulcoites have only experienced small amounts of melting if their precursor material was chondritic. The same values for lodranites point to a more complicated petrologic history – some lodranites are metal cumulates and some have experienced loss of FeNi and FeS. Interesting negative Zr and Hf anomalies in some acapulcoite-lodranites should be investigated in future studies to determine the manifestation and behavior of zircon in the meteorite group.

The Antarctic meteorites MIL 090206 and MIL 090405 were originally compared to ureilites, but petrographic and geochemical studies have shown they have closer ties to the brachinites, and should likely be classified as brachinite-like achondrites. Both meteorites are olivine dominated and sulfide rich, present major- and minor-element mineral chemistries that lie within ranges for brachinite-like achondrites, have oxygen isotopes that lie within the brachinite field, and present whole-rock trace-element abundances that generally lie within the ranges for brachinites and brachinite-like achondrites. MIL 090405 trace-element patterns are of particular note because they nearly exactly compliment the patterns created by the felsic meteorite pair GRA 06128/9. Further study of this observation could unearth an intimate residue/melt relationship between the complimentary meteorites. The expanding compositional range of brachinite-like achondrites suggests that low degree partial melting was a common process on small planetesimals in the early Solar System, yet large oxygen isotope ranges and Mg/Fe values of silicates suggest these bodies formed from diverse materials.

The Lewis Cliff 88763 meteorite is an anomalous stone. It has been compared to many individual meteorite samples (Tafassasset, NWA 6693, Eagles Nest, etc.), as well as a number of groups (acapulcoite-lodranites, brachinites, etc.). The meteorite has acapulcoite-lodranite-like oxygen isotopes, winonaite-like mineral textures, brachinite-like ferroan chemistries, and flat REE abundances. The apparently contrasting nature of LEW 88763 points to the possibility that it may offer petrologic process-related links between meteorite groups. Its existence also points to diverse oxidation environments in the early Solar System. Details of the early stages of asteroid and planet formation in the early Solar System will be explained a great deal as we begin to understand whether

anomalous oxidized samples such as LEW 88763 were created in heterogeneous parent bodies or within discrete homogeneous parent bodies.

Although originally classified as a lodranite, the remarkable meteorite Miller Range 091004 should be classified as a ureilite based on many lines of evidence – existence of large amounts of graphite, mineralogy and textures typical of ureilites, ureilitic major-element mineral compositions (notably in pyroxenes and olivines), ureilitic minor-element mineral compositions, ureilitic whole-rock trace-element abundances, silicon in FeNi metal, and Cr abundances in FeS metal. The meteorite contains two distinct lithologies, one of which – the carbon-rich region – is incredibly rich in large carbon laths and is thought to be an intrusion into the main silicate-rich granoblastic lithology. Evidence supporting this is ample, with the most striking indication being that olivine cores in the region have compositions identical to olivine cores in the main granoblastic region. Many ureilites, including MIL 091004, display REE depletion and some ureilites display LREE enrichment relative to MREEs. This data, combined with the discovery of the intrusive carbon-rich region, allows an auto-fertilization model to be proposed for the ureilite parent body in which the carbon-rich region acted as a pathway for LREE enrichment after initial partial melting and overall REE depletion. This auto-fertilization model could have important implications for the formation of the ureilite parent body, as well as other bodies in our Solar System as it might be possible to compare it to recent studies in which C-rich partial melts are used to explain features of terrestrial melting processes.

References

Barnes, S.-J., Naldrett A.J., and Gorton M.P. (1985) The origin of the fractionation of platinum-group elements in terrestrial magmas. *Chemical Geology* **53**, 303-323.

Benedix G.K., McCoy T.J., Keil K., Bogard D.D., and Garrison D.H. (1998) A petrologic and isotopic study of winonaites: Evidence for early partial melting, brecciation, and metamorphism. *Geochimica et Cosmochimica Acta* **62**, 2535-2553.

Berkley J.L., Taylor G.J., and Keil K. (1980) The nature and origin of ureilites. *Geochimica et Cosmochimica Acta* **44**, 1579-1597.

Bourot-Denise M., Zanda B., and Javoy M. (2002) Tafassasset: An equilibrated CR chondrite. *33rd Lunar and Planetary Science Conference*, abstract #1611.

Bouvier A. and Wadhwa M. (2010) The age of the Solar System redefined by the oldest Pb-Pb age of a meteoritic inclusion. *Nature Geoscience* **3**, 637-641.

Burles S., Nollett K.M., and Turner M.S. (2001) Big Bang nucleosynthesis predictions for precision cosmology. *The Astrophysical Journal* **552**, L1-L5.

Clayton R.N., Onuma N., Grossman L., and Mayeda T.K. (1977) Distribution of the pre-solar component in Allende and other carbonaceous chondrites. *Earth and Planetary Science Letters* **34**, 209-224.

Clayton R.N., Mayeda T.K., and Brownlee D.E. (1986) Oxygen isotopes in deep-sea spherules. *Earth and Planetary Science Letters* **79**, 235-240.

Clayton R.N. and Mayeda T.K. (1996) Oxygen isotope studies of achondrites. *Geochimica et Cosmochimica Acta* **60**, 1999-2017.

Clayton R.N. and Mayeda T.K. (1999) Oxygen isotope studies of carbonaceous chondrites. *Geochimica et Cosmochimica Acta* **63**, 2089-2104.

Corder C.A., Day J.M.D., Patchen A., Marti K., and Taylor L.A. (2013) Petrology of acapulcoites and lodranites and the anomalous achondrite Lewis Cliff 88763. *44th Lunar and Planetary Science Conference*, abstract #2653.

Corder C.A., Day J.M.D., Rumble III D., Assayag N., Cartigny P., and Taylor L.A. (2014a) Petrology and geochemistry of achondrites LEW 88763, MIL 090206 and MIL 090405: Comparisons with acapulcoites-lodranites, brachinites and chondrites. *45th Lunar and Planetary Science Conference*, abstract #2752.

Corder C.A., Day J.M.D., Rumble III D., Assayag N., Cartigny P., and Taylor L.A. (2014b) The unusual case of achondrite Lewis Cliff 88763 and evidence for highly oxidized, partially melted asteroids. *77th Annual Meteoritical Society Meeting*, abstract #5223.

Corder C.A., Day J.M.D., Rumble III D., Assayag N., Cartigny P., and Taylor L.A. (2014c) A carbon-rich region in ureilite Miller Range 091004. *45th Lunar and Planetary Science Conference*, abstract #2304.

Crozaz G., Floss C., and Wadhwa M. (2003) Chemical alteration and REE mobilization in meteorites from hot and cold deserts. *Geochimica et Cosmochimica Acta* **67**, 4727-4741.

Dasgupta R., Mallik A., Tsuno K., Withers A.C., Hirth G., and Hirschmann M.M. (2013) Carbon-dioxide-rich silicate melt in the Earth's upper mantle. *Nature* **493**, 211-215.

Day J.M.D., Floss C., Taylor L.A., Anand M. and Patchen A.D. (2006) Evolved mare basalt magmatism, high Mg/Fe feldspathic crust, chondritic impactors, and the petrogenesis of Antarctic lunar breccia meteorites Meteorite Hills 01210 and Pecora Escarpment 02007. *Geochimica et Cosmochimica Acta* **70**, 5957–5989.

Day J.M.D., Pearson D.G., and Hulbert L.J. (2008) Rhenium-osmium isotope and platinum-group element constraints on the origin and evolution of the 1.27 Muskox layered intrusion. *Journal of Petrology* **49**, 1255-1295.

Day J.M.D., Ash R.D., Liu Y., Bellucci J.J., Rumble III D., McDonough W.F., Walker R.J., and Taylor L.A. (2009) Early formation of evolved asteroidal crust. *Nature* **457**, 179-182.

Day J.M.D., Walker R.J., James O.B., and Puchtel I.S. (2010) Osmium isotope and highly siderophile element systematics of the lunar crust. *Earth and Planetary Science Letters* **289**, 595-605.

Day J.M.D., Walker R.J., Ash R.D., Liu Y., Rumble III D., Irving A.J., Goodrich C.A., Tait K., McDonough W.F., and Taylor L.A. (2012) Origin of felsic achondrites Graves Nunataks 06128 and 06129, and ultramafic brachinites and brachinite-like achondrites by partial melting of volatile-rich primitive parent bodies. *Geochimica et Cosmochimica Acta* **81**, 94-128.

Dhaliwal J.K., Day J.M.D., Corder C.A., Tait K.T., and Marti K. (2015) Highly siderophile element abundances and ^{187}Re-^{187}Os systematics of acapulcoite-lodranite meteorites. *46th Lunar and Planetary Science Conference*, abstract #1595.

El Goresy A., Zinner E., Pellas P., and Caillet C. (2005) A menagerie of graphite morphologies in the Acapulco meteorite with diverse carbon and nitrogen isotopic signatures: implications for the evolution history of acapulcoite meteorites. *Geochimica et Cosmochimica Acta* **69**, 4535-4556.

Floss C. and Crozaz G. (1991) Ce anomalies in the LEW85300 eucrite: evidence for REE mobilization during Antarctic weathering. *Earth and Planetary Science Letters* **107**, 13-24.

Gardner-Vandy K.G., Lauretta D.S., Greenwood R.C., McCoy T.J., Killgore M., and Franchi I.A. (2012) The Tafassasset primitive achondrite: Insights into initial stages of planetary differentiation. *Geochimica et Cosmochimica Acta* **85**, 142-159.

Golabek G.J., Bourdon B., and Gerya T.V. (2014) Numerical models of the thermomechanical evolution of planetesimals: Application to the acapulcoite-lodranite parent body. *Meteoritics & Planetary Science* **49**, 1083-1099.

Goodrich C.A. (1992) Ureilites: A critical review. *Meteoritics* **27**, 327-352.

Goodrich C.A., Scott E.R.D., and Fioretti A.M. (2004) Ureilitic breccias: clues to the petrologic structure and impact disruption of the ureilite parent asteroid. *Chemie der Erde* **64**, 283-327.

Goodrich C.A., Kita N.T., Spicuzza M.J., Valley J.W., Zipfel J., Mikouchi T., and Miyamoto M. (2011) The Northwest Africa 1500 meteorite: Not a ureilite, maybe a brachinite. *Meteoritics & Planetary Science* **45**, 1906-1928.

Goodrich C.A., Kita N.T., Warren P.H., and Rubin A.E. (2012) MIL 090340 and MIL 090206: Two more brachinite-like achondrites mis-identified as ureilites. *75th Annual Meteoritical Society Meeting*, abstract #5272.

Greenwood R.C., Franchi I.A., Gibson J.M., and Benedix G.K. (2012) Oxygen isotope variation in primitive achondrites: The influence of primordial, asteroidal and terrestrial processes. *Geochimica et Cosmochimica Acta* **94**, 146-163.

Haack H. and McCoy T.J. (2007) Iron and Stony-Iron Meteorites. *Treatise on Geochemistry*, **1: Meteorites, Comets, and Planets**, 1-22.

Hoyle F. (1954) On nuclear reactions occurring in very hot stars. I. The synthesis of elements from carbon to nickel. *Astrophysical Journal Supplement* **1**, 121-146.

Hubble E. (1929) A relation between distance and radial velocity among extra-galactic nebulae. *Proceedings of the National Academy of Sciences of the United States of America* **15**, 168-173.

Hubble E. and Humason M.L. (1931) The velocity-distance relation among extra-galactic nebulae. *Astrophysical Journal* **74**, 43-80.

Ivanova M.A., Kononkova N.N., Franchi I.A., Verchovsky A.B., Korochantseva E.V., Trieloff M., Krot A.N., and Brandster F. (2006) Isheyevo Meteorite: Genetic link between CH and CB chondrites? *37th Lunar and Planetary Science Conference*, abstract #1100.

Keil K. (2014) Brachinite meteorites: Partial melt residues from an FeO-rich asteroid. *Chemie der Erde – Geochemistry*, http://dx.doi.org/10.1016/j.chemer.2014.02.001

Kita N.T., Huss G.R., Tachibana S., Amelin Y., Nyquist L.E., and Hutcheon I.D. (2005) Constraints on the origin of chondrules and CAIs from Short-lived and Long-lived Radionuclides. In: Krot A.N., Scott E.R.D. Scott, and Reipurth B. (Eds.) *Chondrites and the Protoplanetary Disk, ASP Conference Series*, **341**, pp. 558 to 587.

Lemaitre G. (1931) The expanding universe. *Monthly Notices of the Royal Astronomical Society* **91**, 490-501.

Lindstrom M., Ed. (1991) *Antarctic Meteorite Newsletter* **14(2)**, p. 22 NASA/Johnson Space Center, Houston, Texas.

Lodders K. (2003) Solar system abundances and condensation temperatures of the elements. *The Astrophysical Journal* **591**, 1220- 1247.

MacPherson G. (1985) *Antarctic Meteorite Newsletter*, **8**(2), 1-64.

MacPherson G. (2007) Calcium-Aluminum-Rich Inclusions in Chondritic Meteorites. *Treatise on Geochemistry*, **1: Meteorites, Comets, and Planets**, 1-47.

McCoy T.J., Keil K., Clayton R.N., Mayeda T.K., Bogard D.D., Garrison D.H., Huss G.R., Hutcheon I.D., and Wieler R. (1996) A petrologic, chemical, and isotopic study of Monument Draw and comparison with other acapulcoites: Evidence for formation by incipient partial melting. *Geochimica et Cosmochimica Acta* **60**, 2681- 2708.

McCoy T.J., Keil K., Clayton R.N., Mayeda T.K., Bogard D.D., Garrison D.H., and Wieler R. (1997a) A petrologic and isotopic study of lodranites: Evidence for early formation as partial melt residues from heterogeneous precursors. *Geochimica et Cosmochimica Acta* **61**, 623-637.

McCoy T.J., Keil K., Muenow D.W., and Wilson L. (1997b) Partial melting and melt migration in the acapulcoite-lodranite parent body. *Geochimica et Cosmochimica Acta* **61**, 639-650.

McCoy T.J., Carlson W.D., Nittler L.R., Stroud R.M., Bogard D.D., and Garrison D.H. (2006) Graves Nunataks 95209: A snapshot of metal segregation and core formation. *Geochimica et Cosmochimica Acta* **70**, 516-531.

McDonough W.F. and Sun S.-s. (1995) The composition of the Earth. *Chemical Geology* **120**, 223-253

Mittlefehldt D.W. and Lindstrom M.M. (1991) Generation of abnormal trace element abundances in Antarctic eucrites by weathering processes. *Geochimica et Cosmochimica Acta* **55**, 77-87.

Mittlefehldt D.W., Lindstrom M.M., Bogard D.D., Garrison D.H., and Field S.W. (1996) Acapulco- and Lodran-like achondrites: Petrology, geochemistry, chronology, and origin. *Geochimica et Cosmochimica Acta* **60**, 867-882.

Mittlefehldt D.W., McCoy T.J., Goodrich C.A., and Kracher A. (1998) Non-chondritic meteorites from asteroidal bodies. In: Papike J.J. (Ed.), *Planetary Materials*, **36**, pp. 4-1 to 4-195.

Mittlefehldt D.W. and Lindstrom M.M. (1998) Petrology and geochemistry of lodranite Graves Nunataks 95209. *Meteoritics & Planetary Science* **33**, A111.

Mittlefehldt D.W., Bogard D.D., Berkley J.L., and Garrison D.H. (2003) Brachinites: Igneous rocks from differentiated asteroid. *Meteoritics & Planetary Science* **38**, 1601-1625.

Mittlefehldt D.W. (2007) Achondrites. *Treatise on Geochemistry*, **1: Meteorites, Comets, and Planets**, 1-40.

Nakamura N. and Morikawa N. (1993) REE and other trace lithophiles in MAC 88177, LEW 88280, and LEW 88763. *24th Lunar and Planetary Science Conference*, abstract #1047.

Nehru C.E., Prinz M., Delaney J.S., Dreibus G., Palme H., Spettel B., and Wänke H. (1983) Brachina: A new type of meteorite, not a chassignite. *Journal of Geophysical Research* **88**, B237-B244.

Niu Y. (2004) Bulk-rock major and trace element compositions of abyssal peridotites: Implications for mantle melting, melt extraction and post-melting processes beneath mid-ocean ridges. *Journal of Petrology* **45**, 2423-2458.

Olive K.A., Steigman G., and Walker T.P. (2000) Primordial nucleosynthesis: theory and observations. *Physics Reports*, **333-334**, 389-407.

Palme H. Schultz L., Spettel B., Weber H.W., and Wänke H. (1981) The Acapulco meteorite: Chemistry, mineralogy and irradiation effects. *Geochimica et Cosmochimica Acta* **45**, 727-752.

Penzias A.A. and Wilson R.W. (1965) A measurement of excess antenna temperature at 4080 Mc/s. *Astrophysical Journal* **142**, 419-421.

Prinz M., Weisberg M.K., Nehru C.E., and Delaney J.S. (1986) ALHA 84025: A second Brachina-like meteorite. *17th Lunar and Planetary Science Conference*, abstract.

Riches A.V.J., Day J.M.D., Walker R.J., Simonetti A., Liu Y., Neal C.R., and Taylor L.A. (2012) Rhenium-osmium isotope and highly-siderophile-element abundance systematics of angrite meteorites. *Earth and Planetary Science Letters* **353-354**, 208-218.

Rubin A.E. (2007) Petrogenesis of acapulcoites and lodranites: A shock-melting model. *Geochimica et Cosmochimica Acta* **71**, 2383-2401.

Rumble III D. and Hoering T.C. (1994) Analysis of oxygen and sulfur isotope ratios in oxide and sulfide minerals by spot heating with a carbon dioxide laser in a fluorine atmosphere. *Accounts of Chemical Research* **27**, 237-241.

Rumble III D., Zolensky M.E., Friedrich J.M., Jenniskens P., and Shaddad M.H. (2010) The oxygen isotope composition of Almahata Sitta. *Meteoritics & Planetary Science* **45**, 1765-1770.

Russell S.S., Zipfel J., Grossman J.N., and Grady M.M. (2002) The Meteoritical Bulletin, No. 86, 2002 July. *Meteoritics & Planetary Science* **37**, A157-A184.

Satterwhite C.E. and Righter K. (2011a) *Antarctic Meteorite Newsletter* **34**(1), 1-29.

Satterwhite C.E. and Righter K. (2011b) *Antarctic Meteorite Newsletter* **34**(2), 1-27.

Satterwhite C.E. and Righter K. (2012) *Antarctic Meteorite Newsletter* **35**(2), 1-25.

Schrader D.L., Franchi I.A., Connolly Jr. H.C., Greenwood R.C., Lauretta D.S., and Gibson J.M. (2011) The formation and alteration of the Renazzo-like carbonaceous chondrites I: Implications of bulk-oxygen isotopic composition. *Geochimica et Cosmochimica Acta* **75**, 308-325.

Scott E.R.D., Taylor G.J., and Keil K. (1993) Origin of ureilite meteorites and implications for planetary accretion. *Geophysical Research Letters* **20**, 415-418.

Scott E.R.D. and Krot A.N. (2007) Chondrites and Their Components. *Treatise on Geochemistry*, **1: Meteorites, Comets, and Planets**, 1-72.

Seeger P.A., Fowler W.A., and Clayton D.D. (1965) Nucleosynthesis of heavy elements by neutron capture. *Astrophysical Journal Supplement* **11**, 121-126.

Shearer C.K., Burger P.V., Neal C., Sharp Z., Spivak-Birndork L., Borg L., Fernandes V.A., Papike J.J., Karner J., Wadhwa M., Gaffney A., Shafer J., Geissman J., Atudorei N.-V., Herd C., Weiss B.P., King P.L., Crowther S.A., and Gilmour J.D. (2010) Non-basaltic asteroidal magmatism during the earliest stages of solar system evolution: A view from Antarctic achondrites Graves Nunatak 06128 and 06129. *Geochimica et Cosmochimia Acta* **74**, 1172-1199.

Singletary S.J. and Grove T.L. (2003) Early petrologic processes on the ureilite parent body. *Meteoritics & Planetary Science* **38**, 95-108.

Spitz A.H. and Boynton W.V. (1991) Trace element analysis of ureilites: New constraints on their petrogenesis. *Geochimica et Cosmochimica Acta* **55**, 3417-3430.

Steele A., McCubbin F.M., Fries M.D., Golden D.C., Ming D.W., and Benning L.G. (2012) Graphite in the martian meteorite Allan Hills 84001. *American Mineralogist* **97**, 1256-1259.

Swindle T.D., Kring D.A., Burkland M.K., Hill D.H., and Boynton W.V. (1998) Noble gases, bulk chemistry, and petrography of olivine-rich achondrites Eagles Nest and Lewis Cliff 88763: Comparison to brachinites. *Meteoritics & Planetary Science* **33**, 31-48.

Takeda H., Mori H., Hiroi T., and Saito J. (1994) Mineralogy of new Antarctic achondrites with affinity to Lodran and a model of their evolution in an asteroid. *Meteoritics* **29**, 830-842.

Touboul M., Kleine T., Bourdon B., Van Orman J.A., Maden C., and Zipfel J. (2009) Hf-W thermochronometry: II. Accretion and thermal history of the acapulcoite-lodranite parent body. *Earth and Planetary Science Letters* **284**, 168-178.

Valley J.W., Kitchen N., Kohn M.J., Niendorf C.R., and Spicuzza M.J. (1995) UWG-2, a garnet standard for oxygen isotope ratios: Strategies for high precision and accuracy with laser heating. *Geochimica et Cosmochimica Acta* **59**, 5223-5231.

Walker D., and Grove T. (1993) Ureilite smelting. *Meteoritics* **28**, 629-636.

Warren P.H. and Kallemeyn G.W. (1989) Allan Hills 84025: The second brachinite, far more differentiated than Brachina, and an ultramafic achondritic clast from L chondrite yamato 75097. *Proceedings of the 19th Lunar and Planetary Science Conference*, 475-486.

Warren P.H. and Kallemeyn G.W. (1992) Explosive volcanism and the graphite-oxygen fugacity buffer on the parent asteroid(s) of the ureilite meteorites. *Icarus* **100**, 110-126.

Warren P.H., Ulff-Møller F., Huber H., and Kallemeyn G.W. (2006) Siderophile geochemistry of ureilites: A record of early stages of planetesimal core formation. *Geochimica et Cosmochimica Acta* **70**, 2104-2126.

Warren P.H. and Rubin A.E. (2010) Pyroxene-selective impact smelting in ureilites. *Geochimica et Cosmochimica Acta* **74**, 5109-5133.

Warren P.H., Rubin A.E., Isa J., Brittenham S., Ahn I., and Choi B.-G. (2013) Northwest Africa 6693: A new type of FeO-rich, low-$\Delta^{17}O$, poikilitic cumulate achondrite. *Geochimica et Cosmochimica Acta* **107**, 135-154.

Yugami K., Miyamoto M., and Takeda H. (1995) The similar reduction processes of primitive achondrites from different parent bodies. *Meteoritics* **30**, 605.

Yugami K., Takeda H., Kojima H., and Miyamoto M. (1998) Modal mineral abundances and the differentiation trends in primitive achondrites. *Antarctic Meteorite Research* **11**, 49-70.

Zipfel J., Palme H., Kennedy A.K., and Hutcheon I.D. (1995) Chemical composition and origin of the Acapulco meteorite. *Geochimica et Cosmochimica Acta* **59**, 3607-3627.